



Measurement of longitudinal flow decorrelations in Pb+Pb collisions at $\sqrt{s_{\text{NN}}} = 2.76$ and 5.02 TeV with the ATLAS detector

The ATLAS Collaboration

Measurements of longitudinal flow correlations are presented for charged particles in the pseudorapidity range $|\eta| < 2.4$ using $7 \mu\text{b}^{-1}$ and $470 \mu\text{b}^{-1}$ of Pb+Pb collisions at $\sqrt{s_{\text{NN}}} = 2.76$ and 5.02 TeV, respectively, recorded by the ATLAS detector at the LHC. It is found that the correlation between the harmonic flow coefficients v_n measured in two separated η intervals does not factorise into the product of single-particle coefficients, and this breaking of factorisation, or flow decorrelation, increases linearly with the η separation between the intervals. The flow decorrelation is stronger at 2.76 TeV than at 5.02 TeV. Higher-order moments of the correlations are also measured, and the corresponding linear coefficients for the k^{th} -moment of the v_n are found to be proportional to k for v_3 , but not for v_2 . The decorrelation effect is separated into contributions from the magnitude of v_n and the event-plane orientation, each as a function of η . These two contributions are found to be comparable. The longitudinal flow correlations are also measured between v_n of different order in n . The decorrelations of v_2 and v_3 are found to be independent of each other, while the decorrelations of v_4 and v_5 are found to be driven by the nonlinear contribution from v_2^2 and v_2v_3 , respectively.

1 Introduction

Heavy-ion collisions at RHIC and the LHC create hot, dense matter whose space-time evolution is well described by relativistic viscous hydrodynamics [1, 2]. Owing to strong event-by-event (EbyE) density fluctuations in the initial state, the space-time evolution of the produced matter also fluctuates event by event. These fluctuations lead to correlations of particle multiplicity in momentum space in both the transverse and longitudinal directions with respect to the collision axis. Studies of particle correlations in the transverse plane have revealed strong harmonic modulation of the particle densities in the azimuthal angle: $dN/d\phi \propto 1 + 2 \sum_{n=1}^{\infty} v_n \cos n(\phi - \Phi_n)$, where v_n and Φ_n represent the magnitude and event-plane angle of the n^{th} -order harmonic flow. The measurements of harmonic flow coefficients v_n and their EbyE fluctuations, as well as the correlations between Φ_n of different order [3–9], have placed important constraints on the properties of the dense matter and on transverse density fluctuations in the initial state [10–15].

Most previous flow studies assumed that the initial condition and space-time evolution of the matter are boost-invariant in the longitudinal direction. Recent model studies of two-particle correlations as a function of pseudorapidity η revealed strong EbyE fluctuations of the flow magnitude and phase between two well-separated pseudorapidities, i.e. $v_n(\eta_1) \neq v_n(\eta_2)$ (forward-backward or FB asymmetry) and $\Phi_n(\eta_1) \neq \Phi_n(\eta_2)$ (event-plane twist) [16–18]. The CMS Collaboration proposed an observable based on the ratio of two correlations: the correlation between η and η_{ref} and the correlation between $-\eta$ and η_{ref} . This ratio is sensitive to the correlation between η and $-\eta$ [19]. The CMS results show that the longitudinal fluctuations lead to a linear decrease of the ratio with η , and the slope of the decrease shows a strong centrality dependence for elliptic flow v_2 but very weak dependences for v_3 and v_4 . This paper extends the CMS result by measuring several new observables based on multi-particle correlations in two or more η intervals [20]. These observables are sensitive to the EbyE fluctuations of the initial condition in the longitudinal direction. They are also sensitive to nonlinear mode-mixing effects, e.g. v_4 contains nonlinear contributions that are proportional to v_2^2 [8, 9, 21–23]. Furthermore, the measurements are performed at two nucleon–nucleon centre-of-mass collision energies, $\sqrt{s_{\text{NN}}} = 2.76$ TeV and 5.02 TeV, to evaluate the $\sqrt{s_{\text{NN}}}$ dependence of the longitudinal flow fluctuations. Recent model calculations predict an increase of longitudinal flow fluctuations at lower $\sqrt{s_{\text{NN}}}$ [24]. Therefore, measurements of these observables at two collision energies can provide new insights into the initial condition along the longitudinal direction and should help in the development of full three-dimensional viscous hydrodynamic models.

Using these new observables, this paper improves the study of the longitudinal dynamics of collective flow in three ways. Firstly, the CMS measurement, which is effectively the first moment of the correlation between v_n in separate η intervals, is extended to the second and the third moments. Secondly, a correlation between four different η intervals is measured to estimate the contributions from the fluctuations of v_n amplitudes as well as the contributions from fluctuations of Φ_n . Thirdly, correlations between harmonics of different order are also measured, e.g. between v_2 and v_4 in different η intervals, to investigate how mode-mixing effects evolve with rapidity. In this way, this paper presents a measurement of flow decorrelation involving v_2 , v_3 , v_4 and v_5 , using Pb+Pb collisions at $\sqrt{s_{\text{NN}}} = 2.76$ and 5.02 TeV.

2 Observables

This section gives a brief summary of the observables measured in this paper, further details can be found in Refs. [19, 20, 25]. The azimuthal anisotropy of the particle production in an event is conveniently

described by harmonic flow vectors $\mathbf{V}_n = v_n e^{in\Phi_n}$ ¹, where v_n and Φ_n are the magnitude and phase (or event plane), respectively. The \mathbf{V}_n are estimated from the observed per-particle normalised flow vector \mathbf{q}_n [5]:

$$\mathbf{q}_n \equiv \frac{\sum_i w_i e^{in\phi_i}}{\sum_i w_i}. \quad (1)$$

The sums run over all particles in a given η interval of the event, and ϕ_i and w_i are the azimuthal angle and the weight assigned to the i^{th} particle, respectively. The weight accounts for detector non-uniformity and tracking inefficiency.

The longitudinal flow fluctuations are studied using the correlation between the k^{th} -moment of the n^{th} -order flow vectors in two different η intervals, averaged over events in a given centrality interval, $r_{n|n;k}$, for $k = 1, 2, 3$:

$$r_{n|n;k}(\eta) = \frac{\langle \mathbf{q}_n^k(-\eta) \mathbf{q}_n^{*k}(\eta_{\text{ref}}) \rangle}{\langle \mathbf{q}_n^k(\eta) \mathbf{q}_n^{*k}(\eta_{\text{ref}}) \rangle} = \frac{\langle [v_n(-\eta)v_n(\eta_{\text{ref}})]^k \cos kn(\Phi_n(-\eta) - \Phi_n(\eta_{\text{ref}})) \rangle}{\langle [v_n(\eta)v_n(\eta_{\text{ref}})]^k \cos kn(\Phi_n(\eta) - \Phi_n(\eta_{\text{ref}})) \rangle}, \quad (2)$$

where η_{ref} is the reference pseudorapidity common to the numerator and the denominator, the subscript “ $n|n;k$ ” denotes the k^{th} -moment of the flow vectors of order n at η , combined with the k^{th} moment of the conjugate of the flow vector of order n at η_{ref} . The sine terms vanish in the last expression in Eq. (2) because any observable must be an even function of $\Phi_n(-\eta) - \Phi_n(\eta_{\text{ref}})$. A schematic illustration of the choice of the η ($|\eta| < 2.4$) and η_{ref} ($4.0 < |\eta_{\text{ref}}| < 4.9$) to be discussed in Section 5, as well as the relations between different flow vectors, are shown in the left panel of Figure 1. This observable is effectively a 2k-particle correlator between two subevents as defined in Ref. [28], and the particle multiplets containing duplicated particle indices are removed using the cumulant framework, with particle weights taken into account [20].

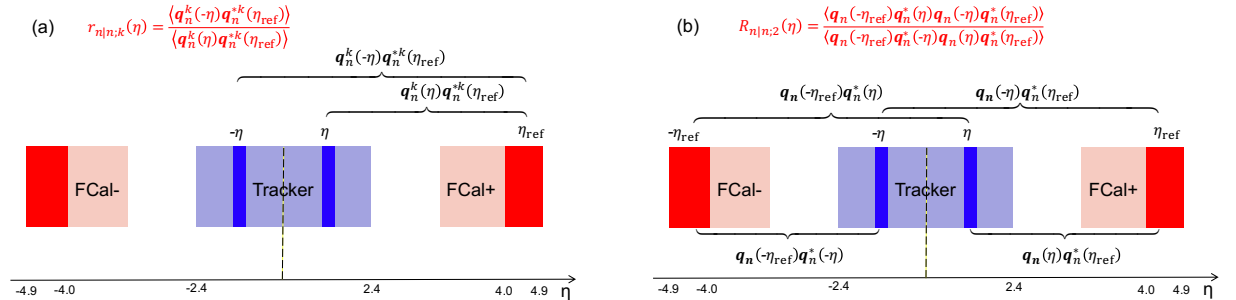


Figure 1: Schematic illustration of the procedure for constructing the correlators $r_{n|n;k}(\eta)$ Eq. (2) (left panel) and $R_{n|n;2}(\eta)$ Eq. (5) (right panel). The acceptance coverages for the ATLAS tracker for η and reference detector used for η_{ref} are discussed in Section 5.

The observable measured by the CMS Collaboration [19] corresponds to $k = 1$, i.e. $r_{n|n;1}$. It should be noted that $\langle \mathbf{q}_n \rangle = 0$ because the event plane changes randomly from event to event. Hence a direct study of the correlation between $+\eta$ and $-\eta$ via a quantity such as $\langle \mathbf{q}_n(+\eta)\mathbf{q}_n^*(-\eta) \rangle / (\langle \mathbf{q}_n(+\eta) \rangle \langle \mathbf{q}_n^*(-\eta) \rangle)$ is not possible. One could also consider a quantity like $\langle \mathbf{q}_n(+\eta)\mathbf{q}_n^*(-\eta) \rangle / (\langle \mathbf{q}_n^2(\eta) \rangle \langle \mathbf{q}_n^2(-\eta) \rangle)^{1/2}$, but the denominator would be affected by short-range correlations. Hence, it is preferable to work with quantities

¹ As in several previous analyses [26, 27], a complex number is used to represent the real two-dimensional flow vector.

of the type used in Eq. (2), which give a correlator sensitive to the flow decorrelation between η and $-\eta$ through the reference flow vector $\mathbf{q}_n^k(\eta_{\text{ref}})$.

One important feature of Eq. (2) is that the detector effects at η_{ref} are expected to cancel out to a great extent (see Section 5). To ensure a sizeable pseudorapidity gap between the flow vectors in both the numerator and denominator of Eq. (2), η_{ref} is usually chosen to be at large pseudorapidity, e.g. $\eta_{\text{ref}} > 4$ or $\eta_{\text{ref}} < -4$, while the pseudorapidity of $\mathbf{q}_n(-\eta)$ and $\mathbf{q}_n(\eta)$ is usually chosen to be close to mid-rapidity, $|\eta| < 2.4$. If flow harmonics from multi-particle correlations factorise into single-particle flow harmonics, e.g. $\langle \mathbf{V}_n^k(\eta) \mathbf{V}_n^{*k}(\eta_{\text{ref}}) \rangle^2 = \langle v_n^{2k}(\eta) \rangle \langle v_n^{2k}(\eta_{\text{ref}}) \rangle$, then it is expected that $r_{n|n;k}(\eta) = 1$. Therefore, a value of $r_{n|n;k}(\eta)$ different from 1 implies a factorisation-breaking effect due to longitudinal flow fluctuations, and such an effect is generally referred to as ‘‘flow decorrelation’’.

Based on the CMS measurement [19] and arguments in Ref. [20], the observable $r_{n|n;k}(\eta)$ is expected to be approximately a linear function of η with a negative slope, and is sensitive to both the asymmetry in the magnitude of v_n and the twist of the event-plane angles between η and $-\eta$:

$$r_{n|n;k}(\eta) \approx 1 - 2F_{n;k}^r \eta, \quad F_{n;k}^r = F_{n;k}^{\text{asy}} + F_{n;k}^{\text{twi}}, \quad (3)$$

where $F_{n;k}^{\text{asy}}$ and $F_{n;k}^{\text{twi}}$ represent the contribution from FB v_n asymmetry and event-plane twist, respectively. The $r_{n|n;k}$ results obtained in Ref. [19] were for $k = 1$ and $n = 2, 3, 4$. The measured $F_{n;1}^r$ show only a weak dependence on η_{ref} for $\eta_{\text{ref}} > 3$ or $\eta_{\text{ref}} < -3$ at the LHC. Measuring $r_{n|n;k}$ for $k > 1$ provides new information on how the v_n asymmetry and event-plane twist fluctuate event by event.

If the amount of decorrelation for the k^{th} -moment of the flow vector is proportional to k , it can be shown that [20]:

$$r_{n|n;k} \approx r_{n|n;1}^k, \quad F_{n;k}^r \approx k F_{n;1}^r. \quad (4)$$

Deviations from Eq. (4) are sensitive to the detailed EbyE structure of the flow fluctuations in the longitudinal direction.

To estimate the separate contributions of the asymmetry and twist effects, a new observable involving correlations of flow vectors in four η intervals is used [20]:

$$\begin{aligned} R_{n|n;2}(\eta) &= \frac{\langle \mathbf{q}_n(-\eta_{\text{ref}}) \mathbf{q}_n^*(\eta) \mathbf{q}_n(-\eta) \mathbf{q}_n^*(\eta_{\text{ref}}) \rangle}{\langle \mathbf{q}_n(-\eta_{\text{ref}}) \mathbf{q}_n^*(-\eta) \mathbf{q}_n(\eta) \mathbf{q}_n^*(\eta_{\text{ref}}) \rangle} \\ &= \frac{\langle v_n(-\eta_{\text{ref}}) v_n(-\eta) v_n(\eta) v_n(\eta_{\text{ref}}) \cos n [\Phi_n(-\eta_{\text{ref}}) - \Phi_n(\eta_{\text{ref}}) + (\Phi_n(-\eta) - \Phi_n(\eta))] \rangle}{\langle v_n(-\eta_{\text{ref}}) v_n(-\eta) v_n(\eta) v_n(\eta_{\text{ref}}) \cos n [\Phi_n(-\eta_{\text{ref}}) - \Phi_n(\eta_{\text{ref}}) - (\Phi_n(-\eta) - \Phi_n(\eta))] \rangle}, \end{aligned} \quad (5)$$

where the notation ‘‘2’’ in the subscript indicates that there are two \mathbf{q}_n and two \mathbf{q}_n^* in the numerator and denominator. A schematic illustration of the relations between different flow vectors is shown in the right panel of Figure 1. Since the effect of an asymmetry is the same in both the numerator and the denominator, this correlator is mainly sensitive to the event-plane twist effects:

$$R_{n|n;2}(\eta) \approx 1 - 2F_{n;2}^R \eta, \quad F_{n;2}^R = F_{n;2}^{\text{twi}}. \quad (6)$$

Therefore, the asymmetry and twist contributions can be estimated by combining Eqs. (3) and (6).

Measurements of longitudinal flow fluctuations can also be extended to correlations between harmonics of different order:

$$r_{2,3|2,3}(\eta) = \frac{\langle \mathbf{q}_2(-\eta) \mathbf{q}_2^*(\eta_{\text{ref}}) \mathbf{q}_3(-\eta) \mathbf{q}_3^*(\eta_{\text{ref}}) \rangle}{\langle \mathbf{q}_2(\eta) \mathbf{q}_2^*(\eta_{\text{ref}}) \mathbf{q}_3(\eta) \mathbf{q}_3^*(\eta_{\text{ref}}) \rangle}, \quad (7)$$

$$r_{2,2|4}(\eta) = \frac{\langle \mathbf{q}_2^2(-\eta) \mathbf{q}_4^*(\eta_{\text{ref}}) \rangle + \langle \mathbf{q}_2^2(\eta_{\text{ref}}) \mathbf{q}_4^*(-\eta) \rangle}{\langle \mathbf{q}_2^2(\eta) \mathbf{q}_4^*(\eta_{\text{ref}}) \rangle + \langle \mathbf{q}_2^2(\eta_{\text{ref}}) \mathbf{q}_4^*(\eta) \rangle}, \quad (8)$$

$$r_{2,3|5}(\eta) = \frac{\langle \mathbf{q}_2(-\eta) \mathbf{q}_3(-\eta) \mathbf{q}_5^*(\eta_{\text{ref}}) \rangle + \langle \mathbf{q}_2(\eta_{\text{ref}}) \mathbf{q}_3(\eta_{\text{ref}}) \mathbf{q}_5^*(-\eta) \rangle}{\langle \mathbf{q}_2(\eta) \mathbf{q}_3(\eta) \mathbf{q}_5^*(\eta_{\text{ref}}) \rangle + \langle \mathbf{q}_2(\eta_{\text{ref}}) \mathbf{q}_3(\eta_{\text{ref}}) \mathbf{q}_5^*(\eta) \rangle}, \quad (9)$$

where the comma in the subscripts denotes the combination of \mathbf{q}_n of different order. If the longitudinal fluctuations for \mathbf{V}_2 and \mathbf{V}_3 are independent of each other, one would expect $r_{2,3|2,3} = r_{2|2;1} r_{3|3;1}$ [20]. On the other hand, $r_{2,2|4}$ and $r_{2,3|5}$ are sensitive to the η dependence of the correlations between v_n and event planes of different order, for example $\langle \mathbf{q}_2^2(-\eta) \mathbf{q}_4^*(\eta_{\text{ref}}) \rangle = \langle v_2^2(-\eta) v_4(\eta_{\text{ref}}) \cos 4(\Phi_2(-\eta) - \Phi_4(\eta_{\text{ref}})) \rangle$. Correlations between different orders have been measured previously at the LHC [8, 9, 23, 29].

It is well established that the \mathbf{V}_4 and \mathbf{V}_5 in Pb+Pb collisions contain a linear contribution associated with initial geometry and mode-mixing contributions from lower-order harmonics due to nonlinear hydrodynamic response [8, 9, 14, 21, 22]:

$$\mathbf{V}_4 = \mathbf{V}_{4L} + \chi_4 \mathbf{V}_2^2, \quad \mathbf{V}_5 = \mathbf{V}_{5L} + \chi_5 \mathbf{V}_2 \mathbf{V}_3, \quad (10)$$

where the linear component \mathbf{V}_{nL} is driven by the corresponding eccentricity in the initial geometry [11]. If the linear component of v_4 and v_5 is uncorrelated with lower-order harmonics, i.e. $\mathbf{V}_2^2 \mathbf{V}_{4L}^* \sim 0$ and $\mathbf{V}_2 \mathbf{V}_3 \mathbf{V}_{5L}^* \sim 0$, one expects [20]:

$$r_{2,2|4} \approx r_{2|2;2}, \quad r_{2,3|5} \approx r_{2,3|2,3}. \quad (11)$$

Furthermore, using Eq. (10) the $r_{n|n;1}$ correlators involving v_4 and v_5 can be approximated by:

$$r_{4|4;1}(\eta) \approx \frac{\langle \mathbf{V}_{4L}(-\eta) \mathbf{V}_{4L}^*(\eta_{\text{ref}}) \rangle + \chi_4^2 \langle \mathbf{V}_2^2(-\eta) \mathbf{V}_2^{*2}(\eta_{\text{ref}}) \rangle}{\langle \mathbf{V}_{4L}(\eta) \mathbf{V}_{4L}^*(\eta_{\text{ref}}) \rangle + \chi_4^2 \langle \mathbf{V}_2^2(\eta) \mathbf{V}_2^{*2}(\eta_{\text{ref}}) \rangle}, \quad (12)$$

$$r_{5|5;1}(\eta) \approx \frac{\langle \mathbf{V}_{5L}(-\eta) \mathbf{V}_{5L}^*(\eta_{\text{ref}}) \rangle + \chi_5^2 \langle \mathbf{V}_2(-\eta) \mathbf{V}_2^*(\eta_{\text{ref}}) \mathbf{V}_3(-\eta) \mathbf{V}_3^*(\eta_{\text{ref}}) \rangle}{\langle \mathbf{V}_{5L}(\eta) \mathbf{V}_{5L}^*(\eta_{\text{ref}}) \rangle + \chi_5^2 \langle \mathbf{V}_2(\eta) \mathbf{V}_2^*(\eta_{\text{ref}}) \mathbf{V}_3(\eta) \mathbf{V}_3^*(\eta_{\text{ref}}) \rangle}. \quad (13)$$

Therefore, both the linear and nonlinear components are important for $r_{4|4;1}$ and $r_{5|5;1}$.

3 ATLAS detector and trigger

The ATLAS detector [30] provides nearly full solid-angle coverage of the collision point with tracking detectors, calorimeters, and muon chambers, and is well suited for measurements of multi-particle correlations over a large pseudorapidity range.² The measurements were performed using the inner detector (ID),

² ATLAS uses a right-handed coordinate system with its origin at the nominal interaction point (IP) in the centre of the detector and the z -axis along the beam pipe. The x -axis points from the IP to the centre of the LHC ring, and the y -axis points upward. Cylindrical coordinates (r, ϕ) are used in the transverse plane, ϕ being the azimuthal angle around the beam pipe. The pseudorapidity is defined in terms of the polar angle θ as $\eta = -\ln \tan(\theta/2)$.

minimum-bias trigger scintillators (MBTS), the forward calorimeters (FCal), and the zero-degree calorimeters (ZDC). The ID detects charged particles within $|\eta| < 2.5$ using a combination of silicon pixel detectors, silicon microstrip detectors (SCT), and a straw-tube transition-radiation tracker (TRT), all immersed in a 2 T axial magnetic field [31]. An additional pixel layer, the “insertable B-layer” (IBL) [32] installed during the 2013-2015 shutdown between Run 1 and Run 2, is used in the 5.02 TeV measurements. The MBTS system detects charged particles over $2.1 \lesssim |\eta| \lesssim 3.9$ using two hodoscopes of counters positioned at $z = \pm 3.6$ m. The FCal consists of three sampling layers, longitudinal in shower depth, and covers $3.2 < |\eta| < 4.9$. The ZDC are positioned at ± 140 m from the IP, detecting neutrons and photons with $|\eta| > 8.3$.

This analysis uses approximately $7 \mu\text{b}^{-1}$ and $470 \mu\text{b}^{-1}$ of Pb+Pb data at $\sqrt{s_{\text{NN}}} = 2.76$ and 5.02 TeV, respectively, recorded by the ATLAS experiment at the LHC. The 2.76 TeV data were collected in 2010, while the 5.02 TeV data were collected in 2015.

The ATLAS trigger system [33] consists of a level-1 (L1) trigger implemented using a combination of dedicated electronics and programmable logic, and a high-level trigger (HLT) implemented in general-purpose processors. The trigger requires signals in both ZDC or either of the two MBTS counters. The ZDC trigger thresholds on each side are set below the maximum corresponding to a single neutron. A timing requirement based on signals from each side of the MBTS was imposed to remove beam backgrounds. This trigger selected $7 \mu\text{b}^{-1}$ and $22 \mu\text{b}^{-1}$ of minimum-bias Pb+Pb data at $\sqrt{s_{\text{NN}}} = 2.76$ TeV and $\sqrt{s_{\text{NN}}} = 5.02$ TeV, respectively. To increase the number of recorded events from very central Pb+Pb collisions, a dedicated L1 trigger was used in 2015 to select events requiring the total transverse energy (ΣE_{T}) in the FCal to be more than 4.54 TeV. This ultra-central trigger sampled $470 \mu\text{b}^{-1}$ of Pb+Pb collisions at 5.02 TeV and was fully efficient for collisions with centrality 0–0.1% (see Section 4).

4 Event and track selection

The offline event selection requires a reconstructed vertex with its z position satisfying $|z_{\text{vtx}}| < 100$ mm. For the $\sqrt{s_{\text{NN}}} = 2.76$ TeV Pb+Pb data, the selection also requires a time difference $|\Delta t| < 3$ ns between signals in the MBTS trigger counters on either side of the nominal centre of ATLAS to suppress non-collision backgrounds. A coincidence between the ZDC signals at forward and backward pseudorapidity is required to reject a variety of background processes such as elastic collisions and non-collision backgrounds, while maintaining high efficiency for inelastic processes. The fraction of events containing more than one inelastic interaction (pile-up) is estimated to be less than 0.1% at both collision energies. The pile-up contribution is studied by exploiting the correlation between the transverse energy ΣE_{T} measured in the FCal or the number of neutrons N_n in the ZDC and the number of tracks associated with a primary vertex $N_{\text{ch}}^{\text{rec}}$. Since the distribution of ΣE_{T} or N_n in events with pile-up is broader than that for the events without pile-up, pile-up events are suppressed by rejecting events with an abnormally large ΣE_{T} or N_n as a function of $N_{\text{ch}}^{\text{rec}}$.

The event centrality [34] is characterised by the ΣE_{T} deposited in the FCal over the pseudorapidity range $3.2 < |\eta| < 4.9$ using a calibration employing the electromagnetic calorimeters to set the energy scale [35]. The FCal ΣE_{T} distribution is divided into a set of centrality intervals. A centrality interval refers to a percentile range, starting at 0% relative to the most central collisions. Thus the 0–5% centrality interval, for example, corresponds to the most central 5% of the events. The ultra-central trigger mentioned in Section 3 selects events in the 0–0.1% centrality interval with full efficiency. A Monte Carlo Glauber analysis [34,36] is used to estimate the average number of participating nucleons, N_{part} , for each centrality

interval. The systematic uncertainty in N_{part} is less than 1% for centrality intervals in the range 0–20% and increases to 6% for centrality intervals in the range 70–80%. The Glauber model also provides a correspondence between the ΣE_{T} distribution and sampling fraction of the total inelastic Pb+Pb cross section, allowing centrality percentiles to be set. For this analysis, a selection of collisions corresponding to 0–70% centrality is used to avoid diffraction or other processes that contribute to very peripheral collisions. Following the convention used in heavy-ion analyses, the centrality dependence of the results in this paper is presented as a function of N_{part} .

Charged-particle tracks and primary vertices [37] are reconstructed from hits in the ID. Tracks are required to have $p_{\text{T}} > 0.5$ GeV and $|\eta| < 2.4$. For the 2.76 TeV data, tracks are required to have at least nine hits in the silicon detectors with no missing pixel hits and not more than one missing SCT hit, taking into account the presence of known dead modules. For the 5.02 TeV data, tracks are required to have at least two pixel hits, with the additional requirement of a hit in the first pixel layer when one is expected, at least eight SCT hits, and at most one missing hit in the SCT. In addition, for both datasets, the point of closest approach of the track is required to be within 1 mm of the primary vertex in both the transverse and longitudinal directions [38].

The efficiency, $\epsilon(p_{\text{T}}, \eta)$, of the track reconstruction and track selection criteria is evaluated using Pb+Pb Monte Carlo events produced with the HIJING event generator [39]. The generated particles in each event were rotated in azimuthal angle according to the procedure described in Ref. [40] to produce harmonic flow consistent with previous ATLAS measurements [5, 41]. The response of the detector was simulated using GEANT4 [42, 43] and the resulting events are reconstructed with the same algorithms applied to the data. For the 5.02 TeV Pb+Pb data, the efficiency ranges from 75% at $\eta \approx 0$ to about 50% for $|\eta| > 2$ for charged particles with $p_{\text{T}} > 0.8$ GeV, falling by about 5% as p_{T} is reduced to 0.5 GeV. The efficiency varies more strongly with η and event multiplicity. For $p_{\text{T}} > 0.8$ GeV, it ranges from 75% at $\eta \approx 0$ to 50% for $|\eta| > 2$ in peripheral collisions, while it ranges from 71% at $\eta \approx 0$ to about 40% for $|\eta| > 2$ in central collisions. The tracking efficiency for the 2.76 TeV data has a similar dependence on p_{T} and η . The efficiency is used in the particle weight, as described in Section 5. However, because the observables studied are ratios (see Section 2), uncertainties in detector and reconstruction efficiencies largely cancel. The rate of falsely reconstructed tracks (“fakes”) is also estimated and found to be significant only at $p_{\text{T}} < 1$ GeV in central collisions, where its percentage per-track ranges from 2% at $|\eta| < 1$ to 8% at the larger $|\eta|$. The fake rate drops rapidly for higher p_{T} and towards more peripheral collisions. The fake rate is accounted for in the tracking efficiency correction following the procedure in Ref. [44].

5 Data analysis

Measurement of the longitudinal flow dynamics requires the calculation of the flow vector \mathbf{q}_n via Eq. (1) in the ID and the FCal. The flow vector from the FCal serves as the reference $\mathbf{q}_n(\eta_{\text{ref}})$, while the ID provides the flow vector as a function of pseudorapidity $\mathbf{q}_n(\eta)$.

In order to account for detector inefficiencies and non-uniformity, a particle weight for the i^{th} -particle in the ID for the flow vector from Eq. (1) is defined as:

$$w_i^{\text{ID}}(\eta, \phi, p_{\text{T}}) = d_{\text{ID}}(\eta, \phi) / \epsilon(\eta, p_{\text{T}}), \quad (14)$$

similar to the procedure in Ref. [44]. The determination of track efficiency $\epsilon(\eta, p_{\text{T}})$ is described in Section 4. The additional weight factor $d_{\text{ID}}(\eta, \phi)$ corrects for variation of tracking efficiency or non-uniformity of detector acceptance as a function of η and ϕ . For a given η interval of 0.1, the distribution

in azimuthal bins, $N(\phi, \eta)$, is built up from reconstructed charged particles summed over all events. The weight factor is then obtained as $d_{\text{ID}}(\eta, \phi) \equiv \langle N(\eta) \rangle / N(\phi, \eta)$, where $\langle N(\eta) \rangle$ is the average of $N(\phi, \eta)$. This ‘‘flattening’’ procedure removes most ϕ -dependent non-uniformity from track reconstruction, which is important for any azimuthal correlation analysis. Similarly, the weight in the FCal for the flow vector from Eq. (1) is defined as:

$$w_i^{\text{FCal}}(\eta, \phi) = d_{\text{FCal}}(\eta, \phi) E_{T,i}, \quad (15)$$

where $E_{T,i}$ is the transverse energy measured in the i^{th} tower in the FCal at η and ϕ . The azimuthal weight $d_{\text{FCal}}(\eta, \phi)$ is calculated in narrow η intervals in a similar way to what is done for the ID. It ensures that the E_T -weighted distribution, averaged over all events in a given centrality interval, is uniform in ϕ . The flow vectors $\mathbf{q}_n(\eta)$ and $\mathbf{q}_n(\eta_{\text{ref}})$ are further corrected by an event-averaged offset: $\mathbf{q}_n - \langle \mathbf{q}_n \rangle_{\text{evts}}$ [8].

The flow vectors obtained after these reweighting and offset procedures are used in the correlation analysis. The correlation quantities used in $r_{n|n;k}$ are calculated as:

$$\langle \mathbf{q}_n^k(\eta) \mathbf{q}_n^{*k}(\eta_{\text{ref}}) \rangle \equiv \langle \mathbf{q}_n^k(\eta) \mathbf{q}_n^{*k}(\eta_{\text{ref}}) \rangle_{\text{s}} - \langle \mathbf{q}_n^k(\eta) \mathbf{q}_n^{*k}(\eta_{\text{ref}}) \rangle_{\text{b}}, \quad (16)$$

where subscripts ‘‘s’’ and ‘‘b’’ represent the correlator constructed from the same event (‘‘signal’’) and from the mixed-event (‘‘background’’), respectively. The mixed-event quantity is constructed by combining $\mathbf{q}_n^k(\eta)$ from each event with $\mathbf{q}_n^{*k}(\eta_{\text{ref}})$ obtained in other events with similar centrality (within 1%) and similar z_{vtx} ($|\Delta z_{\text{vtx}}| < 5$ mm). The $\langle \mathbf{q}_n^k(\eta) \mathbf{q}_n^{*k}(\eta_{\text{ref}}) \rangle_{\text{b}}$, which is typically more than two orders of magnitude smaller than the corresponding signal term, is subtracted to account for any residual detector non-uniformity effects that result from a correlation between different η ranges.

For correlators involving flow vectors in two different η ranges, mixed events are constructed from two different events. For example, the correlation for $r_{2,3|5}$ is calculated as:

$$\langle \mathbf{q}_2(\eta) \mathbf{q}_3(\eta) \mathbf{q}_5^*(\eta_{\text{ref}}) \rangle \equiv \langle \mathbf{q}_2(\eta) \mathbf{q}_3(\eta) \mathbf{q}_5^*(\eta_{\text{ref}}) \rangle_{\text{s}} - \langle \mathbf{q}_2(\eta) \mathbf{q}_3(\eta) \mathbf{q}_5^*(\eta_{\text{ref}}) \rangle_{\text{b}}. \quad (17)$$

The mixed-event correlator is constructed by combining $\mathbf{q}_2(\eta) \mathbf{q}_3(\eta)$ from one event with $\mathbf{q}_5^*(\eta_{\text{ref}})$ obtained in another event with similar centrality (within 1%) and similar z_{vtx} ($|\Delta z_{\text{vtx}}| < 5$ mm). On the other hand, for correlators involving more than two different η ranges, mixed events are constructed from more than two different events, one for each unique η range. One such example is $R_{n|n;2}$, for which each mixed event is constructed from four different events with similar centrality and z_{vtx} .

Most correlators can be symmetrised. For example, in a symmetric system such as Pb+Pb collisions, the condition $\langle \mathbf{q}_n^k(-\eta) \mathbf{q}_n^{*k}(\eta_{\text{ref}}) \rangle = \langle \mathbf{q}_n^k(\eta) \mathbf{q}_n^{*k}(-\eta_{\text{ref}}) \rangle$ holds. So instead of Eq. (2), the actual measured observable is:

$$r_{n|n;k}(\eta) = \frac{\langle \mathbf{q}_n^k(-\eta) \mathbf{q}_n^{*k}(\eta_{\text{ref}}) + \mathbf{q}_n^k(\eta) \mathbf{q}_n^{*k}(-\eta_{\text{ref}}) \rangle}{\langle \mathbf{q}_n^k(\eta) \mathbf{q}_n^{*k}(\eta_{\text{ref}}) + \mathbf{q}_n^k(-\eta) \mathbf{q}_n^{*k}(-\eta_{\text{ref}}) \rangle}. \quad (18)$$

The symmetrisation procedure also allows further cancellation of possible differences between η and $-\eta$ in the tracking efficiency or detector acceptance.

Table 1 gives a summary of the set of correlators measured in this analysis. The analysis is performed in intervals of centrality and the results are presented as a function of η for $|\eta| < 2.4$. The main results are obtained using 5.02 TeV Pb+Pb data. The 2010 2.76 TeV Pb+Pb data are statistically limited, and are used only to obtain $r_{n|n;1}$ and $R_{n|n;2}$ to compare with results obtained from the 5.02 TeV data and study the dependence on collision energy.

Table 1: The list of observables measured in this analysis.

Observables	Pb+Pb datasets
$r_{n n;k}$ for $n = 2,3,4$ and $k = 1$	2.76 and 5.02 TeV
$R_{n n;2}$ for $n = 2,3$	2.76 and 5.02 TeV
$r_{n n;k}$ for $n = 5$ and $k = 1$	5.02 TeV
$r_{n n;k}$ for $n = 2,3$ and $k = 2,3$	5.02 TeV
$R_{n n;2}$ for $n = 4$	5.02 TeV
$r_{2,2 4}, r_{2,3 5}, r_{2,3 2,3}$	5.02 TeV

Figures 2 and 3 show the sensitivity of $r_{2|2;1}$ and $r_{3|3;1}$, respectively, to the choice of the range of η_{ref} . A smaller η_{ref} value implies a smaller pseudorapidity gap between η and η_{ref} . The values of $r_{n|n;1}$ generally decrease with decreasing η_{ref} , possibly reflecting the contributions from the dijet correlations [5]. However, such contributions should be reduced in the most central collisions due to large charged-particle multiplicity and jet-quenching [45] effects. Therefore, the decrease of $r_{n|n;1}$ in the most central collisions may also reflect the η_{ref} dependence of $F_{n;1}^r$, as defined in Eq. (3). In this analysis, the reference flow vector is calculated from $4.0 < \eta_{\text{ref}} < 4.9$, which reduces the effect of dijets and provides good statistical precision. For this choice of η_{ref} range, $r_{2|2;1}$ and $r_{3|3;1}$ show a linear decrease as a function of η in most centrality intervals, indicating a significant breakdown of factorisation. A similar comparison for $r_{4|4;1}$ can be found in the Appendix.

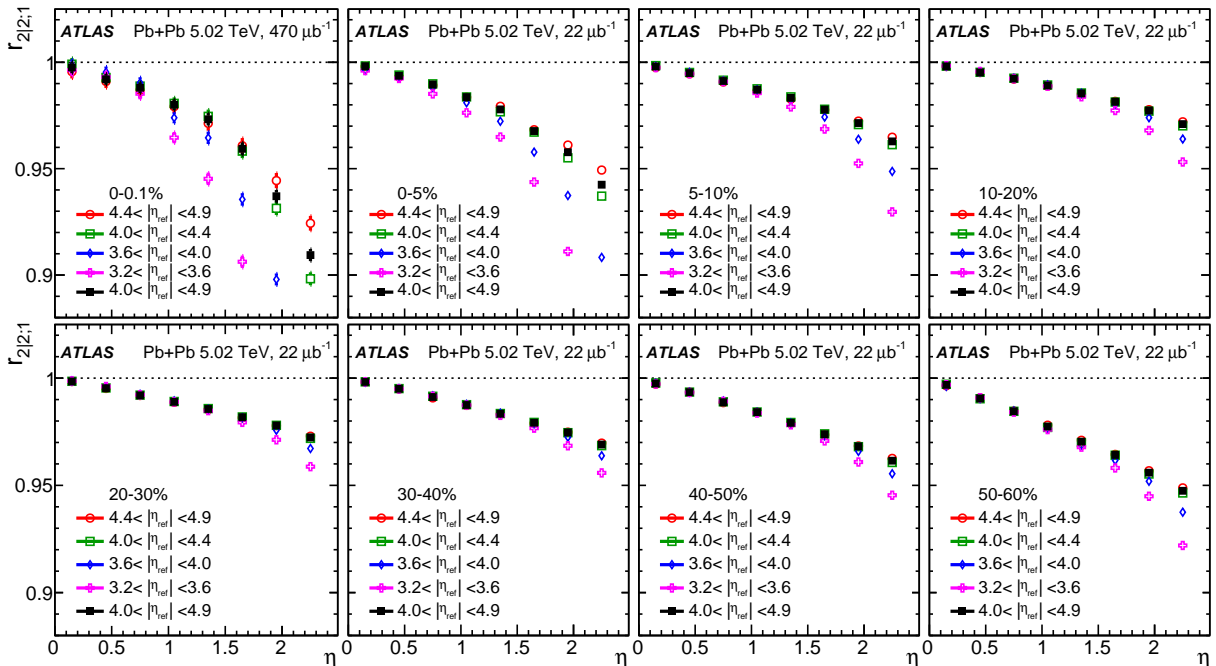


Figure 2: The $r_{2|2;1}(\eta)$ measured for several η_{ref} ranges. Each panel shows the results for one centrality range. The error bars are statistical only.

Figures 4 and 5 show $r_{2|2;1}$ and $r_{3|3;1}$ calculated for several p_T ranges of the charged particles in the ID. A similar comparison for $r_{4|4;1}$ can be found in the Appendix. If the longitudinal-flow asymmetry and twist reflect global properties of the event, the values of $r_{n|n;1}$ should not depend strongly on p_T . Indeed no

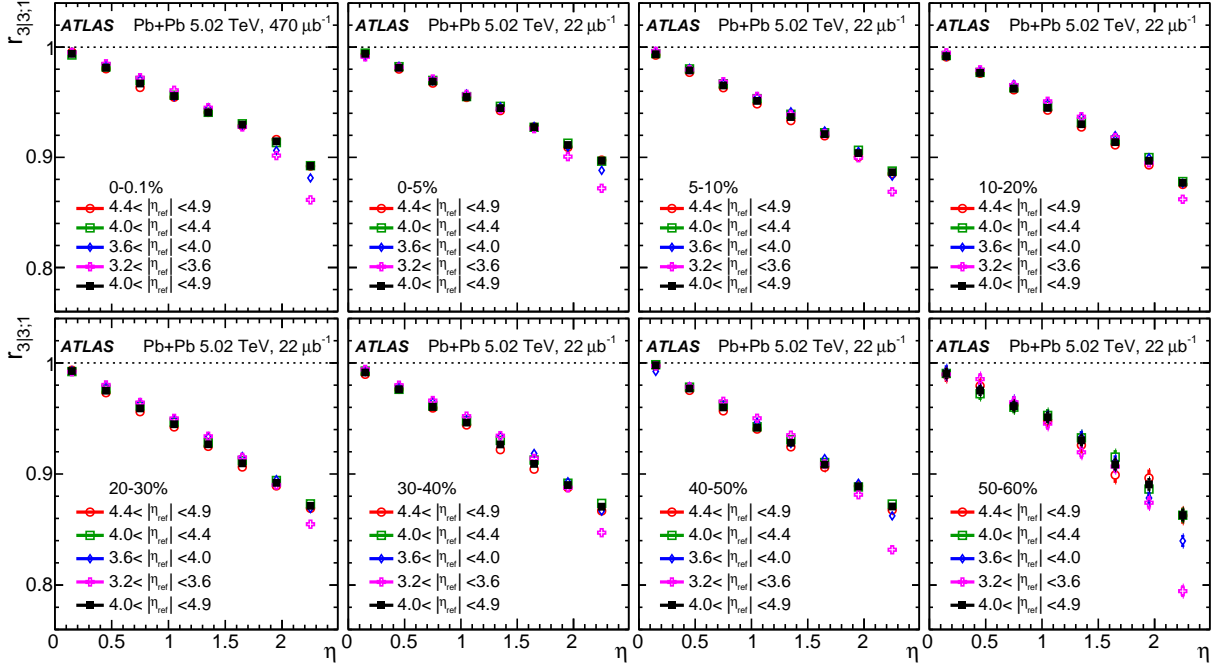


Figure 3: The $r_{3|3;1}(\eta)$ measured for several η_{ref} ranges. Each panel shows the results for one centrality range. The error bars are statistical only.

dependence is observed, except for $r_{2|2;1}$ in the most central collisions and very peripheral collisions. The behaviour in central collisions may be related to the factorisation breaking of the v_2 as a function of p_T and η [5, 19]. The behaviour in peripheral collisions is presumably due to increasing relative contributions from jets and dijets at higher p_T and for peripheral collisions. Based on this, the measurements are performed using charged particles with $0.5 < p_T < 3$ GeV.

6 Systematic uncertainties

Since all observables are found to follow an approximately linear decrease with η , i.e. $D(\eta) \approx 1 - c\eta$ for a given observable $D(\eta)$ where c is a constant, the systematic uncertainty is presented as the relative uncertainty for $1 - D(\eta)$ at $\eta = 1.2$, the mid-point of the η range. The systematic uncertainties in this analysis arise from event mixing, track selection, and reconstruction efficiency. Most of the systematic uncertainties enter the analysis through the particle weights in Eqs. (14) and (15). In general, the uncertainties for $r_{n|n;k}$ increase with n and k , the uncertainties for $R_{n|n;2}$ increase with n , and all uncertainties are larger in the most central and more peripheral collisions. For $r_{2,3|2,3}$, $r_{2,2|4}$ and $r_{2,3|5}$, the uncertainties are significantly larger than for the other correlators. Each source is discussed separately below.

The effect of detector azimuthal non-uniformity is accounted for by the weight factor $d(\eta, \phi)$ in Eqs. (14) and (15). The effect of reweighting is studied by setting the weight to unity and repeating the analysis. The results are consistent with the default (weighted) results within statistical uncertainties, so no additional systematic uncertainty is included. Possible residual detector effects for each observable are further removed by subtracting those obtained from mixed events as described in Section 5. Uncertainties due

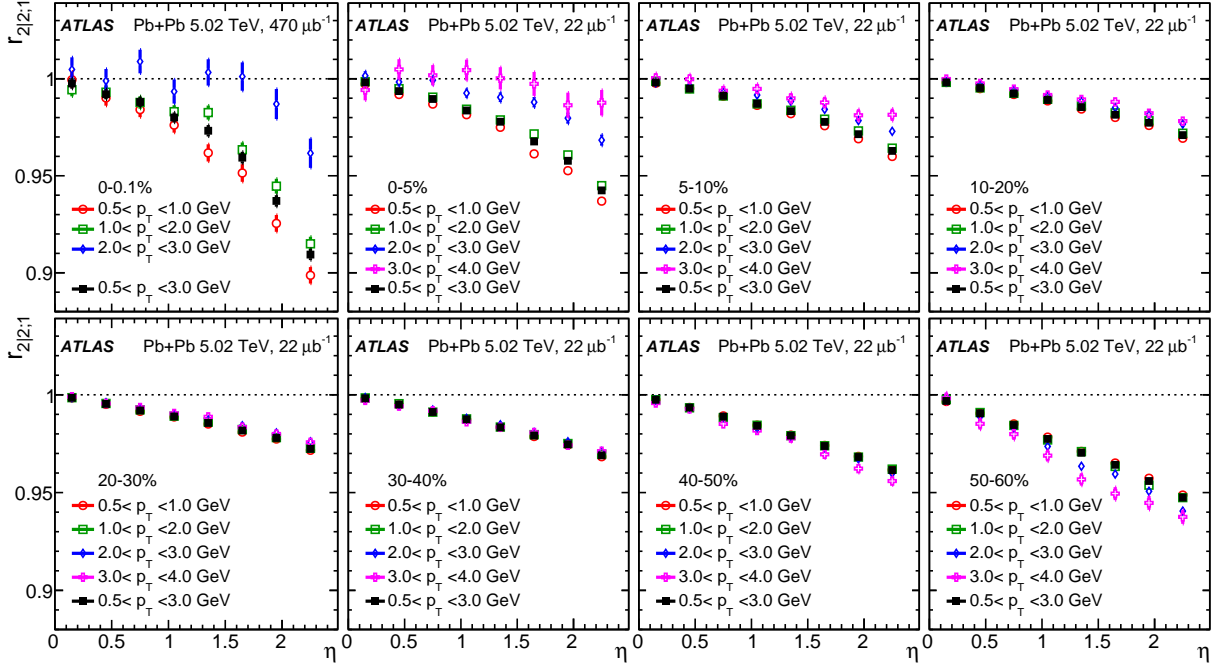


Figure 4: The $r_{2|2;1}(\eta)$ measured in several p_T ranges. Each panel shows the results for one centrality range. The error bars are statistical only.

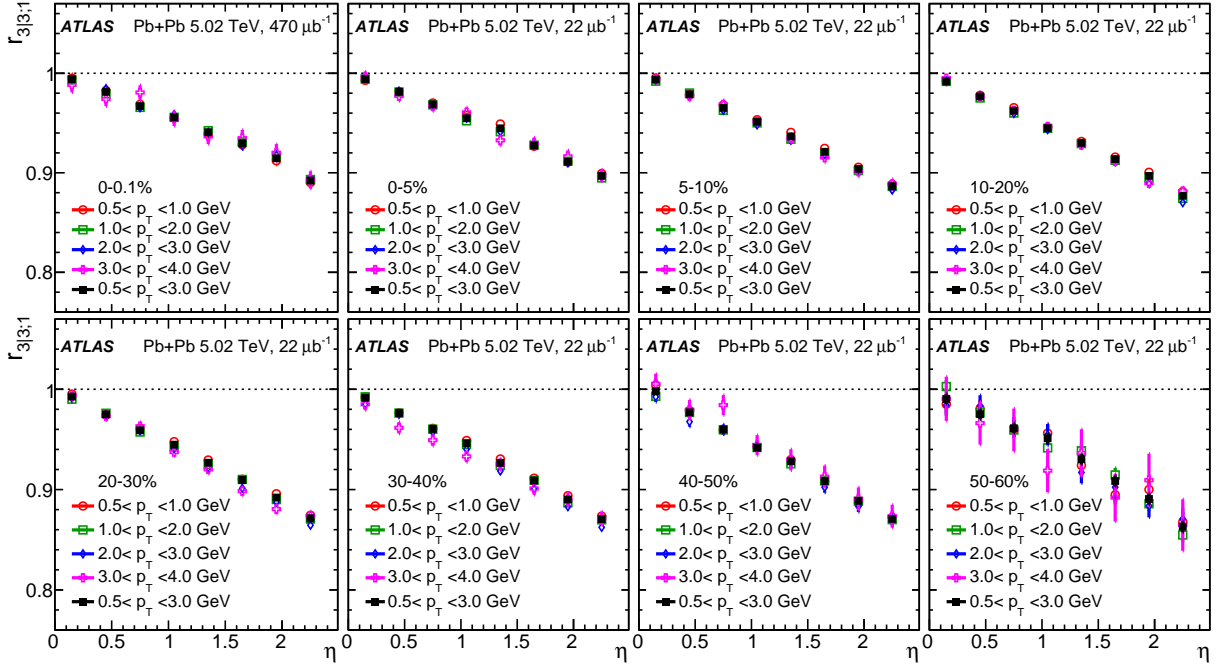


Figure 5: The $r_{3|3;1}(\eta)$ measured in several p_T ranges. Each panel shows the results for one centrality range. The error bars are statistical only.

to the event-mixing procedure are estimated by varying the criteria for matching events in centrality and z_{vtx} . The resulting uncertainty is in general found to be smaller than the statistical uncertainties. The event-mixing uncertainty for $r_{2|2;k}$ and $r_{3|3;k}$ is less than 1% for $k = 1$ and changes to about 0.4–8% for $k = 2$ and 0.6–10% for $k = 3$, while the uncertainty for $r_{4|4;1}$ and $r_{5|5;1}$ is in the range 1.5–3% and 5–13%, respectively. The uncertainty for $R_{n|n;2}$ is 1.5–6% for $n = 2$ and 3–14% for $n = 3$. The uncertainties for $r_{2,3|2,3}$, $r_{2,2|4}$ and $r_{2,2|5}$ are typically larger: 1–4%, 1.5–16% and 3–15%.

The systematic uncertainty associated with the track quality selections is estimated by tightening or loosening the requirements on transverse impact parameter $|d_0|$ and longitudinal impact parameter $|z_0 \sin \theta|$ used to select tracks. In each case, the tracking efficiency is re-evaluated and the analysis is repeated. The difference is observed to be larger in the most central collisions where the flow signal is smaller and the influence of falsely reconstructed tracks is higher. The difference is observed to be in the range 0.2–12% for $r_{2|2;k}$ and $r_{3|3;k}$, 1.1–2% for $r_{4|4;1}$, 3–6% for $r_{5|5;1}$, 0.5–13% for $R_{n|n;2}$, and 1–14% for $r_{2,3|2,3}$, $r_{2,2|4}$ and $r_{2,2|5}$.

From previous measurements [5, 6, 46], the v_n signal has been shown to have a strong dependence on p_T but relatively weak dependence on η . Therefore, a p_T -dependent uncertainty in the track reconstruction efficiency $\epsilon(\eta, p_T)$ could affect the measured longitudinal flow correlation, through the particle weights. The uncertainty in the track reconstruction efficiency is due to differences in the detector conditions and known differences in the material between data and simulations. The uncertainty in the efficiency varies between 1% and 4%, depending on η and p_T [44]. The systematic uncertainty for each observable in Table 1 is evaluated by repeating the analysis with the tracking efficiency varied up and down by its corresponding uncertainty. For $r_{n|n;k}$ the uncertainties are in the range 0.1–2%, depending on n and k . For $R_{n|n;2}$ the uncertainties are in the range 0.1–1%. For $r_{2,3|2,3}$, $r_{2,2|4}$ and $r_{2,2|5}$, the uncertainties are in the range 0.1–2%.

Due to the finite energy resolution and energy scale uncertainty of the FCal, the $\mathbf{q}_n(\eta_{\text{ref}})$ calculated from the azimuthal distribution of the E_T via Eqs. (1) and (15) differs from the true azimuthal distribution. However, since $\mathbf{q}_n(\eta_{\text{ref}})$ appears in both the numerator and the denominator of the correlators studied in this paper, most of the effects associated with the FCal E_T response are expected to cancel out. Two cross-checks are also performed to study the influence of the FCal response. In the first cross-check, only the FCal towers with E_T above the 50th percentile are used to calculate the $\mathbf{q}_n(\eta_{\text{ref}})$. The $|\mathbf{q}_n(\eta_{\text{ref}})|$ value is different from the default analysis, but the values of the correlators are found to be consistent. In the second cross-check, HIJING events with imposed flow (see Section 4) are used to study the FCal response. The $\mathbf{q}_n(\eta_{\text{ref}})$ is calculated using both the generated E_T and the reconstructed E_T , and the resulting correlators are compared with each other. The results are found to be consistent. Accordingly, no additional systematic uncertainty is added for the FCal response.

The systematic uncertainties from the different sources described above are added in quadrature to give the total systematic uncertainty for each observable. They are listed in Tables 2–4.

7 Results

The presentation of the results is structured as follows. Section 7.1 presents the results for $r_{n|n;1}$ and $R_{n|n;2}$ and the comparison between the two collision energies. Section 7.2 shows the results for $r_{n|n;k}$ for $k > 1$. The scaling relation from Eq. (4) is tested and the contributions from v_n FB asymmetry and event-plane twist are estimated. Results for the mixed-harmonic correlators, Eqs. (7)–(9), are presented in Section 7.3

Table 2: Systematic uncertainties in percent for $1 - r_{2|2;k}$ and $1 - r_{3|3;k}$ at $\eta = 1.2$ in selected centrality intervals.

	$1 - r_{2 2;1}$			$1 - r_{2 2;2}$			$1 - r_{2 2;3}$		
	0–5%	20–30%	40–50%	0–5%	20–30%	40–50%	0–5%	20–30%	40–50%
Event mixing[%]	0.8	0.2	0.3	2.2	0.4	0.6	6.0	0.6	2.1
Track selections[%]	0.4	0.3	0.2	1.5	0.4	0.9	9.4	1.0	2.4
Reco. efficiency[%]	0.3	0.1	0.1	0.4	0.1	0.1	0.9	0.1	0.1
Total[%]	1.0	0.4	0.4	2.7	0.6	1.1	12	1.2	3.2
	$1 - r_{3 3;1}$			$1 - r_{3 3;2}$			$1 - r_{3 3;3}$		
	0–5%	20–30%	40–50%	0–5%	20–30%	40–50%	0–5%	20–30%	40–50%
Event mixing[%]	0.6	0.4	0.9	2.2	1.2	7.9	7.0	9.5	
Track selections[%]	0.6	0.2	0.6	2.5	0.7	4.4	12	10	
Reco. efficiency[%]	0.1	0.1	0.1	0.4	0.2	0.9	1.1	1.5	
Total[%]	0.9	0.5	1.1	3.4	1.5	9.1	14	14	

Table 3: Systematic uncertainties in percent for $1 - R_{2|2;2}$, $1 - R_{3|3;2}$, $1 - r_{4|4;1}$ and $1 - r_{5|5;1}$ at $\eta = 1.2$ in selected centrality intervals.

	$1 - R_{2 2;2}$			$1 - R_{3 3;2}$		
	0–5%	20–30%	40–50%	0–5%	20–30%	40–50%
Event mixing [%]	6.1	1.5	1.5	4.6	2.9	14
Track selections [%]	3.5	0.4	0.7	2.0	3.2	13
Reco. efficiency[%]	0.2	0.1	0.1	0.1	0.2	0.5
Total [%]	7.1	1.6	1.7	5.1	4.4	20
	$1 - r_{4 4;1}$			$1 - r_{5 5;1}$		
	0–5%	20–30%	40–50%	0–5%	20–30%	40–50%
Event mixing [%]	1.8	1.5	2.7	13	5.1	9.8
Track selections [%]	1.5	1.1	2.0	6.3	3.6	4.6
Reco. efficiency[%]	0.3	0.3	0.6	2.2	1.6	1.3
Total [%]	2.4	1.9	3.5	15	6.5	11

Table 4: Systematic uncertainties in percent for $1 - r_{2,3|2,3}$, $1 - r_{2,2|4}$ and $1 - r_{2,3|5}$ at $\eta = 1.2$ in selected centrality intervals.

	$1 - r_{2,3 2,3}$			$1 - r_{2,2 4}$			$1 - r_{2,3 5}$		
	0–5%	20–30%	40–50%	0–5%	20–30%	40–50%	0–5%	20–30%	40–50%
Event mixing [%]	4.1	1.7	3.2	16	1.5	2.4	15	3.4	7.8
Track selections [%]	1.4	0.5	2.0	12	1.6	1.5	14	2.0	7.4
Reco. efficiency[%]	0.1	0.0	0.1	1.6	0.1	0.1	1.2	0.1	0.5
Total [%]	4.4	1.8	3.8	21	2.2	2.9	21	4.0	11

and checked for compatibility with the hydrodynamical picture. The measurements are performed using charged particles with $0.5 < p_T < 3$ GeV, and the reference flow vector is calculated with $4.0 < |\eta_{\text{ref}}| < 4.9$. Most results are shown for the $\sqrt{s_{\text{NN}}} = 5.02$ TeV Pb+Pb dataset, which has better statistical precision. The results for the $\sqrt{s_{\text{NN}}} = 2.76$ TeV Pb+Pb dataset are shown only for $r_{n|n;1}$ and $R_{n|n;2}$.

7.1 $r_{n|n;1}$ and $R_{n|n;2}$ at two collision energies

Figure 6 shows $r_{2|2;1}$ in various centrality intervals at the two collision energies. The correlator shows a linear decrease with η , except in the most central collisions. The decreasing trend is weakest around the

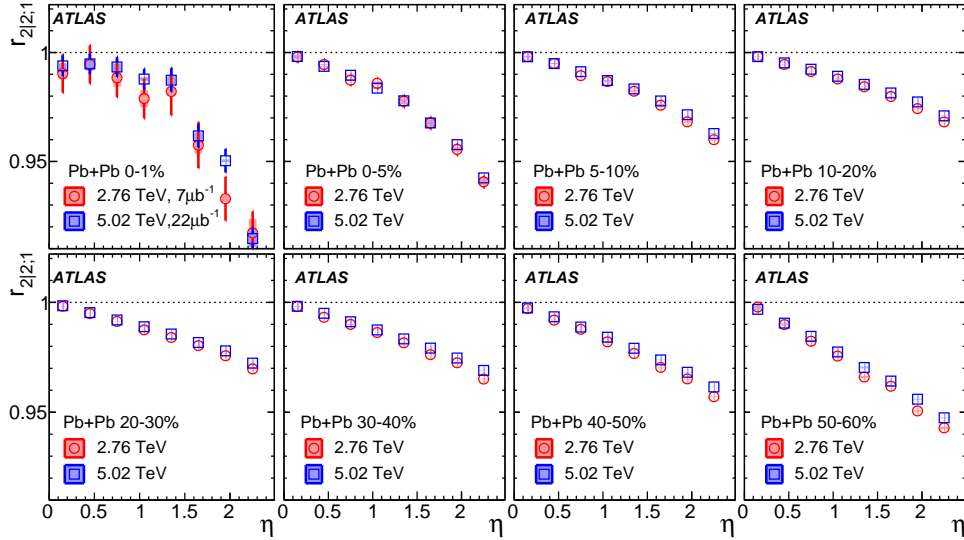


Figure 6: The $r_{2|2;1}(\eta)$ compared between the two collision energies. Each panel shows results from one centrality interval. The error bars and shaded boxes are statistical and systematic uncertainties, respectively.

20–30% centrality range, and is more pronounced in both more central and more peripheral collisions. This centrality dependence is the result of a strong centrality dependence of the v_2 associated with the average elliptic geometry [47]. The decreasing trend at $\sqrt{s_{NN}} = 2.76$ TeV is slightly stronger than that at $\sqrt{s_{NN}} = 5.02$ TeV, which is expected as the collision system becomes less boost-invariant at lower collision energy [24].

Figures 7 and 8 show the results for $r_{3|3;1}$ and $r_{4|4;1}$, respectively, at the two collision energies. A linear

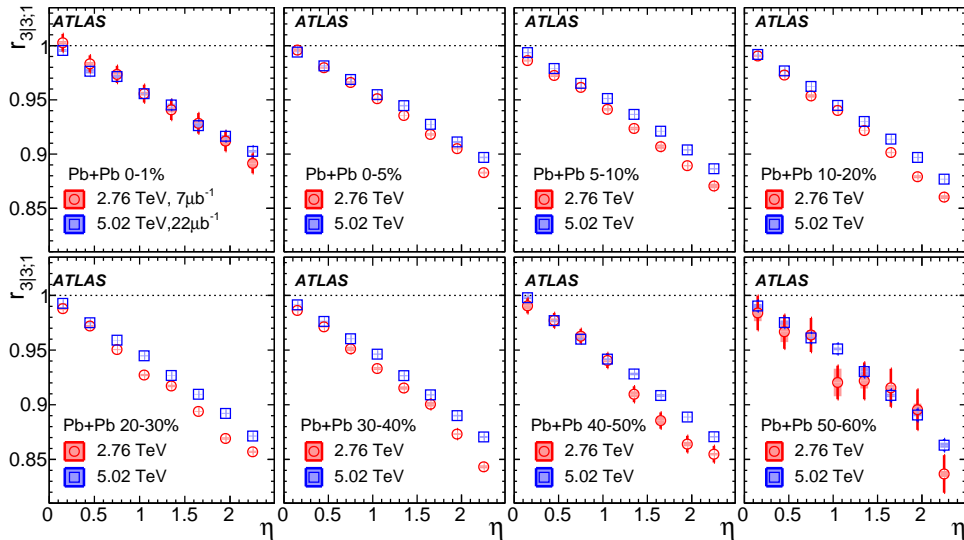


Figure 7: The $r_{3|3;1}(\eta)$ compared between the two collision energies. Each panel shows results from one centrality interval. The error bars and shaded boxes are statistical and systematic uncertainties, respectively.

decrease as a function of η is observed for both correlators, and the rate of the decrease is approximately

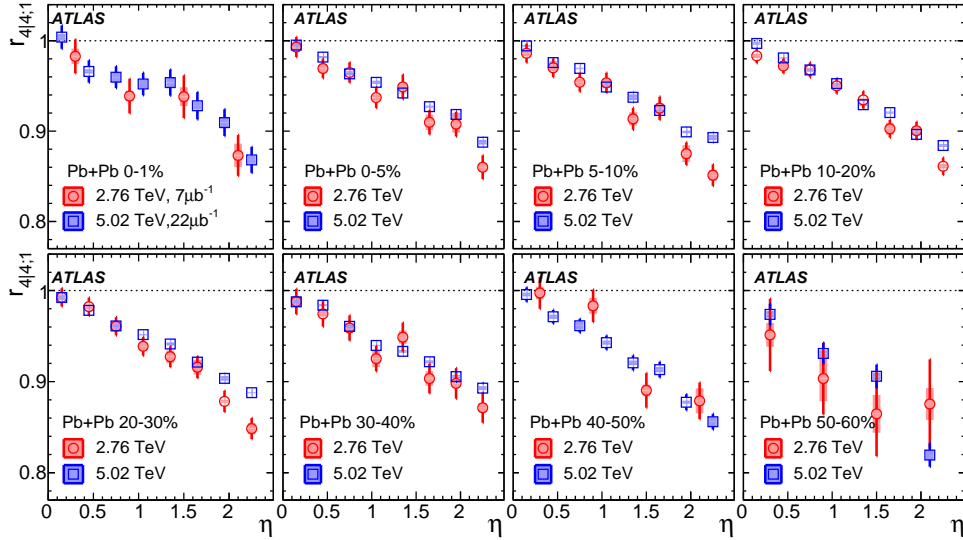


Figure 8: The $r_{4|4;1}(\eta)$ compared between the two collision energies. Each panel shows results from one centrality interval. The error bars and shaded boxes are statistical and systematic uncertainties, respectively.

independent of centrality. This centrality independence could be due to the fact that v_3 and v_4 are driven mainly by fluctuations in the initial state. The rate of the decrease is also observed to be slightly stronger at lower collision energy.

The decreasing trend of $r_{n|n;1}$ for $n = 2-4$ in Figures 6–8 indicates significant breakdown of the factorisation of two-particle flow harmonics into those between different η ranges. However, the size of the factorisation breakdown depends on the harmonic order n , collision centrality, and collision energy. The results have also been compared with those from the CMS Collaboration [19], with the η_{ref} chosen to be $4.4 < |\eta_{\text{ref}}| < 4.9$ to match the CMS choice of η_{ref} . The two results agree very well with each other, and details are shown in the Appendix.

Figures 9 and 10 show $R_{2|2;2}$ and $R_{3|3;2}$ in several centrality intervals. Both observables follow a linear decrease with η and the decreasing trends are stronger at lower collision energy.

The measured $r_{n|n;k}$ and $R_{n|n;2}$ are parameterised with linear functions,

$$r_{n|n;k} = 1 - 2F_{n;k}^r \eta, \quad R_{n|n;2} = 1 - 2F_{n;2}^R \eta, \quad (19)$$

where the slope parameters are calculated as linear-regression coefficients,

$$F_{n;k}^r = \frac{\sum_i (1 - r_{n|n;k}(\eta_i)) \eta_i}{2 \sum_i \eta_i^2}, \quad F_{n;2}^R = \frac{\sum_i (1 - R_{n|n;2}(\eta_i)) \eta_i}{2 \sum_i \eta_i^2}, \quad (20)$$

which characterise the average η -weighted deviation of $r_{n|n;1}(\eta)$ and $R_{n|n;2}(\eta)$ from unity. The sum runs over all data points. If $r_{n|n;k}$ and $R_{n|n;2}$ are a linear function in η , the linear-regression coefficients are equivalent to a fit to Eq. (19). However, these coefficients are well defined even if the observables have significant nonlinear behaviour, which is the case for $r_{2|2;k}$ and $R_{2|2;2}$ in the 0–20% centrality range.

The extracted slope parameters $F_{n;1}^r$ and $F_{n;2}^R$ are plotted as a function of centrality in terms of N_{part} , in Figures 11 and 12, respectively. The values of $F_{2;1}^r$ and $F_{2;2}^R$ first decrease and then increase as a function of increasing N_{part} . The larger values in central and peripheral collisions are related to the fact

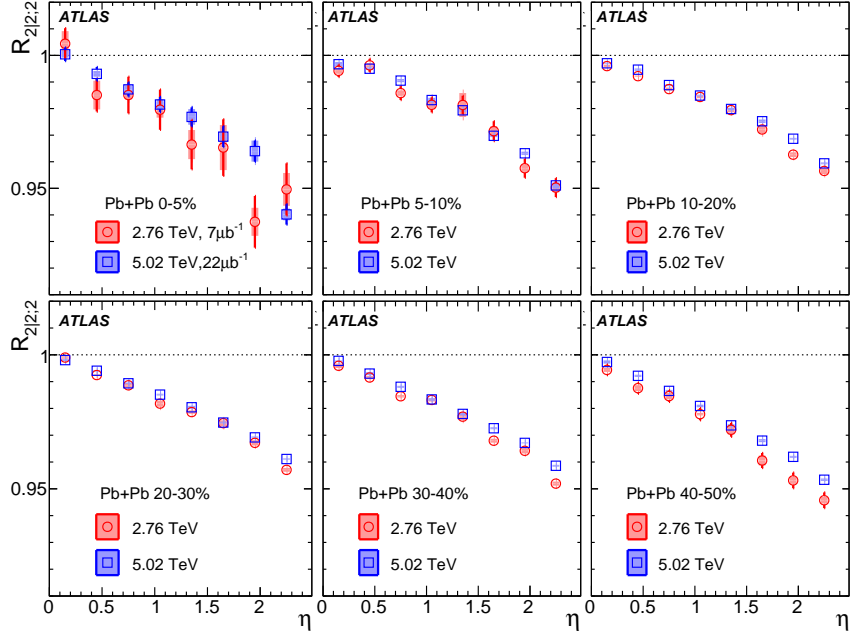


Figure 9: The $R_{2|2;2}(\eta)$ compared between the two collision energies. Each panel shows results from one centrality interval. The error bars and shaded boxes are statistical and systematic uncertainties, respectively.

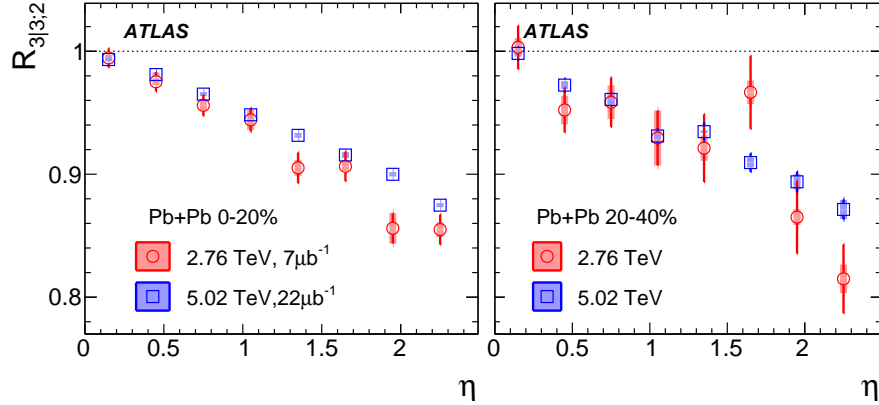


Figure 10: The $R_{3|3;2}(\eta)$ compared between the two collision energies. Each panel shows results from one centrality interval. The error bars and shaded boxes are statistical and systematic uncertainties, respectively.

that v_2 is more dominated by the initial geometry fluctuations. The slopes for higher-order harmonics are significantly larger. As a function of N_{part} , a slight decrease in $F_{3;1}^r$ and $F_{3;2}^R$ is observed for $N_{\text{part}} > 200$, as well as an increase in $F_{4;1}^r$ for $N_{\text{part}} < 100$. The values of $F_{n;1}^r$ and $F_{n;2}^R$ are larger with decreasing $\sqrt{s_{\text{NN}}}$, as the rapidity profile of the initial state is more compressed due to smaller beam rapidity y_{beam} at lower $\sqrt{s_{\text{NN}}}$. This energy dependence has been predicted for $F_{n;1}^r$ in hydrodynamic model calculations [24], and it is quantified in Figure 13 via the ratio of $F_{2;1}^r$ values and of $F_{2;2}^R$ values at the two energies. The weighted averages of the ratios calculated in the range $30 < N_{\text{part}} < 400$ are given in Table 5. Compared to $\sqrt{s_{\text{NN}}} = 5.02$ TeV, the values of $F_{2;1}^r$ and $F_{2;2}^R$ at $\sqrt{s_{\text{NN}}} = 2.76$ TeV are about 10% higher, and the values of $F_{3;1}^r$ and $F_{4;1}^r$ are about 16% higher.

If the change of correlators with $\sqrt{s_{\text{NN}}}$ were entirely due to the change of y_{beam} , then the correlators would be expected to follow a universal curve when they are rescaled by y_{beam} , i. e. $r_{n|n;k}(\eta/y_{\text{beam}})$ and $R_{n|n;2}(\eta/y_{\text{beam}})$ should not depend on $\sqrt{s_{\text{NN}}}$. In this case, the slopes parameters multiplied by the beam rapidity, $\hat{F}_{n;1}^r \equiv F_{n;1}^r y_{\text{beam}}$ and $\hat{F}_{n;2}^R \equiv F_{n;2}^R y_{\text{beam}}$, should not depend on $\sqrt{s_{\text{NN}}}$. The beam rapidity is $y_{\text{beam}} = 7.92$ and 8.52 for $\sqrt{s_{\text{NN}}} = 2.76$ and 5.02 TeV, respectively, which leads to a 7.5% reduction in the ratio. Figure 14 shows the ratio of $\hat{F}_{2;1}^r$ values and of $\hat{F}_{2;2}^R$ values at the two energies, and the weighted averages of the ratios calculated in the range $30 < N_{\text{part}} < 400$ are given in Table 5. The y_{beam} -scaling accounts for a large part of the $\sqrt{s_{\text{NN}}}$ dependence. Compared to $\sqrt{s_{\text{NN}}} = 5.02$ TeV, the values of $\hat{F}_{2;1}^r$ and $\hat{F}_{2;2}^R$ at $\sqrt{s_{\text{NN}}} = 2.76$ TeV are about 3% higher, and the values of $\hat{F}_{3;1}^r$ and $\hat{F}_{4;1}^r$ are about 8% higher, so this level of difference remains after accounting for the change in the beam rapidity.

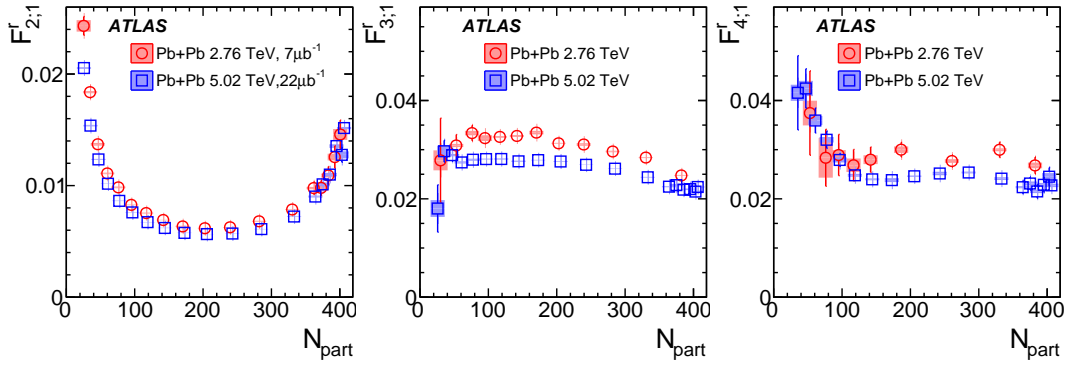


Figure 11: Centrality dependence of $F_{2;1}^r$ (left panel), $F_{3;1}^r$ (middle panel) and $F_{4;1}^r$ (right panel) for Pb+Pb at 2.76 TeV (circles) and 5.02 TeV (squares). The error bars and shaded boxes are statistical and systematic uncertainties, respectively. The widths of the centrality intervals are not fixed but are optimised to reduce the uncertainty.

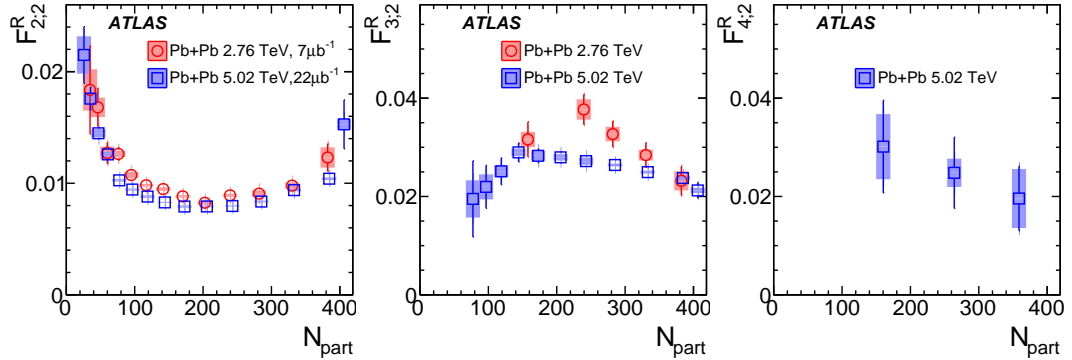


Figure 12: Centrality dependence of $F_{2;2}^R$ (left panel), $F_{3;2}^R$ (middle panel) and $F_{4;2}^R$ (right panel) for Pb+Pb at 2.76 TeV (circles) and 5.02 TeV (squares). The error bars and shaded boxes are statistical and systematic uncertainties, respectively. The widths of the centrality intervals are not fixed but are optimised to reduce the uncertainty.

7.2 Higher-order moments

The longitudinal correlations of higher-order moments of harmonic flow carry information about the EbyE flow fluctuations in pseudorapidity. In the simple model described in Ref. [20], the decrease in $r_{n|n;k}$ is expected to scale with k as given by Eq. (4).

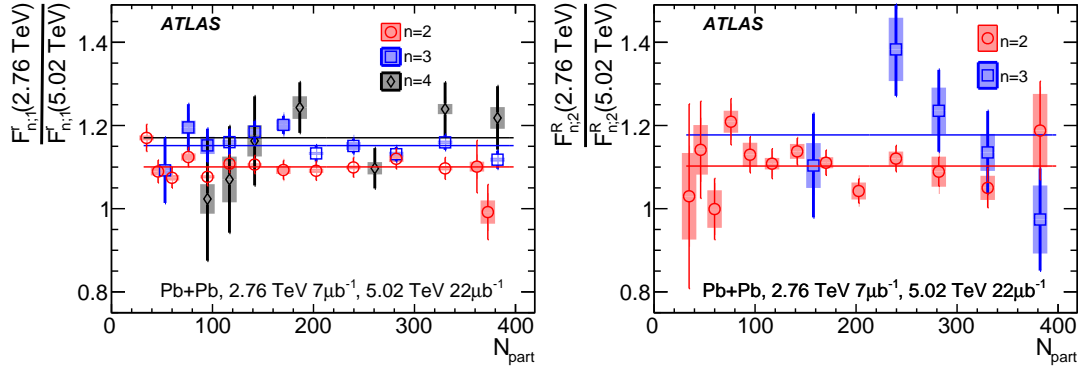


Figure 13: Centrality dependence of ratio of $F_{n;1}^r$ values (left panel) and $F_{n;2}^R$ values (right panel) at 2.76 TeV and 5.02 TeV. The lines indicate the average values in the range $30 < N_{\text{part}} < 400$, with the results and fit uncertainties given by Table 5. The error bars and shaded boxes are statistical and systematic uncertainties, respectively.

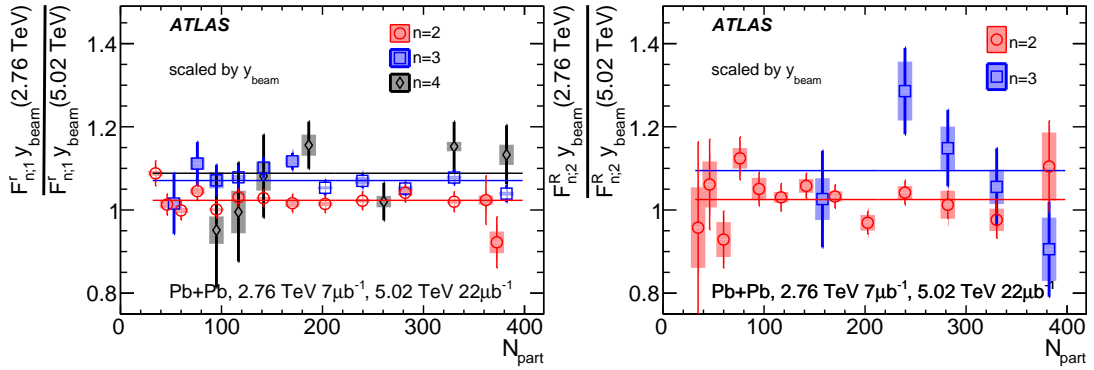


Figure 14: Centrality dependence of ratio of $\hat{F}_{n;1}^r \equiv F_{n;1}^r y_{\text{beam}}$ values (left panel) and $\hat{F}_{n;2}^R \equiv F_{n;2}^R y_{\text{beam}}$ values (right panel) at 2.76 TeV and 5.02 TeV. The lines indicate the average values in the range $30 < N_{\text{part}} < 400$, with the results and fit uncertainties given by Table 5. The error bars and shaded boxes are statistical and systematic uncertainties, respectively.

Table 5: Results of the fits to the ratio of $F_{n;1}^r$, $F_{n;2}^R$, $\hat{F}_{n;1}^r \equiv F_{n;1}^r y_{\text{beam}}$ and $\hat{F}_{n;2}^R \equiv F_{n;2}^R y_{\text{beam}}$ values at the two energies in the range $30 < N_{\text{part}} < 400$ shown in Figures 13 and 14. The uncertainties include both statistical and systematic uncertainties.

	$n = 2$	$n = 3$	$n = 4$
$F_{n;1}^r(2.76 \text{ TeV})/F_{n;1}^r(5.02 \text{ TeV})$	1.100 ± 0.010	1.152 ± 0.011	1.17 ± 0.036
$F_{n;2}^R(2.76 \text{ TeV})/F_{n;2}^R(5.02 \text{ TeV})$	1.103 ± 0.026	1.18 ± 0.08	–
$\hat{F}_{n;1}^r(2.76 \text{ TeV})/\hat{F}_{n;1}^r(5.02 \text{ TeV})$	1.023 ± 0.009	1.071 ± 0.010	1.088 ± 0.033
$\hat{F}_{n;2}^R(2.76 \text{ TeV})/\hat{F}_{n;2}^R(5.02 \text{ TeV})$	1.025 ± 0.024	1.10 ± 0.07	–

Figure 15 compares the results for $r_{2|2;k}$ for $k = 1-3$ (solid symbols) with $r_{2|2;1}^k$ for $k = 2-3$ (open symbols). The data follow the scaling relation from Eq. (4) in the most central collisions (0–5% centrality) where

v_2 is driven by the initial-state fluctuations. In other centrality intervals, where the average geometry is more important for v_2 , the $r_{2|2;k}$ ($k = 2$ and 3) data show stronger decreases with η than $r_{2|2;1}^k$.

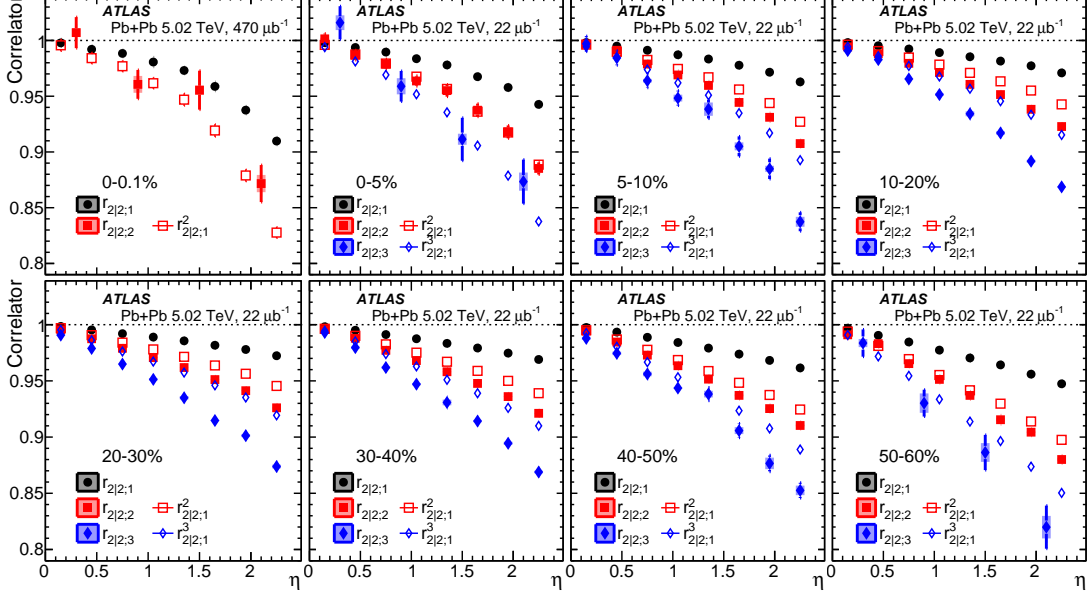


Figure 15: The $r_{2|2;k}$ for $k = 1-3$ compared with $r_{2|2;1}^k$ for $k = 2-3$ in various centrality intervals for Pb+Pb collisions at 5.02 TeV. The error bars and shaded boxes are statistical and systematic uncertainties, respectively. The data points for $k = 2$ or 3 in some centrality intervals are rebinned to reduce the uncertainty.

A similar study is performed for third-order harmonics, and the results are shown in Figure 16. The data follow approximately the scaling relation Eq. (4) in all centrality intervals.

To quantify the difference between $r_{n|n;k}$ and $r_{n|n;1}^k$, the slopes ($F_{n;k}^r$) of $r_{n|n;k}$ are calculated via Eqs. (19) and (20). The scaled quantities, $F_{n;k}^r/k$, are then compared with each other as a function of centrality in Figure 17. For second-order harmonics, the data show clearly that over most of the centrality range $F_{2;3}^r/3 > F_{2;2}^r/2 > F_{2;1}^r$, implying $F_{2;k}^r > kF_{2;1}^r$. However, for the most central and most peripheral collisions the quantities approach each other. On the other hand, a slightly opposite trend for the third-order harmonics, $F_{3;3}^r/3 \lesssim F_{3;2}^r/2 \lesssim F_{3;1}^r$, i.e. $F_{3;k}^r \lesssim kF_{3;1}^r$, is observed in mid-central collisions ($150 < N_{\text{part}} < 350$).

Figures 18 and 19 compare the $r_{n|n;2}$ with $R_{n|n;2}$ for $n = 2$ and $n = 3$, respectively. The decorrelation of $R_{n|n;2}$ is significantly weaker than that for the $r_{n|n;2}$. This is because the $R_{n|n;2}$ is mainly affected by the event-plane twist effects, while the $r_{n|n;2}$ receives contributions from both FB asymmetry and event-plane twist [20].

Following the discussion in Section 2, Eqs. (3) and (6), the measured $F_{n;2}^r$ and $F_{n;2}^R$ values can be used to estimate the separate contributions from FB asymmetry and event-plane twist, $F_{n;2}^{\text{asy}}$ and $F_{n;2}^{\text{twi}}$, respectively, via the relation:

$$F_{n;2}^{\text{twi}} = F_{n;2}^R, \quad F_{n;2}^{\text{asy}} = F_{n;2}^r - F_{n;2}^R. \quad (21)$$

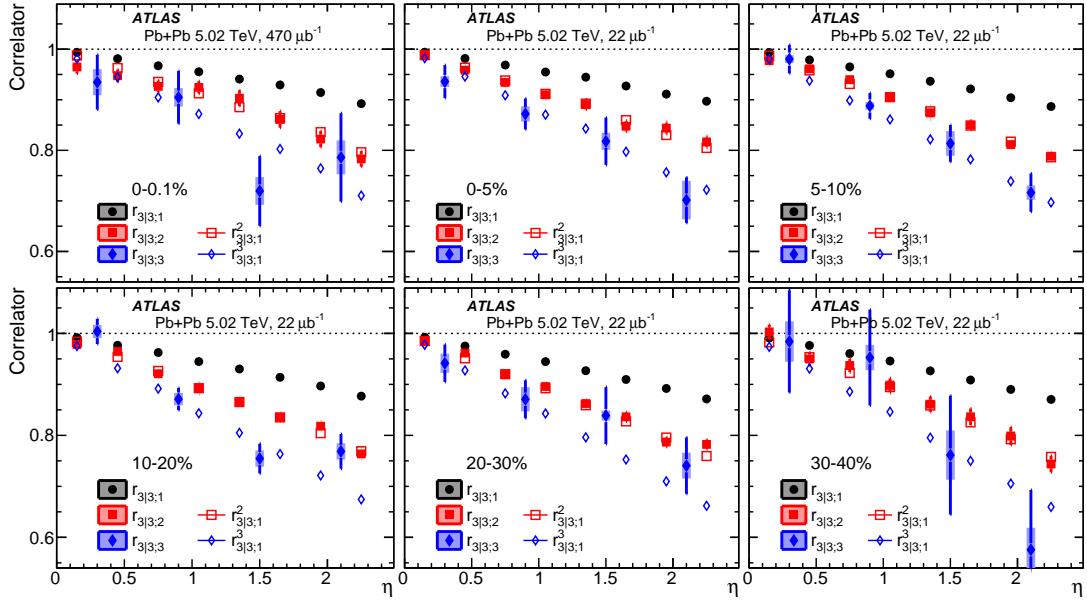


Figure 16: The $r_{3|3;k}$ for $k = 1-3$ compared with $r_{3|3;1}^k$ for $k = 2-3$ in various centrality intervals for Pb+Pb collisions at 5.02 TeV. The error bars and shaded boxes are statistical and systematic uncertainties, respectively. The data points for $k = 2$ or 3 in some centrality intervals are rebinned to reduce the uncertainty.

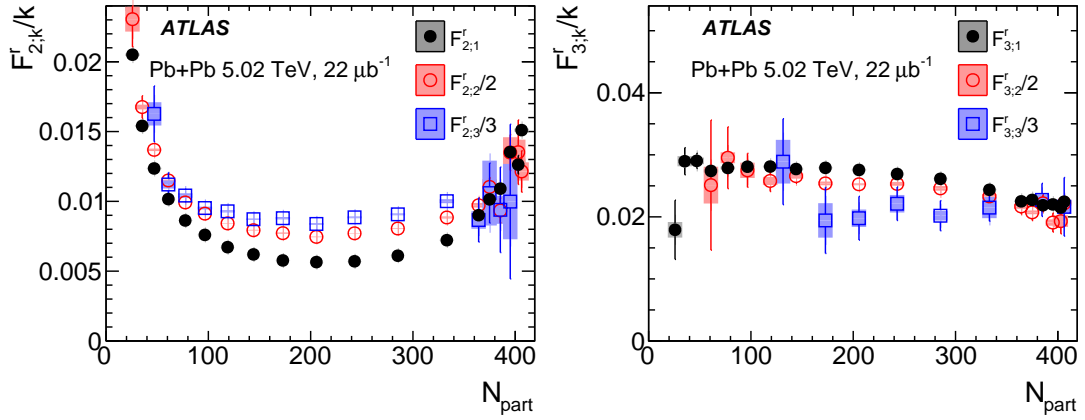


Figure 17: The values of $F_{n;k}^r/k$ for $k = 1, 2$ and 3 for $n = 2$ (left panel) and $n = 3$ (right panel), respectively. The error bars and shaded boxes are statistical and systematic uncertainties, respectively. The widths of the centrality intervals are not fixed but are optimised to reduce the uncertainty.

The results are shown in Figure 20. The contributions from the two components are similar to each other for $n = 2$, for which the harmonic flow arises primarily from the average collision shape, as well as for $n = 3$, for which the harmonic flow is driven mainly by fluctuations in the initial geometry.

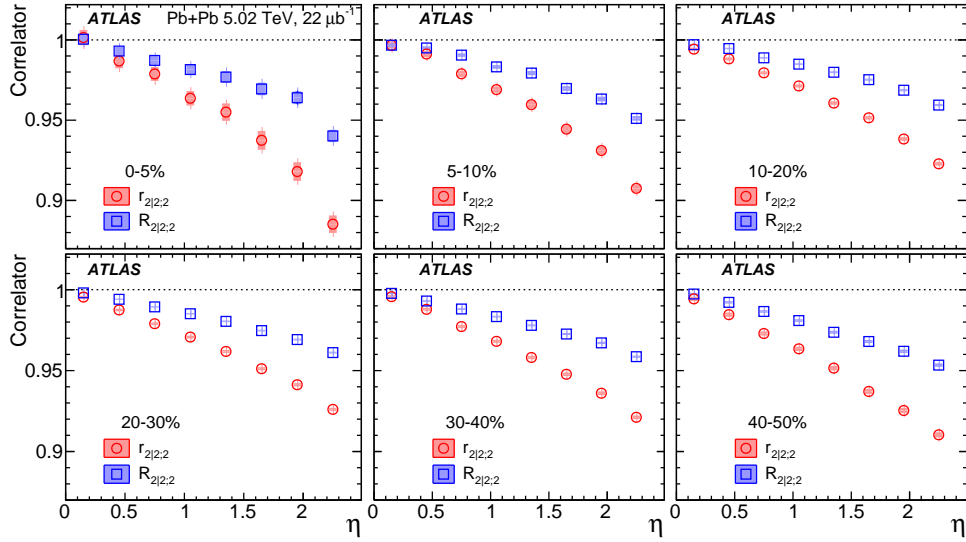


Figure 18: The $r_{2|2,2}(\eta)$ and $R_{2|2,2}(\eta)$ in various centrality intervals for Pb+Pb collisions at 5.02 TeV. The error bars and shaded boxes are statistical and systematic uncertainties, respectively.

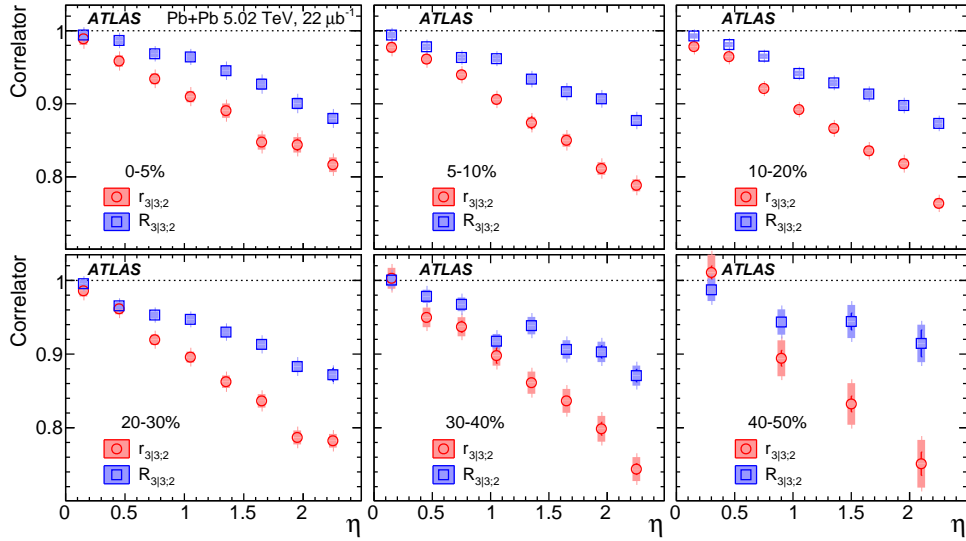


Figure 19: The $r_{3|3,2}(\eta)$ and $R_{3|3,2}(\eta)$ in various centrality intervals for Pb+Pb collisions at 5.02 TeV. The error bars and shaded boxes are statistical and systematic uncertainties, respectively. The data points in 40–50% centrality interval are rebinned to reduce the uncertainty.

7.3 Mixed-harmonics correlation

Figure 21 compares the $r_{2,3|2,3}$ with the product of $r_{2|2,1}$ and $r_{3|3,1}$. The data show that they are consistent with each other, suggesting the previously observed anticorrelation between v_2 and v_3 is a property of the entire event [9, 48], and that longitudinal fluctuations of v_2 and v_3 are uncorrelated. Figure 22 compares $r_{2|2,2}$ with the mixed-harmonic correlator $r_{2,2|4}$, as well as $r_{4|4,1}$. As discussed in Section 2 in the context

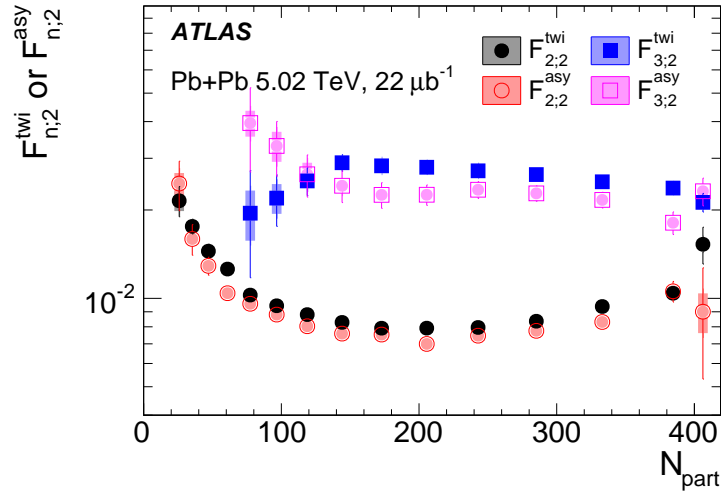


Figure 20: The estimated event-plane twist component $F_{n;2}^{\text{twi}}$ and FB asymmetry component $F_{n;2}^{\text{asy}}$ as a function of N_{part} for $n = 2$ and 3 for Pb+Pb collisions at 5.02 TeV. The error bars and shaded boxes are statistical and systematic uncertainties, respectively.

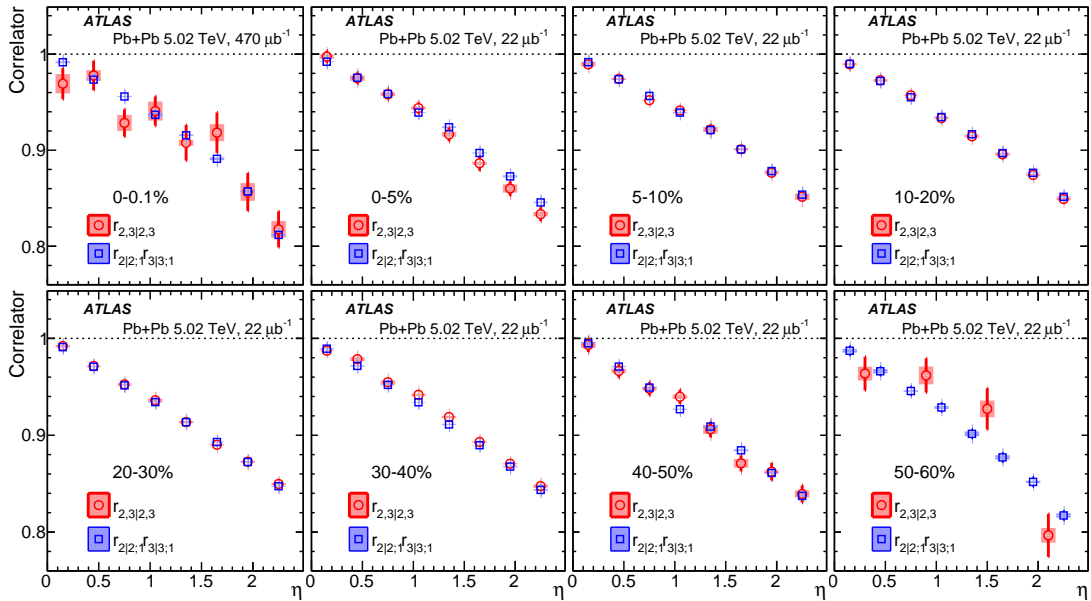


Figure 21: The $r_{2,3|2,3}$ (circles) and $r_{2|2;1}r_{3|3;1}$ (squares) as a function of η for several centrality intervals. The error bars and shaded boxes are statistical and systematic uncertainties, respectively. The $r_{2,3|2,3}$ data in the 50–60% centrality interval are rebinned to reduce the uncertainty.

of the first relation in Eq. (10), if the linear and non-linear components of v_4 in Eq. (10) are uncorrelated, then $r_{2,2|4}$ would be expected to be similar to $r_{2|2;24}$. This is indeed confirmed by the comparisons of the η and centrality dependence of $r_{2|2;2}$ and $r_{2,2|4}$ in Figure 22. Figure 22 also shows that the η dependence for $r_{4|4;1}$ is stronger than for $r_{2|2;2}$ in all centrality intervals, suggesting that the decorrelation effects are

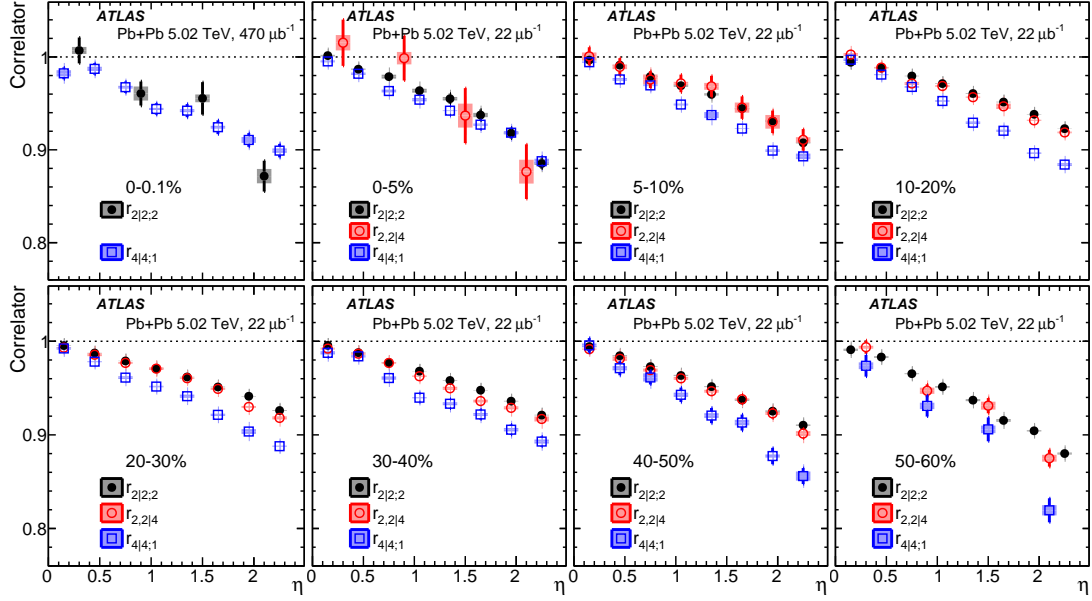


Figure 22: Comparison of $r_{2|2;2}$, $r_{2,2|4}$ and $r_{4|4;1}$ for several centrality intervals. The error bars and shaded boxes are statistical and systematic uncertainties, respectively. The data points in some centrality intervals are rebinned to reduce the uncertainty.

stronger for the linear component of v_4 than for the nonlinear component (see Eq. (12)).

A similar study of the influence of the linear and nonlinear effects for v_5 was also performed, and results are shown in Figure 23. The three observables $r_{2,3|2,3}$, $r_{2,3|5}$, and $r_{5|5;1}$ show similar values in all centrality intervals, albeit with large statistical uncertainties.

The decorrelations shown in Figures 21–23 can be quantified by calculating the slopes of the distributions in each centrality interval and presenting the results as a function of centrality. Following the example for $r_{n|n;k}$, the slopes for the mixed-harmonic correlators are obtained via the linear regression procedure of Eqs. (19) and (20):

$$r_{2,3|2,3} = 1 - 2F_{2,3|2,3}^r \eta, \quad r_{2,2|4} = 1 - 2F_{2,2|4}^r \eta, \quad r_{2,3|5} = 1 - 2F_{2,3|5}^r \eta. \quad (22)$$

The results are summarised in Figure 24, with each panel corresponding to the slopes of distributions in Figures 21, 22, and 23, respectively. The only significant difference is seen between $F_{4|4;1}$ and $F_{2|2;2}$ or $F_{2,2|4}$.

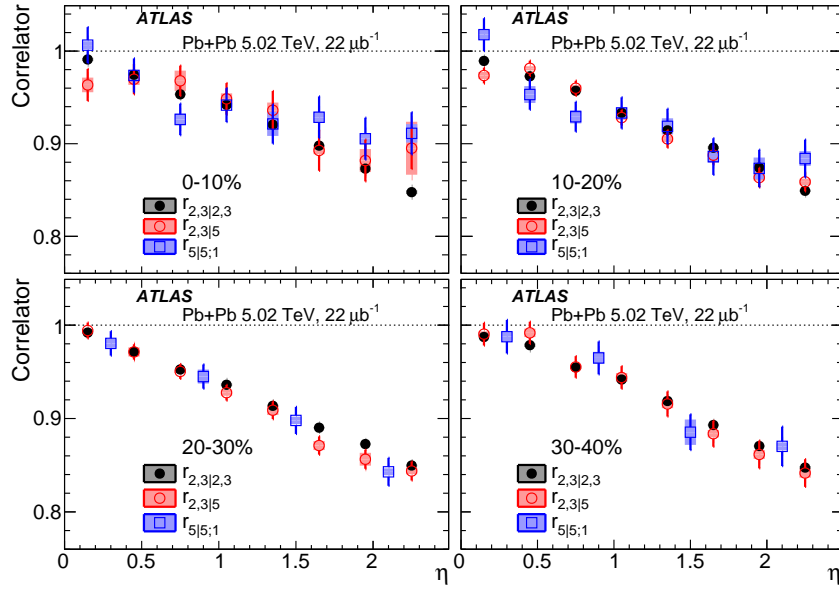


Figure 23: Comparison of $r_{2,3|2,3}$, $r_{2,3|5}$ and $r_{5|5;1}$ for several centrality intervals. The error bars and shaded boxes are statistical and systematic uncertainties, respectively. The $r_{5|5;1}$ data in some centrality intervals are rebinned to reduce the uncertainty.

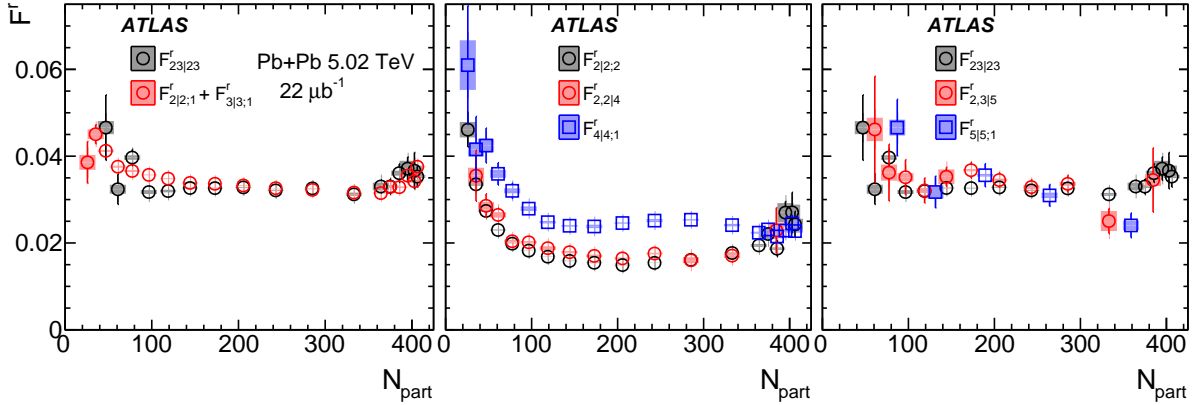


Figure 24: Comparison of the slopes of the correlators as a function of N_{part} for three groups of correlators: $r_{2,3|2,3}$ and $r_{2|2;1}r_{3|3;1}$ (for which the slope is $F_{2|2;1} + F_{3|3;1}$) in Figure 21 (left panel), $r_{2|2;2}$, $r_{2,2|4}$ and $r_{4|4;1}$ in Figure 22 (middle panel), and $r_{2,3|2,3}$, $r_{2,3|5}$ and $r_{5|5;1}$ in Figure 23 (right panel). The error bars and shaded boxes are statistical and systematic uncertainties, respectively.

8 Summary

Measurements of longitudinal flow correlations for charged particles are presented in the pseudorapidity range $|\eta| < 2.4$ using $7 \mu\text{b}^{-1}$ and $470 \mu\text{b}^{-1}$ of Pb+Pb data at $\sqrt{s_{\text{NN}}} = 2.76$ and 5.02 TeV, respectively, recorded by the ATLAS detector at the LHC. The factorisation of two-particle azimuthal correlations into single-particle flow harmonics v_n is found to be broken, and the amount of factorisation breakdown

increases approximately linearly as a function of the η separation between the two particles. The slope of this dependence is nearly independent of centrality and p_T for $n > 2$. However, for $n = 2$ the effect is smallest in mid-central collisions and increases toward more central or more peripheral collisions, and in central collisions the effect also depends strongly on p_T . Furthermore, the effect is found to be larger at 2.76 TeV than 5.02 TeV for all harmonics, which cannot be explained entirely by the change in the beam rapidity.

The higher moments of the η -dependent flow correlations are also measured and the corresponding linear coefficients of the η dependence are extracted. The coefficient for the k^{th} -moment of v_n scales with k for $n > 2$, but scales faster than k for $n = 2$. The factorisation breakdown is separated into contributions from forward-backward asymmetry of the flow magnitude and event-plane twist, which are found to be comparable to each other.

The longitudinal flow correlations are also measured between harmonic flows of different order. The correlation of v_2v_3 between two η ranges is found to factorise into the product of the correlation for v_2 and the correlation for v_3 , suggesting that the longitudinal fluctuations of v_2 and v_3 are independent of each other. The correlations between v_4 and v_2^2 suggest that the longitudinal fluctuations of v_4 have a significant nonlinear contribution from v_2 , i.e. $v_4 \propto v_2^2$. Similarly, the correlations between v_5 and v_2v_3 suggest that the longitudinal fluctuations of v_5 are driven by the nonlinear contribution from v_2v_3 , i.e. $v_5 \propto v_2v_3$. The results presented in this paper provide new insights into the fluctuations and correlations of harmonic flow in the longitudinal direction, which can be used to improve full three-dimensional viscous hydrodynamic models.

Acknowledgements

We thank CERN for the very successful operation of the LHC, as well as the support staff from our institutions without whom ATLAS could not be operated efficiently.

We acknowledge the support of ANPCyT, Argentina; YerPhI, Armenia; ARC, Australia; BMWFW and FWF, Austria; ANAS, Azerbaijan; SSTC, Belarus; CNPq and FAPESP, Brazil; NSERC, NRC and CFI, Canada; CERN; CONICYT, Chile; CAS, MOST and NSFC, China; COLCIENCIAS, Colombia; MSMT CR, MPO CR and VSC CR, Czech Republic; DNRF and DNSRC, Denmark; IN2P3-CNRS, CEA-DRF/IRFU, France; SRNSF, Georgia; BMBF, HGF, and MPG, Germany; GSRT, Greece; RGC, Hong Kong SAR, China; ISF, I-CORE and Benoziyo Center, Israel; INFN, Italy; MEXT and JSPS, Japan; CNRST, Morocco; NWO, Netherlands; RCN, Norway; MNiSW and NCN, Poland; FCT, Portugal; MNE/IFA, Romania; MES of Russia and NRC KI, Russian Federation; JINR; MESTD, Serbia; MSSR, Slovakia; ARRS and MIZŠ, Slovenia; DST/NRF, South Africa; MINECO, Spain; SRC and Wallenberg Foundation, Sweden; SERI, SNSF and Cantons of Bern and Geneva, Switzerland; MOST, Taiwan; TAEK, Turkey; STFC, United Kingdom; DOE and NSF, United States of America. In addition, individual groups and members have received support from BCKDF, the Canada Council, CANARIE, CRC, Compute Canada, FQRNT, and the Ontario Innovation Trust, Canada; EPLANET, ERC, ERDF, FP7, Horizon 2020 and Marie Skłodowska-Curie Actions, European Union; Investissements d’Avenir Labex and Idex, ANR, Région Auvergne and Fondation Partager le Savoir, France; DFG and AvH Foundation, Germany; Herakleitos, Thales and Aristeia programmes co-financed by EU-ESF and the Greek NSRF; BSF, GIF and Minerva, Israel; BRF, Norway; CERCA Programme Generalitat de Catalunya, Generalitat Valenciana, Spain; the Royal Society and Leverhulme Trust, United Kingdom.

The crucial computing support from all WLCG partners is acknowledged gratefully, in particular from CERN, the ATLAS Tier-1 facilities at TRIUMF (Canada), NDGF (Denmark, Norway, Sweden), CC-IN2P3 (France), KIT/GridKA (Germany), INFN-CNAF (Italy), NL-T1 (Netherlands), PIC (Spain), ASGC (Taiwan), RAL (UK) and BNL (USA), the Tier-2 facilities worldwide and large non-WLCG resource providers. Major contributors of computing resources are listed in Ref. [49].

Appendix

Figure 25 and 26 show a comparison of $r_{2|2;1}$ and $r_{3|3;1}$ between ATLAS and CMS for Pb+Pb collisions at 2.76 TeV, where the ATLAS η_{ref} is chosen to be $4.4 < |\eta_{\text{ref}}| < 4.9$ to match that of the CMS Collaboration. Excellent agreement is observed. Figure 27 and 28 show the detailed p_T and η_{ref} dependence of $r_{4|4;1}$; these figures complement Figures 2–5. Figure 29 compiles the results of $r_{n|n;1}$ and $R_{n|n;2}$ for 0–0.1% ultra-central collisions.

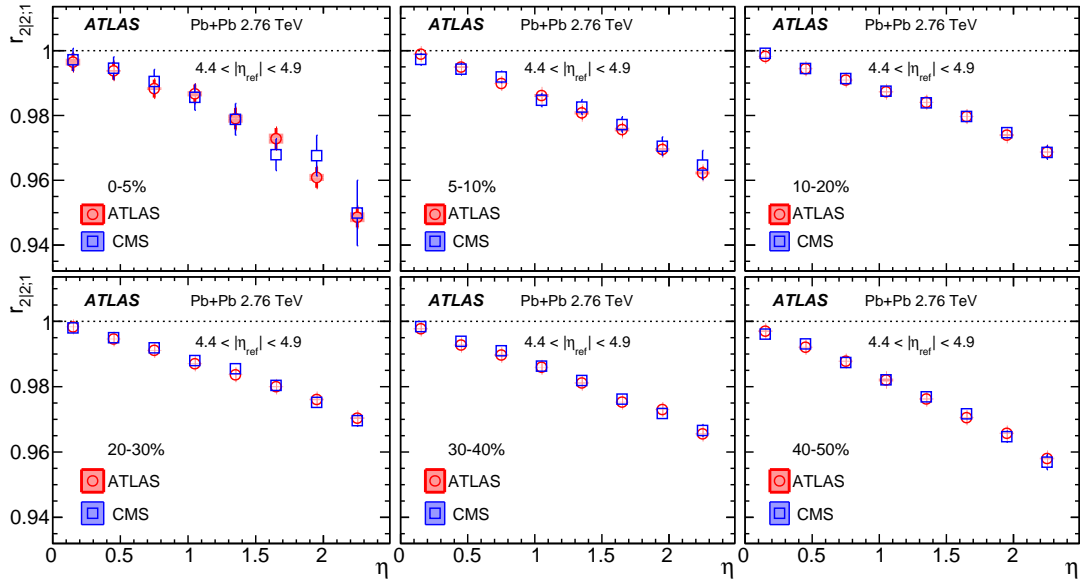


Figure 25: The values of $r_{2|2;1}$ measured by ATLAS and by CMS [19] for Pb+Pb collisions at 2.76 TeV, for the same reference pseudorapidity $4.4 < |\eta_{\text{ref}}| < 4.9$.

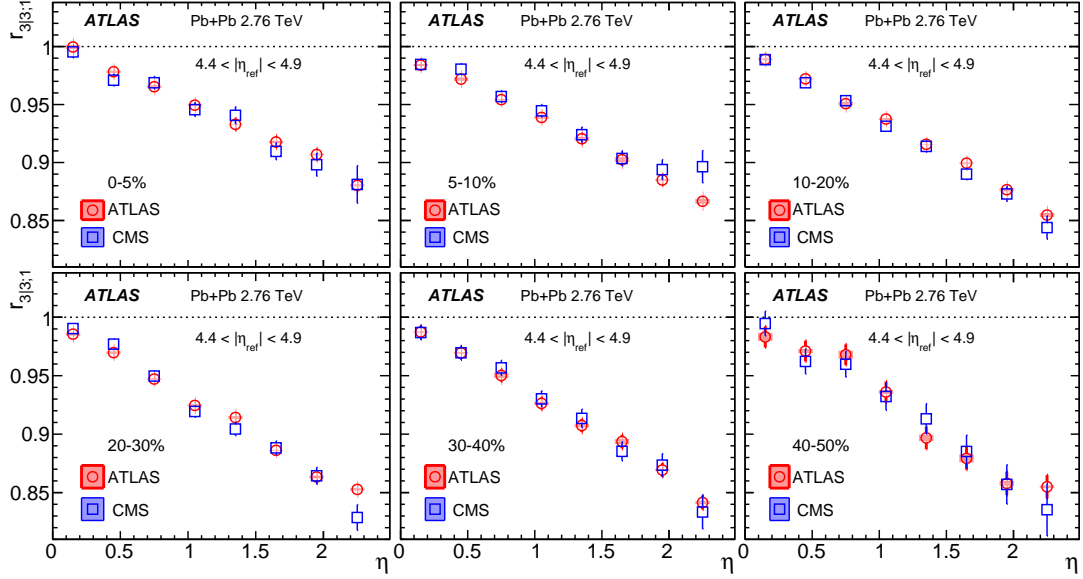


Figure 26: The values of $r_{3|3;1}$ measured by ATLAS and by CMS [19] for Pb+Pb collisions at 2.76 TeV, for the same reference pseudorapidity $4.4 < |\eta_{\text{ref}}| < 4.9$.

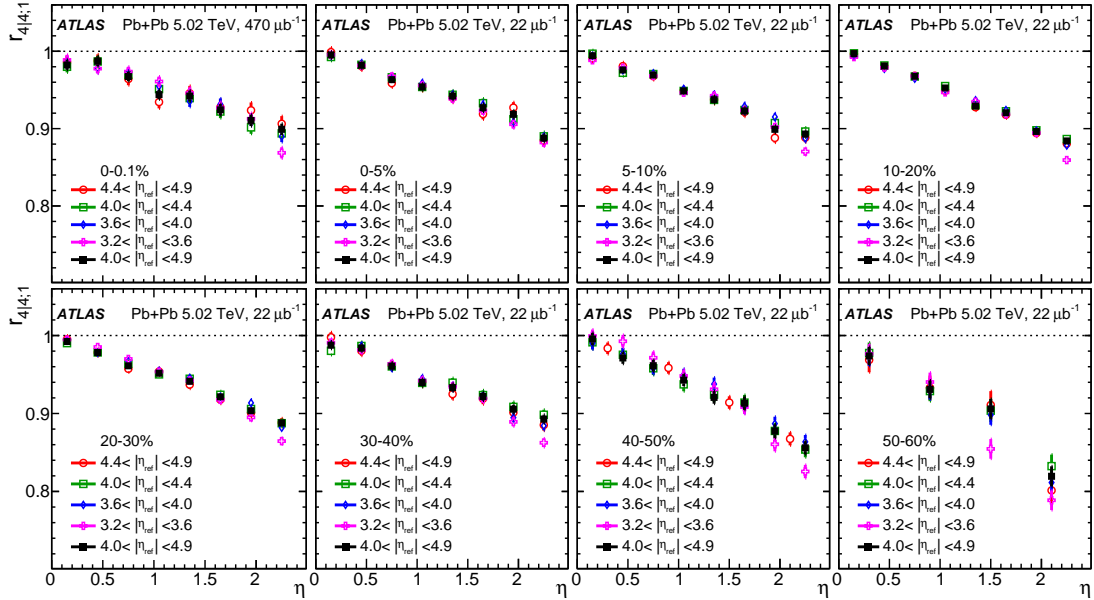


Figure 27: The $r_{4|4;1}(\eta)$ measured for several η_{ref} ranges for Pb+Pb collisions at 5.02 TeV. Each panel represents one centrality range. The error bars are statistical only. The data points in some centrality intervals are rebinned to reduce the uncertainty.

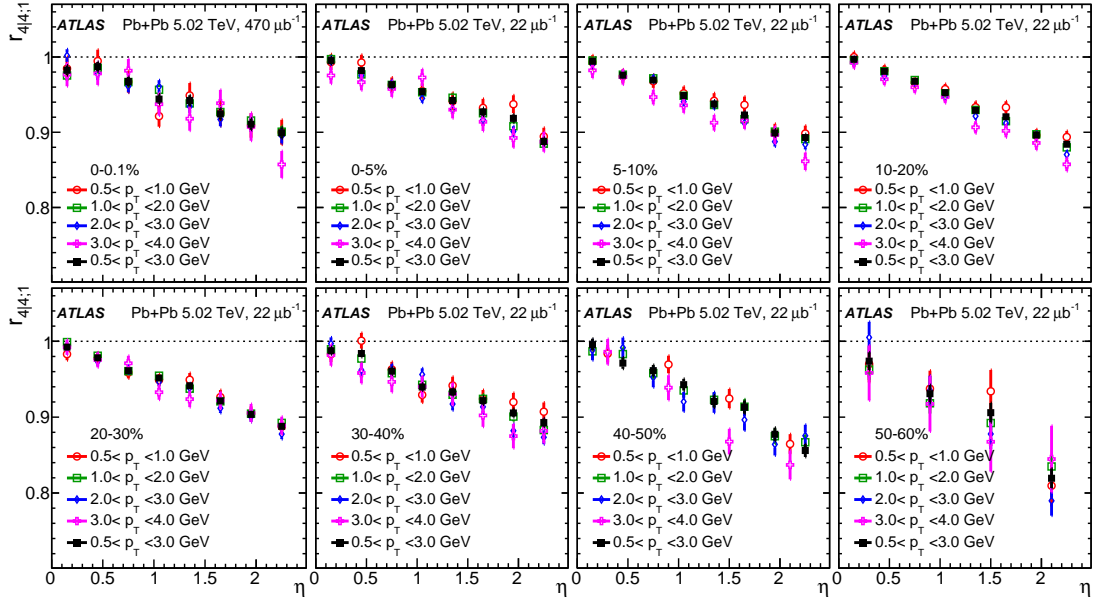


Figure 28: The $r_{4|4;1}(\eta)$ measured in several p_T ranges for Pb+Pb collisions at 5.02 TeV. Each panel shows the results for one centrality range. The error bars are statistical only. The data points in some centrality intervals are rebinned to reduce the uncertainty.

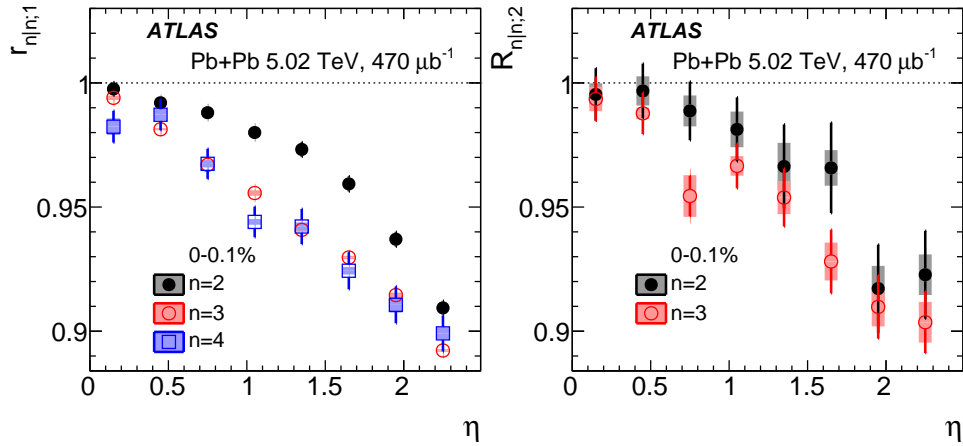


Figure 29: The $r_{n|n;1}(\eta)$ (left panel) and $R_{n|n;2}(\eta)$ (right panel) in ultra-central Pb+Pb collisions at 5.02 TeV. The error bars and shaded boxes are statistical and systematic uncertainties, respectively.

References

- [1] C. Gale, S. Jeon, and B. Schenke, *Hydrodynamic Modeling of Heavy-Ion Collisions*, *Int. J. Mod. Phys. A* **28** (2013) 1340011, [arXiv:1301.5893](#) [nucl-th].
- [2] U. Heinz and R. Snellings, *Collective flow and viscosity in relativistic heavy-ion collisions*, *Ann. Rev. Nucl. Part. Sci.* **63** (2013) 123, [arXiv:1301.2826](#) [nucl-th].
- [3] PHENIX Collaboration, A. Adare et al., *Measurements of Higher-Order Flow Harmonics in Au+Au Collisions at $\sqrt{s_{NN}} = 200$ GeV*, *Phys. Rev. Lett.* **107** (2011) 252301, [arXiv:1105.3928](#) [nucl-ex].
- [4] ALICE Collaboration, K. Aamodt et al., *Higher harmonic anisotropic flow measurements of charged particles in Pb-Pb collisions at $\sqrt{s_{NN}} = 2.76$ TeV*, *Phys. Rev. Lett.* **107** (2011) 032301, [arXiv:1105.3865](#) [nucl-ex].
- [5] ATLAS Collaboration, *Measurement of the azimuthal anisotropy for charged particle production in $\sqrt{s_{NN}} = 2.76$ TeV lead-lead collisions with the ATLAS detector*, *Phys. Rev. C* **86** (2012) 014907, [arXiv:1203.3087](#) [hep-ex].
- [6] CMS Collaboration, *Measurement of higher-order harmonic azimuthal anisotropy in PbPb collisions at $\sqrt{s_{NN}} = 2.76$ TeV*, *Phys. Rev. C* **89** (2014) 044906, [arXiv:1310.8651](#) [nucl-ex].
- [7] ATLAS Collaboration, *Measurement of the distributions of event-by-event flow harmonics in lead-lead collisions at $\sqrt{s_{NN}} = 2.76$ TeV with the ATLAS detector at the LHC*, *JHEP* **11** (2013) 183, [arXiv:1305.2942](#) [hep-ex].
- [8] ATLAS Collaboration, *Measurement of event-plane correlations in $\sqrt{s_{NN}} = 2.76$ TeV lead-lead collisions with the ATLAS detector*, *Phys. Rev. C* **90** (2014) 024905, [arXiv:1403.0489](#) [hep-ex].
- [9] ATLAS Collaboration, *Measurement of the correlation between flow harmonics of different order in lead-lead collisions at $\sqrt{s_{NN}} = 2.76$ TeV with the ATLAS detector*, *Phys. Rev. C* **92** (2015) 034903, [arXiv:1504.01289](#) [hep-ex].
- [10] M. Luzum and J.-Y. Ollitrault, *Extracting the shear viscosity of the quark-gluon plasma from flow in ultra-central heavy-ion collisions*, *Nucl. Phys. A* **904-905** (2013) 377c, [arXiv:1210.6010](#) [nucl-th].
- [11] D. Teaney and L. Yan, *Triangularity and Dipole Asymmetry in Heavy Ion Collisions*, *Phys. Rev. C* **83** (2011) 064904, [arXiv:1010.1876](#) [nucl-th].
- [12] C. Gale, S. Jeon, B. Schenke, P. Tribedy, and R. Venugopalan, *Event-by-event anisotropic flow in heavy-ion collisions from combined Yang-Mills and viscous fluid dynamics*, *Phys. Rev. Lett.* **110** (2013) 012302, [arXiv:1209.6330](#) [nucl-th].
- [13] H. Niemi, G. Denicol, H. Holopainen, and P. Huovinen, *Event-by-event distributions of azimuthal asymmetries in ultrarelativistic heavy-ion collisions*, *Phys. Rev. C* **87** (2013) 054901, [arXiv:1212.1008](#) [nucl-th].
- [14] Z. Qiu and U. Heinz, *Hydrodynamic event-plane correlations in Pb+Pb collisions at $\sqrt{s} = 2.76$ ATeV*, *Phys. Lett. B* **717** (2012) 261, [arXiv:1208.1200](#) [nucl-th].

- [15] D. Teaney and L. Yan, *Event-plane correlations and hydrodynamic simulations of heavy ion collisions*, *Phys. Rev. C* **90** (2014) 024902, [arXiv:1312.3689](#) [[nucl-th](#)].
- [16] P. Bozek, W. Broniowski, and J. Moreira, *Torqued fireballs in relativistic heavy-ion collisions*, *Phys. Rev. C* **83** (2011) 034911, [arXiv:1011.3354](#) [[nucl-th](#)].
- [17] K. Xiao, F. Liu, and F. Wang, *Event-plane decorrelation over pseudorapidity and its effect on azimuthal anisotropy measurements in relativistic heavy-ion collisions*, *Phys. Rev. C* **87** (2013) 011901, [arXiv:1208.1195](#) [[nucl-th](#)].
- [18] J. Jia and P. Huo, *Forward-backward eccentricity and participant-plane angle fluctuations and their influences on longitudinal dynamics of collective flow*, *Phys. Rev. C* **90** (2014) 034915, [arXiv:1403.6077](#) [[nucl-th](#)].
- [19] CMS Collaboration, *Evidence for transverse momentum and pseudorapidity dependent event plane fluctuations in PbPb and pPb collisions*, *Phys. Rev. C* **92** (2015) 034911, [arXiv:1503.01692](#) [[nucl-ex](#)].
- [20] J. Jia, P. Huo, G. Ma, and M. Nie, *Observables for longitudinal flow correlations in heavy-ion collisions*, *J. Phys. G* **44** (2017) 075106, [arXiv:1701.02183](#) [[nucl-th](#)].
- [21] F. G. Gardim, F. Grassi, M. Luzum, and J.-Y. Ollitrault, *Mapping the hydrodynamic response to the initial geometry in heavy-ion collisions*, *Phys. Rev. C* **85** (2012) 024908, [arXiv:1111.6538](#) [[nucl-th](#)].
- [22] D. Teaney and L. Yan, *Non linearities in the harmonic spectrum of heavy ion collisions with ideal and viscous hydrodynamics*, *Phys. Rev. C* **86** (2012) 044908, [arXiv:1206.1905](#) [[nucl-th](#)].
- [23] ALICE Collaboration, S. Acharya et al., *Linear and non-linear flow modes in Pb-Pb collisions at $\sqrt{s_{NN}} = 2.76$ TeV*, *Phys. Lett. B* **773** (2017) 68–80, [arXiv:1705.04377](#) [[nucl-ex](#)].
- [24] L.-G. Pang, H. Petersen, G.-Y. Qin, V. Roy, and X.-N. Wang, *Decorrelation of anisotropic flow along the longitudinal direction*, *Eur. Phys. J. A* **52** (2016) 97, [arXiv:1511.04131](#) [[nucl-th](#)].
- [25] P. Bozek and W. Broniowski, *The torque effect and fluctuations of entropy deposition in rapidity in ultra-relativistic nuclear collisions*, *Phys. Lett. B* **752** (2016) 206, [arXiv:1506.02817](#) [[nucl-th](#)].
- [26] M. Luzum and H. Petersen, *Initial State Fluctuations and Final State Correlations in Relativistic Heavy-Ion Collisions*, *J. Phys. G* **41** (2014) 063102, [arXiv:1312.5503](#) [[nucl-th](#)].
- [27] A. Bilandzic, R. Snellings, and S. Voloshin, *Flow analysis with cumulants: Direct calculations*, *Phys. Rev. C* **83** (2011) 044913, [arXiv:1010.0233](#) [[nucl-ex](#)].
- [28] J. Jia, M. Zhou, and A. Trzupek, *Revealing long-range multiparticle collectivity in small collision systems via subevent cumulants*, *Phys. Rev. C* **96** (2017) 034906, [arXiv:1701.03830](#) [[nucl-th](#)].
- [29] ALICE Collaboration, J. Adam et al., *Correlated event-by-event fluctuations of flow harmonics in Pb-Pb collisions at $\sqrt{s_{NN}} = 2.76$ TeV*, *Phys. Rev. Lett.* **117** (2016) 182301, [arXiv:1604.07663](#) [[nucl-ex](#)].
- [30] ATLAS Collaboration, *The ATLAS Experiment at the CERN Large Hadron Collider*, *JINST* **3** (2008) S08003.

- [31] ATLAS Collaboration, *The ATLAS Inner Detector commissioning and calibration*, *Eur. Phys. J. C* **70** (2010) 787, [arXiv:1004.5293](#) [[physics.ins-det](#)].
- [32] ATLAS Collaboration, *ATLAS Insertable B-Layer Technical Design Report*, ATLAS-TDR-19, 2010, <https://cds.cern.ch/record/1291633>, *ATLAS Insertable B-Layer Technical Design Report Addendum*, ATLAS-TDR-19-ADD-1, 2012, URL: <https://cds.cern.ch/record/1451888>.
- [33] ATLAS Collaboration, *Performance of the ATLAS Trigger System in 2010*, *Eur. Phys. J. C* **72** (2012) 1849, [arXiv:1110.1530](#) [[hep-ex](#)].
- [34] ATLAS Collaboration, *Measurement of the centrality dependence of the charged particle pseudorapidity distribution in lead-lead collisions at $\sqrt{s_{NN}} = 2.76$ TeV with the ATLAS detector*, *Phys. Lett. B* **710** (2012) 363, [arXiv:1108.6027](#) [[hep-ex](#)].
- [35] ATLAS Collaboration, *Jet energy measurement with the ATLAS detector in proton-proton collisions at $\sqrt{s} = 7$ TeV*, *Eur. Phys. J. C* **73** (2013) 2304, [arXiv:1112.6426](#) [[hep-ex](#)].
- [36] M. L. Miller, K. Reygers, S. J. Sanders, and P. Steinberg, *Glauber modeling in high energy nuclear collisions*, *Ann. Rev. Nucl. Part. Sci.* **57** (2007) 205, [arXiv:nucl-ex/0701025](#).
- [37] ATLAS Collaboration, *Measurement of charged-particle spectra in Pb+Pb collisions at $\sqrt{s_{NN}} = 2.76$ TeV with the ATLAS detector at the LHC*, *JHEP* **09** (2015) 050, [arXiv:1504.04337](#) [[hep-ex](#)].
- [38] ATLAS Collaboration, *Measurement of the pseudorapidity and transverse momentum dependence of the elliptic flow of charged particles in lead-lead collisions at $\sqrt{s_{NN}} = 2.76$ TeV with the ATLAS detector*, *Phys. Lett. B* **707** (2012) 330, [arXiv:1108.6018](#) [[hep-ex](#)].
- [39] M. Gyulassy and X.-N. Wang, *HIJING 1.0: A Monte Carlo program for parton and particle production in high-energy hadronic and nuclear collisions*, *Comput. Phys. Commun.* **83** (1994) 307, [arXiv:nucl-th/9502021](#).
- [40] M. Masera, G. Ortona, M. Poghosyan, and F. Prino, *Anisotropic transverse flow introduction in Monte Carlo generators for heavy ion collisions*, *Phys. Rev. C* **79** (2009) 064909.
- [41] ATLAS Collaboration, *Measurement of the pseudorapidity and transverse momentum dependence of the elliptic flow of charged particles in lead-lead collisions at $\sqrt{s_{NN}} = 2.76$ TeV with the ATLAS detector*, *Phys. Lett. B* **707** (2012) 330, [arXiv:1108.6018](#) [[hep-ex](#)].
- [42] GEANT4 Collaboration, S. Agostinelli et al., *GEANT4: A Simulation toolkit*, *Nucl. Instrum. Meth. A* **506** (2003) 250.
- [43] ATLAS Collaboration, *The ATLAS Simulation Infrastructure*, *Eur. Phys. J. C* **70** (2010) 823, [arXiv:1005.4568](#) [[physics.ins-det](#)].
- [44] ATLAS Collaboration, *Measurement of flow harmonics with multi-particle cumulants in Pb+Pb collisions at $\sqrt{s_{NN}} = 2.76$ TeV with the ATLAS detector*, *Eur. Phys. J. C* **74** (2014) 3157, [arXiv:1408.4342](#) [[hep-ex](#)].
- [45] M. Gyulassy, I. Vitev, X.-N. Wang, and B.-W. Zhang, *Jet quenching and radiative energy loss in dense nuclear matter*, [arXiv:nucl-th/0302077](#).

- [46] ALICE Collaboration, J. Adam et al., *Pseudorapidity dependence of the anisotropic flow of charged particles in Pb-Pb collisions at $\sqrt{s_{NN}} = 2.76$ TeV*, *Phys. Lett. B* **762** (2016) 376, [arXiv:1605.02035 \[nucl-ex\]](#).
- [47] P. Huo, J. Jia, and S. Mohapatra, *Elucidating the event-by-event flow fluctuations in heavy-ion collisions via the event shape selection technique*, *Phys. Rev. C* **90** (2014) 024910, [arXiv:1311.7091 \[nucl-ex\]](#).
- [48] ALICE Collaboration, S. Acharya et al., *Systematic studies of correlations between different order flow harmonics in Pb-Pb collisions at $\sqrt{s_{NN}} = 2.76$ TeV*, [arXiv:1709.01127 \[nucl-ex\]](#).
- [49] ATLAS Collaboration, *ATLAS Computing Acknowledgements 2016–2017*, ATL-GEN-PUB-2016-002, <https://cds.cern.ch/record/2202407>.

The ATLAS Collaboration

M. Aaboud^{137d}, G. Aad⁸⁸, B. Abbott¹¹⁵, O. Abdinov^{12,*}, B. Abeloos¹¹⁹, S.H. Abidi¹⁶¹, O.S. AbouZeid¹³⁹, N.L. Abraham¹⁵¹, H. Abramowicz¹⁵⁵, H. Abreu¹⁵⁴, R. Abreu¹¹⁸, Y. Abulaiti^{148a,148b}, B.S. Acharya^{167a,167b,a}, S. Adachi¹⁵⁷, L. Adamczyk^{41a}, J. Adelman¹¹⁰, M. Adersberger¹⁰², T. Adye¹³³, A.A. Affolder¹³⁹, Y. Afik¹⁵⁴, T. Agatonovic-Jovin¹⁴, C. Agheorghiesei^{28c}, J.A. Aguilar-Saavedra^{128a,128f}, S.P. Ahlen²⁴, F. Ahmadov^{68,b}, G. Aielli^{135a,135b}, S. Akatsuka⁷¹, H. Akerstedt^{148a,148b}, T.P.A. Åkesson⁸⁴, E. Akilli⁵², A.V. Akimov⁹⁸, G.L. Alberghi^{22a,22b}, J. Albert¹⁷², P. Albicocco⁵⁰, M.J. Alconada Verzini⁷⁴, S.C. Alderweireldt¹⁰⁸, M. Aleksa³², I.N. Aleksandrov⁶⁸, C. Alexa^{28b}, G. Alexander¹⁵⁵, T. Alexopoulos¹⁰, M. Alhroob¹¹⁵, B. Ali¹³⁰, M. Aliev^{76a,76b}, G. Alimonti^{94a}, J. Alison³³, S.P. Alkire³⁸, B.M.M. Allbrooke¹⁵¹, B.W. Allen¹¹⁸, P.P. Allport¹⁹, A. Aloisio^{106a,106b}, A. Alonso³⁹, F. Alonso⁷⁴, C. Alpigiani¹⁴⁰, A.A. Alshehri⁵⁶, M.I. Alstary⁸⁸, B. Alvarez Gonzalez³², D. Álvarez Piqueras¹⁷⁰, M.G. Alvigi^{106a,106b}, B.T. Amadio¹⁶, Y. Amaral Coutinho^{26a}, C. Amelung²⁵, D. Amidei⁹², S.P. Amor Dos Santos^{128a,128c}, S. Amoroso³², G. Amundsen²⁵, C. Anastopoulos¹⁴¹, L.S. Ancu⁵², N. Andari¹⁹, T. Andeen¹¹, C.F. Anders^{60b}, J.K. Anders⁷⁷, K.J. Anderson³³, A. Andreazza^{94a,94b}, V. Andrei^{60a}, S. Angelidakis³⁷, I. Angelozzi¹⁰⁹, A. Angerami³⁸, A.V. Anisenkov^{111,c}, N. Anjos¹³, A. Annovi^{126a,126b}, C. Antel^{160a}, M. Antonelli⁵⁰, A. Antonov^{100,*}, D.J. Antrim¹⁶⁶, F. Anulli^{134a}, M. Aoki⁶⁹, L. Aperio Bella³², G. Arabidze⁹³, Y. Arai⁶⁹, J.P. Araque^{128a}, V. Araujo Ferraz^{26a}, A.T.H. Arce⁴⁸, R.E. Ardell⁸⁰, F.A. Arduh⁷⁴, J-F. Arguin⁹⁷, S. Argyropoulos⁶⁶, M. Arik^{20a}, A.J. Armbruster³², L.J. Armitage⁷⁹, O. Arnaez¹⁶¹, H. Arnold⁵¹, M. Arratia³⁰, O. Arslan²³, A. Artamonov^{99,*}, G. Artoni¹²², S. Artz⁸⁶, S. Asai¹⁵⁷, N. Asbah⁴⁵, A. Ashkenazi¹⁵⁵, L. Asquith¹⁵¹, K. Assamagan²⁷, R. Astalos^{146a}, M. Atkinson¹⁶⁹, N.B. Atlay¹⁴³, K. Augsten¹³⁰, G. Avolio³², B. Axen¹⁶, M.K. Ayoub^{35a}, G. Azuelos^{97,d}, A.E. Baas^{60a}, M.J. Baca¹⁹, H. Bachacou¹³⁸, K. Bachas^{76a,76b}, M. Backes¹²², P. Bagnaia^{134a,134b}, M. Bahmani⁴², H. Bahrasemani¹⁴⁴, J.T. Baines¹³³, M. Bajic³⁹, O.K. Baker¹⁷⁹, P.J. Bakker¹⁰⁹, E.M. Baldin^{111,c}, P. Balek¹⁷⁵, F. Balli¹³⁸, W.K. Balunas¹²⁴, E. Banas⁴², A. Bandyopadhyay²³, Sw. Banerjee^{176,e}, A.A.E. Bannoura¹⁷⁸, L. Barak¹⁵⁵, E.L. Barberio⁹¹, D. Barberis^{53a,53b}, M. Barbero⁸⁸, T. Barillari¹⁰³, M-S Barisits³², J.T. Barkeloo¹¹⁸, T. Barklow¹⁴⁵, N. Barlow³⁰, S.L. Barnes^{36c}, B.M. Barnett¹³³, R.M. Barnett¹⁶, Z. Barnovska-Blenessy^{36a}, A. Baroncelli^{136a}, G. Barone²⁵, A.J. Barr¹²², L. Barranco Navarro¹⁷⁰, F. Barreiro⁸⁵, J. Barreiro Guimarães da Costa^{35a}, R. Bartoldus¹⁴⁵, A.E. Barton⁷⁵, P. Bartos^{146a}, A. Basalae¹²⁵, A. Bassalat^{119,f}, R.L. Bates⁵⁶, S.J. Batista¹⁶¹, J.R. Batley³⁰, M. Battaglia¹³⁹, M. Bauce^{134a,134b}, F. Bauer¹³⁸, H.S. Bawa^{145,g}, J.B. Beacham¹¹³, M.D. Beattie⁷⁵, T. Beau⁸³, P.H. Beauchemin¹⁶⁵, P. Bechtel²³, H.P. Beck^{18,h}, H.C. Beck⁵⁷, K. Becker¹²², M. Becker⁸⁶, C. Becot¹¹², A.J. Beddall^{20e},

A. Beddall^{20b}, V.A. Bednyakov⁶⁸, M. Bedognetti¹⁰⁹, C.P. Bee¹⁵⁰, T.A. Beermann³², M. Begalli^{26a},
 M. Begel²⁷, J.K. Behr⁴⁵, A.S. Bell⁸¹, G. Bella¹⁵⁵, L. Bellagamba^{22a}, A. Bellerive³¹, M. Bellomo¹⁵⁴,
 K. Belotskiy¹⁰⁰, O. Beltramello³², N.L. Belyaev¹⁰⁰, O. Benary^{155,*}, D. Benchekroun^{137a}, M. Bender¹⁰²,
 N. Benekos¹⁰, Y. Benhammou¹⁵⁵, E. Benhar Noccioli¹⁷⁹, J. Benitez⁶⁶, D.P. Benjamin⁴⁸, M. Benoit⁵²,
 J.R. Bensingher²⁵, S. Bentvelsen¹⁰⁹, L. Beresford¹²², M. Beretta⁵⁰, D. Berge¹⁰⁹,
 E. Bergeaas Kuutmann¹⁶⁸, N. Berger⁵, L.J. Bergsten²⁵, J. Beringer¹⁶, S. Berlendis⁵⁸, N.R. Bernard⁸⁹,
 G. Bernardi⁸³, C. Bernius¹⁴⁵, F.U. Bernlochner²³, T. Berry⁸⁰, P. Berta⁸⁶, C. Bertella^{35a},
 G. Bertoli^{148a,148b}, I.A. Bertram⁷⁵, C. Bertsche⁴⁵, G.J. Besjes³⁹, O. Bessidskaia Bylund^{148a,148b},
 M. Bessner⁴⁵, N. Besson¹³⁸, A. Bethani⁸⁷, S. Bethke¹⁰³, A. Betti²³, A.J. Bevan⁷⁹, J. Beyer¹⁰³,
 R.M. Bianchi¹²⁷, O. Biebel¹⁰², D. Biedermann¹⁷, R. Bielski⁸⁷, K. Bierwagen⁸⁶, N.V. Biesuz^{126a,126b},
 M. Biglietti^{136a}, T.R.V. Billoud⁹⁷, H. Bilokon⁵⁰, M. Bindi⁵⁷, A. Bingul^{20b}, C. Bini^{134a,134b},
 S. Biondi^{22a,22b}, T. Bisanz⁵⁷, C. Bittrich⁴⁷, D.M. Bjergaard⁴⁸, J.E. Black¹⁴⁵, K.M. Black²⁴, R.E. Blair⁶,
 T. Blazek^{146a}, I. Bloch⁴⁵, C. Blocker²⁵, A. Blue⁵⁶, U. Blumenschein⁷⁹, S. Blunier^{34a}, G.J. Bobbink¹⁰⁹,
 V.S. Bobrovnikov^{111,c}, S.S. Bocchetta⁸⁴, A. Bocci⁴⁸, C. Bock¹⁰², M. Boehler⁵¹, D. Boerner¹⁷⁸,
 D. Bogavac¹⁰², A.G. Bogdanchikov¹¹¹, C. Bohm^{148a}, V. Boisvert⁸⁰, P. Bokan^{168,i}, T. Bold^{41a},
 A.S. Boldyrev¹⁰¹, A.E. Bolz^{60b}, M. Bomben⁸³, M. Bona⁷⁹, M. Boonekamp¹³⁸, A. Borisov¹³²,
 G. Borissov⁷⁵, J. Bortfeldt³², D. Bortoletto¹²², V. Bortolotto^{62a}, D. Boscherini^{22a}, M. Bosman¹³,
 J.D. Bossio Sola²⁹, J. Boudreau¹²⁷, E.V. Bouhova-Thacker⁷⁵, D. Boumediene³⁷, C. Bourdarios¹¹⁹,
 S.K. Boutle⁵⁶, A. Boveia¹¹³, J. Boyd³², I.R. Boyko⁶⁸, A.J. Bozson⁸⁰, J. Bracinik¹⁹, A. Brandt⁸,
 G. Brandt⁵⁷, O. Brandt^{60a}, F. Braren⁴⁵, U. Bratzler¹⁵⁸, B. Brau⁸⁹, J.E. Brau¹¹⁸, W.D. Breaden Madden⁵⁶,
 K. Brendlinger⁴⁵, A.J. Brennan⁹¹, L. Brenner¹⁰⁹, R. Brenner¹⁶⁸, S. Bressler¹⁷⁵, D.L. Briglin¹⁹,
 T.M. Bristow⁴⁹, D. Britton⁵⁶, D. Britzger⁴⁵, F.M. Brochu³⁰, I. Brock²³, R. Brock⁹³, G. Brooijmans³⁸,
 T. Brooks⁸⁰, W.K. Brooks^{34b}, J. Brosamer¹⁶, E. Brost¹¹⁰, J.H. Broughton¹⁹,
 P.A. Bruckman de Renstrom⁴², D. Bruncko^{146b}, A. Bruni^{22a}, G. Bruni^{22a}, L.S. Bruni¹⁰⁹,
 S. Bruno^{135a,135b}, BH Brunt³⁰, M. Bruschi^{22a}, N. Bruscinò¹²⁷, P. Bryant³³, L. Bryngemark⁴⁵,
 T. Buanes¹⁵, Q. Buat¹⁴⁴, P. Buchholz¹⁴³, A.G. Buckley⁵⁶, I.A. Budagov⁶⁸, F. Buehrer⁵¹, M.K. Bugge¹²¹,
 O. Bulekov¹⁰⁰, D. Bullock⁸, T.J. Burch¹¹⁰, S. Burdin⁷⁷, C.D. Burgard¹⁰⁹, A.M. Burger⁵,
 B. Burghgrave¹¹⁰, K. Burka⁴², S. Burke¹³³, I. Burmeister⁴⁶, J.T.P. Burr¹²², D. Büscher⁵¹, V. Büscher⁸⁶,
 P. Bussey⁵⁶, J.M. Butler²⁴, C.M. Buttar⁵⁶, J.M. Butterworth⁸¹, P. Butti³², W. Buttinger²⁷, A. Buzatu¹⁵³,
 A.R. Buzykaev^{111,c}, S. Cabrera Urbán¹⁷⁰, D. Caforio¹³⁰, H. Cai¹⁶⁹, V.M. Cairo^{40a,40b}, O. Cakir^{4a},
 N. Calace⁵², P. Calafiura¹⁶, A. Calandri⁸⁸, G. Calderini⁸³, P. Calfayan⁶⁴, G. Callea^{40a,40b}, L.P. Caloba^{26a},
 S. Calvente Lopez⁸⁵, D. Calvet³⁷, S. Calvet³⁷, T.P. Calvet⁸⁸, R. Camacho Toro³³, S. Camarda³²,
 P. Camarri^{135a,135b}, D. Cameron¹²¹, R. Caminal Armadans¹⁶⁹, C. Camincher⁵⁸, S. Campana³²,
 M. Campanelli⁸¹, A. Camplani^{94a,94b}, A. Campoverde¹⁴³, V. Canale^{106a,106b}, M. Cano Bret^{36c},
 J. Cantero¹¹⁶, T. Cao¹⁵⁵, M.D.M. Capeans Garrido³², I. Caprini^{28b}, M. Caprini^{28b}, M. Capua^{40a,40b},
 R.M. Carbone³⁸, R. Cardarelli^{135a}, F. Cardillo⁵¹, I. Carli¹³¹, T. Carli³², G. Carlino^{106a}, B.T. Carlson¹²⁷,
 L. Carminati^{94a,94b}, R.M.D. Carney^{148a,148b}, S. Caron¹⁰⁸, E. Carquin^{34b}, S. Carrá^{94a,94b},
 G.D. Carrillo-Montoya³², D. Casadei¹⁹, M.P. Casado^{13,j}, A.F. Casha¹⁶¹, M. Casolino¹³, D.W. Casper¹⁶⁶,
 R. Castelijns¹⁰⁹, V. Castillo Gimenez¹⁷⁰, N.F. Castro^{128a,k}, A. Catinaccio³², J.R. Catmore¹²¹, A. Cattai³²,
 J. Caudron²³, V. Cavaliere¹⁶⁹, E. Cavallaro¹³, D. Cavalli^{94a}, M. Cavalli-Sforza¹³, V. Cavasinni^{126a,126b},
 E. Celebi^{20d}, F. Ceradini^{136a,136b}, L. Cerda Alberich¹⁷⁰, A.S. Cerqueira^{26b}, A. Cerri¹⁵¹,
 L. Cerrito^{135a,135b}, F. Cerutti¹⁶, A. Cervelli^{22a,22b}, S.A. Cetin^{20d}, A. Chafaq^{137a}, D. Chakraborty¹¹⁰,
 S.K. Chan⁵⁹, W.S. Chan¹⁰⁹, Y.L. Chan^{62a}, P. Chang¹⁶⁹, J.D. Chapman³⁰, D.G. Charlton¹⁹, C.C. Chau³¹,
 C.A. Chavez Barajas¹⁵¹, S. Che¹¹³, S. Cheatham^{167a,167c}, A. Chegwidden⁹³, S. Chekanov⁶,
 S.V. Chekulaev^{163a}, G.A. Chelkov^{68,l}, M.A. Chelstowska³², C. Chen^{36a}, C. Chen⁶⁷, H. Chen²⁷,
 J. Chen^{36a}, S. Chen^{35b}, S. Chen¹⁵⁷, X. Chen^{35c,m}, Y. Chen⁷⁰, H.C. Cheng⁹², H.J. Cheng^{35a,35d},
 A. Cheplakov⁶⁸, E. Cheremushkina¹³², R. Cherkaoui El Moursli^{137e}, E. Cheu⁷, K. Cheung⁶³,

L. Chevalier¹³⁸, V. Chiarella⁵⁰, G. Chiarelli^{126a,126b}, G. Chiodini^{76a}, A.S. Chisholm³², A. Chitan^{28b},
 Y.H. Chiu¹⁷², M.V. Chizhov⁶⁸, K. Choi⁶⁴, A.R. Chomont³⁷, S. Chouridou¹⁵⁶, Y.S. Chow^{62a},
 V. Christodoulou⁸¹, M.C. Chu^{62a}, J. Chudoba¹²⁹, A.J. Chuinard⁹⁰, J.J. Chwastowski⁴², L. Chytka¹¹⁷,
 A.K. Ciftci^{4a}, D. Cinca⁴⁶, V. Cindro⁷⁸, I.A. Cioara²³, A. Ciocio¹⁶, F. Cirotto^{106a,106b}, Z.H. Citron¹⁷⁵,
 M. Citterio^{94a}, M. Ciubancan^{28b}, A. Clark⁵², B.L. Clark⁵⁹, M.R. Clark³⁸, P.J. Clark⁴⁹, R.N. Clarke¹⁶,
 C. Clement^{148a,148b}, Y. Coadou⁸⁸, M. Cobal^{167a,167c}, A. Coccaro⁵², J. Cochran⁶⁷, L. Colasurdo¹⁰⁸,
 B. Cole³⁸, A.P. Colijn¹⁰⁹, J. Collot⁵⁸, T. Colombo¹⁶⁶, P. Conde Muiño^{128a,128b}, E. Coniavitis⁵¹,
 S.H. Connell^{147b}, I.A. Connelly⁸⁷, S. Constantinescu^{28b}, G. Conti³², F. Conventi^{106a,n}, M. Cooke¹⁶,
 A.M. Cooper-Sarkar¹²², F. Cormier¹⁷¹, K.J.R. Cormier¹⁶¹, M. Corradi^{134a,134b}, F. Corriveau^{90,o},
 A. Cortes-Gonzalez³², G. Costa^{94a}, M.J. Costa¹⁷⁰, D. Costanzo¹⁴¹, G. Cottin³⁰, G. Cowan⁸⁰, B.E. Cox⁸⁷,
 K. Cranmer¹¹², S.J. Crawley⁵⁶, R.A. Creager¹²⁴, G. Cree³¹, S. Crépe-Renaudin⁵⁸, F. Crescioli⁸³,
 W.A. Cribbs^{148a,148b}, M. Cristinziani²³, V. Croft¹¹², G. Crosetti^{40a,40b}, A. Cueto⁸⁵,
 T. Cuhadar Donszelmann¹⁴¹, A.R. Cukierman¹⁴⁵, J. Cummings¹⁷⁹, M. Curatolo⁵⁰, J. Cúth⁸⁶,
 S. Czekierda⁴², P. Czodrowski³², G. D'amen^{22a,22b}, S. D'Auria⁵⁶, L. D'eraimo⁸³, M. D'Onofrio⁷⁷,
 M.J. Da Cunha Sargedas De Sousa^{128a,128b}, C. Da Via⁸⁷, W. Dabrowski^{41a}, T. Dado^{146a}, T. Dai⁹²,
 O. Dale¹⁵, F. Dallaire⁹⁷, C. Dallapiccola⁸⁹, M. Dam³⁹, J.R. Dandoy¹²⁴, M.F. Daneri²⁹, N.P. Dang¹⁷⁶,
 A.C. Daniells¹⁹, N.S. Dann⁸⁷, M. Danninger¹⁷¹, M. Dano Hoffmann¹³⁸, V. Dao¹⁵⁰, G. Darbo^{53a},
 S. Darmora⁸, J. Dassoulas³, A. Dattagupta¹¹⁸, T. Daubney⁴⁵, W. Davey²³, C. David⁴⁵, T. Davidek¹³¹,
 D.R. Davis⁴⁸, P. Davison⁸¹, E. Dawe⁹¹, I. Dawson¹⁴¹, K. De⁸, R. de Asmundis^{106a}, A. De Benedetti¹¹⁵,
 S. De Castro^{22a,22b}, S. De Cecco⁸³, N. De Groot¹⁰⁸, P. de Jong¹⁰⁹, H. De la Torre⁹³, F. De Lorenzi⁶⁷,
 A. De Maria⁵⁷, D. De Pedis^{134a}, A. De Salvo^{134a}, U. De Sanctis^{135a,135b}, A. De Santo¹⁵¹,
 K. De Vasconcelos Corga⁸⁸, J.B. De Vivie De Regie¹¹⁹, R. Debbe²⁷, C. Debenedetti¹³⁹,
 D.V. Dedovich⁶⁸, N. Dehghanian³, I. Deigaard¹⁰⁹, M. Del Gaudio^{40a,40b}, J. Del Peso⁸⁵, D. Delgove¹¹⁹,
 F. Deliot¹³⁸, C.M. Delitzsch⁷, A. Dell'Acqua³², L. Dell'Asta²⁴, M. Dell'Orso^{126a,126b},
 M. Della Pietra^{106a,106b}, D. della Volpe⁵², M. Delmastro⁵, C. Delporte¹¹⁹, P.A. Delsart⁵⁸,
 D.A. DeMarco¹⁶¹, S. Demers¹⁷⁹, M. Demichev⁶⁸, A. Demilly⁸³, S.P. Denisov¹³², D. Denysiuk¹³⁸,
 D. Derendarz⁴², J.E. Derkaoui^{137d}, F. Derue⁸³, P. Dervan⁷⁷, K. Desch²³, C. Deterre⁴⁵, K. Dette¹⁶¹,
 M.R. Devesa²⁹, P.O. Deviveiros³², A. Dewhurst¹³³, S. Dhaliwal²⁵, F.A. Di Bello⁵²,
 A. Di Ciaccio^{135a,135b}, L. Di Ciaccio⁵, W.K. Di Clemente¹²⁴, C. Di Donato^{106a,106b}, A. Di Girolamo³²,
 B. Di Girolamo³², B. Di Micco^{136a,136b}, R. Di Nardo³², K.F. Di Petrillo⁵⁹, A. Di Simone⁵¹,
 R. Di Sipio¹⁶¹, D. Di Valentino³¹, C. Diaconu⁸⁸, M. Diamond¹⁶¹, F.A. Dias³⁹, M.A. Diaz^{34a},
 E.B. Diehl⁹², J. Dietrich¹⁷, S. Díez Cornell⁴⁵, A. Dimitrievska¹⁴, J. Dingfelder²³, P. Dita^{28b}, S. Dita^{28b},
 F. Dittus³², F. Djama⁸⁸, T. Djobava^{54b}, J.I. Djuvslund^{160a}, M.A.B. do Vale^{26c}, D. Dobos³², M. Dobre^{28b},
 D. Dodsworth²⁵, C. Doglioni⁸⁴, J. Dolejsi¹³¹, Z. Dolezal¹³¹, M. Donadelli^{26d}, S. Donati^{126a,126b},
 P. Dondero^{123a,123b}, J. Donini³⁷, J. Dopke¹³³, A. Doria^{106a}, M.T. Dova⁷⁴, A.T. Doyle⁵⁶, E. Drechsler⁵⁷,
 M. Dris¹⁰, Y. Du^{36b}, J. Duarte-Campderros¹⁵⁵, F. Dubinin⁹⁸, A. Dubreuil⁵², E. Duchovni¹⁷⁵,
 G. Duckeck¹⁰², A. Ducourthial⁸³, O.A. Ducu^{97,p}, D. Duda¹⁰⁹, A. Dudarev³², A.Chr. Dudder⁸⁶,
 E.M. Duffield¹⁶, L. Dufлот¹¹⁹, M. Dührssen³², C. Dulsen¹⁷⁸, M. Dumancic¹⁷⁵, A.E. Dumitriu^{28b},
 A.K. Duncan⁵⁶, M. Dunford^{160a}, A. Duperrin⁸⁸, H. Duran Yildiz^{4a}, M. Düren⁵⁵, A. Durglishvili^{54b},
 D. Duschinger⁴⁷, B. Dutta⁴⁵, D. Duvnjak¹, M. Dyndal⁴⁵, B.S. Dziedzic⁴², C. Eckardt⁴⁵, K.M. Ecker¹⁰³,
 R.C. Edgar⁹², T. Eifert³², G. Eigen¹⁵, K. Einsweiler¹⁶, T. Ekelof¹⁶⁸, M. El Kacimi^{137c}, R. El Kosseifi⁸⁸,
 V. Ellajosyula⁸⁸, M. Ellert¹⁶⁸, S. Elles⁵, F. Ellinghaus¹⁷⁸, A.A. Elliot¹⁷², N. Ellis³², J. Elmsheuser²⁷,
 M. Elsing³², D. Emeliyanov¹³³, Y. Enari¹⁵⁷, J.S. Ennis¹⁷³, M.B. Epland⁴⁸, J. Erdmann⁴⁶, A. Ereditato¹⁸,
 M. Ernst²⁷, S. Errede¹⁶⁹, M. Escalier¹¹⁹, C. Escobar¹⁷⁰, B. Esposito⁵⁰, O. Estrada Pastor¹⁷⁰,
 A.I. Etienvre¹³⁸, E. Etzion¹⁵⁵, H. Evans⁶⁴, A. Ezhilov¹²⁵, M. Ezzi^{137e}, F. Fabbri^{22a,22b}, L. Fabbri^{22a,22b},
 V. Fabiani¹⁰⁸, G. Facini⁸¹, R.M. Fakhruddinov¹³², S. Falciano^{134a}, R.J. Falla⁸¹, J. Faltova³², Y. Fang^{35a},
 M. Fanti^{94a,94b}, A. Farbin⁸, A. Farilla^{136a}, C. Farina¹²⁷, E.M. Farina^{123a,123b}, T. Farooque⁹³, S. Farrell¹⁶,

S.M. Farrington¹⁷³, P. Farthouat³², F. Fassi^{137e}, P. Fassnacht³², D. Fassouliotis⁹, M. Faucci Giannelli⁴⁹,
 A. Favareto^{53a,53b}, W.J. Fawcett¹²², L. Fayard¹¹⁹, O.L. Fedin^{125.g}, W. Fedorko¹⁷¹, S. Feigl¹²¹,
 L. Feligioni⁸⁸, C. Feng^{36b}, E.J. Feng³², M.J. Fenton⁵⁶, A.B. Fenyuk¹³², L. Feremenga⁸,
 P. Fernandez Martinez¹⁷⁰, J. Ferrando⁴⁵, A. Ferrari¹⁶⁸, P. Ferrari¹⁰⁹, R. Ferrari^{123a},
 D.E. Ferreira de Lima^{60b}, A. Ferrer¹⁷⁰, D. Ferrere⁵², C. Ferretti⁹², F. Fiedler⁸⁶, A. Filipčić⁷⁸,
 M. Filipuzzi⁴⁵, F. Filthaut¹⁰⁸, M. Fincke-Keeler¹⁷², K.D. Finelli²⁴, M.C.N. Fiolhais^{128a,128c,r},
 L. Fiorini¹⁷⁰, A. Fischer², C. Fischer¹³, J. Fischer¹⁷⁸, W.C. Fisher⁹³, N. Flaschel⁴⁵, I. Fleck¹⁴³,
 P. Fleischmann⁹², R.R.M. Fletcher¹²⁴, T. Flick¹⁷⁸, B.M. Flierl¹⁰², L.R. Flores Castillo^{62a},
 M.J. Flowerdew¹⁰³, G.T. Forcolin⁸⁷, A. Formica¹³⁸, F.A. Förster¹³, A. Forti⁸⁷, A.G. Foster¹⁹,
 D. Fournier¹¹⁹, H. Fox⁷⁵, S. Fracchia¹⁴¹, P. Francavilla^{126a,126b}, M. Franchini^{22a,22b}, S. Franchino^{60a},
 D. Francis³², L. Franconi¹²¹, M. Franklin⁵⁹, M. Frate¹⁶⁶, M. Fraternali^{123a,123b}, D. Freeborn⁸¹,
 S.M. Fressard-Batraneanu³², B. Freund⁹⁷, D. Froidevaux³², J.A. Frost¹²², C. Fukunaga¹⁵⁸,
 T. Fusayasu¹⁰⁴, J. Fuster¹⁷⁰, O. Gabizon¹⁵⁴, A. Gabrielli^{22a,22b}, A. Gabrielli¹⁶, G.P. Gach^{41a},
 S. Gadatsch³², S. Gadomski⁸⁰, G. Gagliardi^{53a,53b}, L.G. Gagnon⁹⁷, C. Galea¹⁰⁸, B. Galhardo^{128a,128c},
 E.J. Gallas¹²², B.J. Gallop¹³³, P. Gallus¹³⁰, G. Galster³⁹, K.K. Gan¹¹³, S. Ganguly³⁷, Y. Gao⁷⁷,
 Y.S. Gao^{145.g}, F.M. Garay Walls^{34a}, C. García¹⁷⁰, J.E. García Navarro¹⁷⁰, J.A. García Pascual^{35a},
 M. Garcia-Sciveres¹⁶, R.W. Gardner³³, N. Garelli¹⁴⁵, V. Garonne¹²¹, A. Gascon Bravo⁴⁵,
 K. Gasnikova⁴⁵, C. Gatti⁵⁰, A. Gaudiello^{53a,53b}, G. Gaudio^{123a}, I.L. Gavrilenko⁹⁸, C. Gay¹⁷¹,
 G. Gaycken²³, E.N. Gazis¹⁰, C.N.P. Gee¹³³, J. Geisen⁵⁷, M. Geisen⁸⁶, M.P. Geisler^{60a},
 K. Gellerstedt^{148a,148b}, C. Gemme^{53a}, M.H. Genest⁵⁸, C. Geng⁹², S. Gentile^{134a,134b}, C. Gentsos¹⁵⁶,
 S. George⁸⁰, D. Gerbaudo¹³, G. Geßner⁴⁶, S. Ghasemi¹⁴³, M. Ghneimat²³, B. Giacobbe^{22a},
 S. Giagu^{134a,134b}, N. Giangiacomi^{22a,22b}, P. Giannetti^{126a,126b}, S.M. Gibson⁸⁰, M. Gignac¹⁷¹,
 M. Gilchriese¹⁶, D. Gillberg³¹, G. Gilles¹⁷⁸, D.M. Gingrich^{3,d}, M.P. Giordani^{167a,167c}, F.M. Giorgi^{22a},
 P.F. Giraud¹³⁸, P. Giromini⁵⁹, G. Giugliarelli^{167a,167c}, D. Giugni^{94a}, F. Giuli¹²², C. Giuliani¹⁰³,
 M. Giulini^{60b}, B.K. Gjelsten¹²¹, S. Gkaitatzis¹⁵⁶, I. Gkialas^{9,s}, E.L. Gkoukousis¹³, P. Gkoutoumis¹⁰,
 L.K. Gladilin¹⁰¹, C. Glasman⁸⁵, J. Glatzer¹³, P.C.F. Glaysher⁴⁵, A. Glazov⁴⁵, M. Goblirsch-Kolb²⁵,
 J. Godlewski⁴², S. Goldfarb⁹¹, T. Golling⁵², D. Golubkov¹³², A. Gomes^{128a,128b,128d}, R. Gonçalves^{128a},
 R. Goncalves Gama^{26a}, J. Goncalves Pinto Firmino Da Costa¹³⁸, G. Gonella⁵¹, L. Gonella¹⁹,
 A. Gongadze⁶⁸, J.L. Gonski⁵⁹, S. González de la Hoz¹⁷⁰, S. Gonzalez-Sevilla⁵², L. Goossens³²,
 P.A. Gorbounov⁹⁹, H.A. Gordon²⁷, I. Gorelov¹⁰⁷, B. Gorini³², E. Gorini^{76a,76b}, A. Gorišek⁷⁸,
 A.T. Goshaw⁴⁸, C. Gössling⁴⁶, M.I. Gostkin⁶⁸, C.A. Gottardo²³, C.R. Goudet¹¹⁹, D. Goujdami^{137c},
 A.G. Goussiou¹⁴⁰, N. Govender^{147b,t}, E. Gozani¹⁵⁴, I. Grabowska-Bold^{41a}, P.O.J. Gradin¹⁶⁸,
 J. Gramling¹⁶⁶, E. Gramstad¹²¹, S. Grancagnolo¹⁷, V. Gratchev¹²⁵, P.M. Gravila^{28f}, C. Gray⁵⁶,
 H.M. Gray¹⁶, Z.D. Greenwood^{82,u}, C. Grefe²³, K. Gregersen⁸¹, I.M. Gregor⁴⁵, P. Grenier¹⁴⁵,
 K. Grevtsov⁵, J. Griffiths⁸, A.A. Grillo¹³⁹, K. Grimm⁷⁵, S. Grinstein^{13,v}, Ph. Gris³⁷, J.-F. Grivaz¹¹⁹,
 S. Groh⁸⁶, E. Gross¹⁷⁵, J. Grosse-Knetter⁵⁷, G.C. Grossi⁸², Z.J. Grout⁸¹, A. Grummer¹⁰⁷, L. Guan⁹²,
 W. Guan¹⁷⁶, J. Guenther³², F. Guescini^{163a}, D. Guest¹⁶⁶, O. Gueta¹⁵⁵, B. Gui¹¹³, E. Guido^{53a,53b},
 T. Guillemin⁵, S. Guindon³², U. Gul⁵⁶, C. Gumpert³², J. Guo^{36c}, W. Guo⁹², Y. Guo^{36a,w}, R. Gupta⁴³,
 S. Gurbuz^{20a}, G. Gustavino¹¹⁵, B.J. Gutelman¹⁵⁴, P. Gutierrez¹¹⁵, N.G. Gutierrez Ortiz⁸¹,
 C. Gutschow⁸¹, C. Guyot¹³⁸, M.P. Guzik^{41a}, C. Gwenlan¹²², C.B. Gwilliam⁷⁷, A. Haas¹¹², C. Haber¹⁶,
 H.K. Hadavand⁸, N. Haddad^{137e}, A. Hadeef⁸⁸, S. Hageböck²³, M. Hagihara¹⁶⁴, H. Hakobyan^{180,*},
 M. Haleem⁴⁵, J. Haley¹¹⁶, G. Halladjian⁹³, G.D. Hallewell⁸⁸, K. Hamacher¹⁷⁸, P. Hamal¹¹⁷,
 K. Hamano¹⁷², A. Hamilton^{147a}, G.N. Hamity¹⁴¹, P.G. Hamnett⁴⁵, L. Han^{36a}, S. Han^{35a,35d},
 K. Hanagaki^{69,x}, K. Hanawa¹⁵⁷, M. Hance¹³⁹, D.M. Handl¹⁰², B. Haney¹²⁴, P. Hanke^{60a}, J.B. Hansen³⁹,
 J.D. Hansen³⁹, M.C. Hansen²³, P.H. Hansen³⁹, K. Hara¹⁶⁴, A.S. Hard¹⁷⁶, T. Harenberg¹⁷⁸, F. Hariri¹¹⁹,
 S. Harkusha⁹⁵, P.F. Harrison¹⁷³, N.M. Hartmann¹⁰², Y. Hasegawa¹⁴², A. Hasib⁴⁹, S. Hassani¹³⁸,
 S. Haug¹⁸, R. Hauser⁹³, L. Hauswald⁴⁷, L.B. Havener³⁸, M. Havranek¹³⁰, C.M. Hawkes¹⁹,

R.J. Hawkings³², D. Hayakawa¹⁵⁹, D. Hayden⁹³, C.P. Hays¹²², J.M. Hays⁷⁹, H.S. Hayward⁷⁷, S.J. Haywood¹³³, S.J. Head¹⁹, T. Heck⁸⁶, V. Hedberg⁸⁴, L. Heelan⁸, S. Heer²³, K.K. Heidegger⁵¹, S. Heim⁴⁵, T. Heim¹⁶, B. Heinemann^{45,y}, J.J. Heinrich¹⁰², L. Heinrich¹¹², C. Heinz⁵⁵, J. Hejbal¹²⁹, L. Helary³², A. Held¹⁷¹, S. Hellman^{148a,148b}, C. Helsens³², R.C.W. Henderson⁷⁵, Y. Heng¹⁷⁶, S. Henkelmann¹⁷¹, A.M. Henriques Correia³², S. Henrot-Versille¹¹⁹, G.H. Herbert¹⁷, H. Herde²⁵, V. Herget¹⁷⁷, Y. Hernández Jiménez^{147c}, H. Herr⁸⁶, G. Herten⁵¹, R. Hertenberger¹⁰², L. Hervas³², T.C. Herwig¹²⁴, G.G. Hesketh⁸¹, N.P. Hessay^{163a}, J.W. Hetherly⁴³, S. Higashino⁶⁹, E. Higón-Rodríguez¹⁷⁰, K. Hildebrand³³, E. Hill¹⁷², J.C. Hill³⁰, K.H. Hiller⁴⁵, S.J. Hillier¹⁹, M. Hils⁴⁷, I. Hinchliffe¹⁶, M. Hirose⁵¹, D. Hirschbuehl¹⁷⁸, B. Hiti⁷⁸, O. Hladik¹²⁹, D.R. Hlaluku^{147c}, X. Hoad⁴⁹, J. Hobbs¹⁵⁰, N. Hod^{163a}, M.C. Hodgkinson¹⁴¹, P. Hodgson¹⁴¹, A. Hoecker³², M.R. Hoferkamp¹⁰⁷, F. Hoenig¹⁰², D. Hohn²³, T.R. Holmes³³, M. Homann⁴⁶, S. Honda¹⁶⁴, T. Honda⁶⁹, T.M. Hong¹²⁷, B.H. Hooberman¹⁶⁹, W.H. Hopkins¹¹⁸, Y. Hori¹⁰⁵, A.J. Horton¹⁴⁴, J.-Y. Hostachy⁵⁸, A. Hostiuc¹⁴⁰, S. Hou¹⁵³, A. Hoummada^{137a}, J. Howarth⁸⁷, J. Hoya⁷⁴, M. Hrabovsky¹¹⁷, J. Hrdinka³², I. Hristova¹⁷, J. Hrivnac¹¹⁹, T. Hryn'ova⁵, A. Hrynevich⁹⁶, P.J. Hsu⁶³, S.-C. Hsu¹⁴⁰, Q. Hu²⁷, S. Hu^{36c}, Y. Huang^{35a}, Z. Hubacek¹³⁰, F. Hubaut⁸⁸, F. Huegging²³, T.B. Huffman¹²², E.W. Hughes³⁸, M. Huhtinen³², R.F.H. Hunter³¹, P. Huo¹⁵⁰, N. Huseynov^{68,b}, J. Huston⁹³, J. Huth⁵⁹, R. Hyneman⁹², G. Iacobucci⁵², G. Iakovidis²⁷, I. Ibragimov¹⁴³, L. Iconomidou-Fayard¹¹⁹, Z. Idrissi^{137e}, P. Iengo³², O. Igonkina^{109,z}, T. Iizawa¹⁷⁴, Y. Ikegami⁶⁹, M. Ikeno⁶⁹, Y. Ilchenko^{11,aa}, D. Iliadis¹⁵⁶, N. Ilic¹⁴⁵, F. Iltzsche⁴⁷, G. Introzzi^{123a,123b}, P. Ioannou^{9,*}, M. Iodice^{136a}, K. Iordanidou³⁸, V. Ippolito⁵⁹, M.F. Isacson¹⁶⁸, N. Ishijima¹²⁰, M. Ishino¹⁵⁷, M. Ishitsuka¹⁵⁹, C. Issever¹²², S. Istin^{20a}, F. Ito¹⁶⁴, J.M. Iturbe Ponce^{62a}, R. Iuppa^{162a,162b}, H. Iwasaki⁶⁹, J.M. Izen⁴⁴, V. Izzo^{106a}, S. Jabbar³, P. Jackson¹, R.M. Jacobs²³, V. Jain², K.B. Jakobi⁸⁶, K. Jakobs⁵¹, S. Jakobsen⁶⁵, T. Jakoubek¹²⁹, D.O. Jamin¹¹⁶, D.K. Jana⁸², R. Jansky⁵², J. Janssen²³, M. Janus⁵⁷, P.A. Janus^{41a}, G. Jarlskog⁸⁴, N. Javadov^{68,b}, T. Javůrek⁵¹, M. Javurkova⁵¹, F. Jeanneau¹³⁸, L. Jeanty¹⁶, J. Jejelava^{54a,ab}, A. Jelinskas¹⁷³, P. Jenni^{51,ac}, C. Jeske¹⁷³, S. Jézéquel⁵, H. Ji¹⁷⁶, J. Jia¹⁵⁰, H. Jiang⁶⁷, Y. Jiang^{36a}, Z. Jiang¹⁴⁵, S. Jiggins⁸¹, J. Jimenez Pena¹⁷⁰, S. Jin^{35b}, A. Jinaru^{28b}, O. Jinnouchi¹⁵⁹, H. Jivan^{147c}, P. Johansson¹⁴¹, K.A. Johns⁷, C.A. Johnson⁶⁴, W.J. Johnson¹⁴⁰, K. Jon-And^{148a,148b}, R.W.L. Jones⁷⁵, S.D. Jones¹⁵¹, S. Jones⁷, T.J. Jones⁷⁷, J. Jongmanns^{60a}, P.M. Jorge^{128a,128b}, J. Jovicevic^{163a}, X. Ju¹⁷⁶, A. Juste Rozas^{13,v}, M.K. Köhler¹⁷⁵, A. Kaczmarska⁴², M. Kado¹¹⁹, H. Kagan¹¹³, M. Kagan¹⁴⁵, S.J. Kahn⁸⁸, T. Kaji¹⁷⁴, E. Kajomovitz¹⁵⁴, C.W. Kalderon⁸⁴, A. Kaluza⁸⁶, S. Kama⁴³, A. Kamenshchikov¹³², N. Kanaya¹⁵⁷, L. Kanjir⁷⁸, V.A. Kantserov¹⁰⁰, J. Kanzaki⁶⁹, B. Kaplan¹¹², L.S. Kaplan¹⁷⁶, D. Kar^{147c}, K. Karakostas¹⁰, N. Karastathis¹⁰, M.J. Kareem^{163b}, E. Karentzos¹⁰, S.N. Karpov⁶⁸, Z.M. Karpova⁶⁸, K. Karthik¹¹², V. Kartvelishvili⁷⁵, A.N. Karyukhin¹³², K. Kasahara¹⁶⁴, L. Kashif¹⁷⁶, R.D. Kass¹¹³, A. Kastanas¹⁴⁹, Y. Kataoka¹⁵⁷, C. Kato¹⁵⁷, A. Katre⁵², J. Katzy⁴⁵, K. Kawade⁷⁰, K. Kawagoe⁷³, T. Kawamoto¹⁵⁷, G. Kawamura⁵⁷, E.F. Kay⁷⁷, V.F. Kazanin^{111,c}, R. Keeler¹⁷², R. Kehoe⁴³, J.S. Keller³¹, E. Kellermann⁸⁴, J.J. Kempster⁸⁰, J. Kendrick¹⁹, H. Keoshkerian¹⁶¹, O. Kepka¹²⁹, B.P. Kerševan⁷⁸, S. Kersten¹⁷⁸, R.A. Keyes⁹⁰, M. Khader¹⁶⁹, F. Khalil-zada¹², A. Khanov¹¹⁶, A.G. Kharlamov^{111,c}, T. Kharlamova^{111,c}, A. Khodinov¹⁶⁰, T.J. Khoo⁵², V. Khovanskiy^{99,*}, E. Khramov⁶⁸, J. Khubua^{54b,ad}, S. Kido⁷⁰, C.R. Kilby⁸⁰, H.Y. Kim⁸, S.H. Kim¹⁶⁴, Y.K. Kim³³, N. Kimura¹⁵⁶, O.M. Kind¹⁷, B.T. King⁷⁷, D. Kirchmeier⁴⁷, J. Kirk¹³³, A.E. Kiryunin¹⁰³, T. Kishimoto¹⁵⁷, D. Kisielewska^{41a}, V. Kitali⁴⁵, O. Kivernyk⁵, E. Kladiva^{146b}, T. Klapdor-Kleingrothaus⁵¹, M.H. Klein⁹², M. Klein⁷⁷, U. Klein⁷⁷, K. Kleinknecht⁸⁶, P. Klimek¹¹⁰, A. Klimentov²⁷, R. Klingenberg^{46,*}, T. Klingl²³, T. Klioutchnikova³², F.F. Klitzner¹⁰², E.-E. Kluge^{60a}, P. Kluit¹⁰⁹, S. Kluth¹⁰³, E. Kneringer⁶⁵, E.B.F.G. Knoops⁸⁸, A. Knue¹⁰³, A. Kobayashi¹⁵⁷, D. Kobayashi⁷³, T. Kobayashi¹⁵⁷, M. Kobel⁴⁷, M. Kocian¹⁴⁵, P. Kodys¹³¹, T. Koffas³¹, E. Koffeman¹⁰⁹, N.M. Köhler¹⁰³, T. Koi¹⁴⁵, M. Kolb^{60b}, I. Koletsou⁵, A.A. Komar^{98,*}, T. Kondo⁶⁹, N. Kondrashova^{36c}, K. Köneke⁵¹, A.C. König¹⁰⁸, T. Kono^{69,ae}, R. Konoplich^{112,af}, N. Konstantinidis⁸¹, B. Konya⁸⁴, R. Kopeliansky⁶⁴, S. Koperny^{41a}, A.K. Kopp⁵¹, K. Korcyl⁴², K. Kordas¹⁵⁶, A. Korn⁸¹,

A.A. Korol^{111,c}, I. Korolkov¹³, E.V. Korolkova¹⁴¹, O. Kortner¹⁰³, S. Kortner¹⁰³, T. Kosek¹³¹,
 V.V. Kostyukhin²³, A. Kotwal⁴⁸, A. Koulouris¹⁰, A. Kourkoumeli-Charalampidi^{123a,123b},
 C. Kourkoumelis⁹, E. Kourlitis¹⁴¹, V. Kouskoura²⁷, A.B. Kowalewska⁴², R. Kowalewski¹⁷²,
 T.Z. Kowalski^{41a}, C. Kozakai¹⁵⁷, W. Kozanecki¹³⁸, A.S. Kozhin¹³², V.A. Kramarenko¹⁰¹,
 G. Kramberger⁷⁸, D. Krasnopevtsev¹⁰⁰, M.W. Krasny⁸³, A. Krasznahorkay³², D. Krauss¹⁰³,
 J.A. Kremer^{41a}, J. Kretschmar⁷⁷, K. Kreutzfeldt⁵⁵, P. Krieger¹⁶¹, K. Krizka¹⁶, K. Kroeninger⁴⁶,
 H. Kroha¹⁰³, J. Kroll¹²⁹, J. Kroll¹²⁴, J. Kroseberg²³, J. Krstic¹⁴, U. Kruchonak⁶⁸, H. Krüger²³,
 N. Krumnack⁶⁷, M.C. Kruse⁴⁸, T. Kubota⁹¹, H. Kucuk⁸¹, S. Kудay^{4b}, J.T. Kuechler¹⁷⁸, S. Kuehn³²,
 A. Kugel^{60a}, F. Kuger¹⁷⁷, T. Kuhl⁴⁵, V. Kukhtin⁶⁸, R. Kukla⁸⁸, Y. Kulchitsky⁹⁵, S. Kuleshov^{34b},
 Y.P. Kulinich¹⁶⁹, M. Kuna^{134a,134b}, T. Kunigo⁷¹, A. Kupco¹²⁹, T. Kupfer⁴⁶, O. Kuprash¹⁵⁵,
 H. Kurashige⁷⁰, L.L. Kurchaninov^{163a}, Y.A. Kurochkin⁹⁵, M.G. Kurth^{35a,35d}, E.S. Kuwertz¹⁷²,
 M. Kuze¹⁵⁹, J. Kvita¹¹⁷, T. Kwan¹⁷², D. Kyriazopoulos¹⁴¹, A. La Rosa¹⁰³, J.L. La Rosa Navarro^{26d},
 L. La Rotonda^{40a,40b}, F. La Ruffa^{40a,40b}, C. Lacasta¹⁷⁰, F. Lacava^{134a,134b}, J. Lacey⁴⁵, D.P.J. Lack⁸⁷,
 H. Lacker¹⁷, D. Lacour⁸³, E. Ladygin⁶⁸, R. Lafaye⁵, B. Laforge⁸³, T. Lagouri¹⁷⁹, S. Lai⁵⁷,
 S. Lammers⁶⁴, W. Lampl⁷, E. Lançon²⁷, U. Landgraf⁵¹, M.P.J. Landon⁷⁹, M.C. Lanfermann⁵²,
 V.S. Lang⁴⁵, J.C. Lange¹³, R.J. Langenberg³², A.J. Lankford¹⁶⁶, F. Lanni²⁷, K. Lantzsch²³, A. Lanza^{123a},
 A. Lapertosa^{53a,53b}, S. Laplace⁸³, J.F. Laporte¹³⁸, T. Lari^{94a}, F. Lasagni Manghi^{22a,22b}, M. Lassnig³²,
 T.S. Lau^{62a}, P. Laurelli⁵⁰, W. Lavrijsen¹⁶, A.T. Law¹³⁹, P. Laycock⁷⁷, T. Lazovich⁵⁹, M. Lazzaroni^{94a,94b},
 B. Le⁹¹, O. Le Dortz⁸³, E. Le Guirriec⁸⁸, E.P. Le Quilleuc¹³⁸, M. LeBlanc¹⁷², T. LeCompte⁶,
 F. Ledroit-Guillon⁵⁸, C.A. Lee²⁷, G.R. Lee^{34a}, S.C. Lee¹⁵³, L. Lee⁵⁹, B. Lefebvre⁹⁰, G. Lefebvre⁸³,
 M. Lefebvre¹⁷², F. Legger¹⁰², C. Leggett¹⁶, G. Lehmann Miotto³², X. Lei⁷, W.A. Leight⁴⁵,
 M.A.L. Leite^{26d}, R. Leitner¹³¹, D. Lellouch¹⁷⁵, B. Lemmer⁵⁷, K.J.C. Leney⁸¹, T. Lenz²³, B. Lenzi³²,
 R. Leone⁷, S. Leone^{126a,126b}, C. Leonidopoulos⁴⁹, G. Lerner¹⁵¹, C. Leroy⁹⁷, R. Les¹⁶¹, A.A.J. Lesage¹³⁸,
 C.G. Lester³⁰, M. Levchenko¹²⁵, J. Levêque⁵, D. Levin⁹², L.J. Levinson¹⁷⁵, M. Levy¹⁹, D. Lewis⁷⁹,
 B. Li^{36a,w}, Changqiao Li^{36a}, H. Li¹⁵⁰, L. Li^{36c}, Q. Li^{35a,35d}, Q. Li^{36a}, S. Li⁴⁸, X. Li^{36c}, Y. Li¹⁴³,
 Z. Liang^{35a}, B. Liberti^{135a}, A. Liblong¹⁶¹, K. Lie^{62c}, J. Liebal²³, W. Liebig¹⁵, A. Limosani¹⁵²,
 C.Y. Lin³⁰, K. Lin⁹³, S.C. Lin¹⁸², T.H. Lin⁸⁶, R.A. Linck⁶⁴, B.E. Lindquist¹⁵⁰, A.E. Lioni⁵²,
 E. Lipeles¹²⁴, A. Lipniacka¹⁵, M. Lisovyi^{60b}, T.M. Liss^{169,ag}, A. Lister¹⁷¹, A.M. Litke¹³⁹, B. Liu⁶⁷,
 H. Liu⁹², H. Liu²⁷, J.K.K. Liu¹²², J. Liu^{36b}, J.B. Liu^{36a}, K. Liu⁸⁸, L. Liu¹⁶⁹, M. Liu^{36a}, Y.L. Liu^{36a},
 Y. Liu^{36a}, M. Livan^{123a,123b}, A. Lleres⁵⁸, J. Llorente Merino^{35a}, S.L. Lloyd⁷⁹, C.Y. Lo^{62b}, F. Lo Sterzo⁴³,
 E.M. Lobodzinska⁴⁵, P. Loch⁷, F.K. Loebinger⁸⁷, A. Loesle⁵¹, K.M. Loew²⁵, T. Lohse¹⁷,
 K. Lohwasser¹⁴¹, M. Lokajicek¹²⁹, B.A. Long²⁴, J.D. Long¹⁶⁹, R.E. Long⁷⁵, L. Longo^{76a,76b},
 K.A. Looper¹¹³, J.A. Lopez^{34b}, I. Lopez Paz¹³, A. Lopez Solis⁸³, J. Lorenz¹⁰², N. Lorenzo Martinez⁵,
 M. Losada²¹, P.J. Lösel¹⁰², X. Lou^{35a}, A. Lounis¹¹⁹, J. Love⁶, P.A. Love⁷⁵, H. Lu^{62a}, N. Lu⁹², Y.J. Lu⁶³,
 H.J. Lubatti¹⁴⁰, C. Luci^{134a,134b}, A. Lucotte⁵⁸, C. Luedtke⁵¹, F. Luehring⁶⁴, W. Lukas⁶⁵, L. Luminari^{134a},
 O. Lundberg^{148a,148b}, B. Lund-Jensen¹⁴⁹, M.S. Lutz⁸⁹, P.M. Luzi⁸³, D. Lynn²⁷, R. Lysak¹²⁹, E. Lytken⁸⁴,
 F. Lyu^{35a}, V. Lyubushkin⁶⁸, H. Ma²⁷, L.L. Ma^{36b}, Y. Ma^{36b}, G. Maccarrone⁵⁰, A. Macchiolo¹⁰³,
 C.M. Macdonald¹⁴¹, B. Maček⁷⁸, J. Machado Miguens^{124,128b}, D. Madaffari¹⁷⁰, R. Madar³⁷,
 W.F. Mader⁴⁷, A. Madsen⁴⁵, N. Madysa⁴⁷, J. Maeda⁷⁰, S. Maeland¹⁵, T. Maeno²⁷, A.S. Maevskiy¹⁰¹,
 V. Magerl⁵¹, C. Maiani¹¹⁹, C. Maidantchik^{26a}, T. Maier¹⁰², A. Maio^{128a,128b,128d}, O. Majersky^{146a},
 S. Majewski¹¹⁸, Y. Makida⁶⁹, N. Makovec¹¹⁹, B. Malaescu⁸³, Pa. Malecki⁴², V.P. Maleev¹²⁵, F. Malek⁵⁸,
 U. Mallik⁶⁶, D. Malon⁶, C. Malone³⁰, S. Maltezos¹⁰, S. Malyukov³², J. Mamuzic¹⁷⁰, G. Mancini⁵⁰,
 I. Mandić⁷⁸, J. Maneira^{128a,128b}, L. Manhaes de Andrade Filho^{26b}, J. Manjarres Ramos⁴⁷,
 K.H. Mankinen⁸⁴, A. Mann¹⁰², A. Manousos³², B. Mansoulie¹³⁸, J.D. Mansour^{35a}, R. Mantifel⁹⁰,
 M. Mantoani⁵⁷, S. Manzoni^{94a,94b}, L. Mapelli³², G. Marceca²⁹, L. March⁵², L. Marchese¹²²,
 G. Marchiori⁸³, M. Marcisovsky¹²⁹, C.A. Marin Tobon³², M. Marjanovic³⁷, D.E. Marley⁹²,
 F. Marroquim^{26a}, S.P. Marsden⁸⁷, Z. Marshall¹⁶, M.U.F. Martensson¹⁶⁸, S. Marti-Garcia¹⁷⁰,

C.B. Martin¹¹³, T.A. Martin¹⁷³, V.J. Martin⁴⁹, B. Martin dit Latour¹⁵, M. Martinez^{13,v},
 V.I. Martinez Outschoorn¹⁶⁹, S. Martin-Haugh¹³³, V.S. Martoiu^{28b}, A.C. Martyniuk⁸¹, A. Marzin³²,
 L. Masetti⁸⁶, T. Mashimo¹⁵⁷, R. Mashinistov⁹⁸, J. Masik⁸⁷, A.L. Maslennikov^{111.c}, L.H. Mason⁹¹,
 L. Massa^{135a,135b}, P. Mastrandrea⁵, A. Mastroberardino^{40a,40b}, T. Masubuchi¹⁵⁷, P. Mättig¹⁷⁸,
 J. Maurer^{28b}, S.J. Maxfield⁷⁷, D.A. Maximov^{111.c}, R. Mazini¹⁵³, I. Maznas¹⁵⁶, S.M. Mazza^{94a,94b},
 N.C. Mc Fadden¹⁰⁷, G. Mc Goldrick¹⁶¹, S.P. Mc Kee⁹², A. McCarn⁹², R.L. McCarthy¹⁵⁰,
 T.G. McCarthy¹⁰³, L.I. McClymont⁸¹, E.F. McDonald⁹¹, J.A. Mcfayden³², G. Mchedlidze⁵⁷,
 S.J. McMahon¹³³, P.C. McNamara⁹¹, C.J. McNicol¹⁷³, R.A. McPherson^{172,o}, S. Meehan¹⁴⁰,
 T.J. Megy⁵¹, S. Mehlhase¹⁰², A. Mehta⁷⁷, T. Meideck⁵⁸, K. Meier^{60a}, B. Meirose⁴⁴, D. Melini^{170,ah},
 B.R. Mellado Garcia^{147c}, J.D. Mellenthin⁵⁷, M. Melo^{146a}, F. Meloni¹⁸, A. Melzer²³, S.B. Menary⁸⁷,
 L. Meng⁷⁷, X.T. Meng⁹², A. Mengarelli^{22a,22b}, S. Menke¹⁰³, E. Meoni^{40a,40b}, S. Mergelmeyer¹⁷,
 C. Merlassino¹⁸, P. Mermod⁵², L. Merola^{106a,106b}, C. Meroni^{94a}, F.S. Merritt³³, A. Messina^{134a,134b},
 J. Metcalfe⁶, A.S. Mete¹⁶⁶, C. Meyer¹²⁴, J-P. Meyer¹³⁸, J. Meyer¹⁰⁹, H. Meyer Zu Theenhausen^{60a},
 F. Miano¹⁵¹, R.P. Middleton¹³³, S. Miglioranzi^{53a,53b}, L. Mijović⁴⁹, G. Mikenberg¹⁷⁵,
 M. Mikestikova¹²⁹, M. Mikuž⁷⁸, M. Milesi⁹¹, A. Milic¹⁶¹, D.A. Millar⁷⁹, D.W. Miller³³, C. Mills⁴⁹,
 A. Milov¹⁷⁵, D.A. Milstead^{148a,148b}, A.A. Minaenko¹³², Y. Minami¹⁵⁷, I.A. Minashvili^{54b},
 A.I. Mincer¹¹², B. Mindur^{41a}, M. Mineev⁶⁸, Y. Minegishi¹⁵⁷, Y. Ming¹⁷⁶, L.M. Mir¹³, A. Mirto^{76a,76b},
 K.P. Mistry¹²⁴, T. Mitani¹⁷⁴, J. Mitrevski¹⁰², V.A. Mitsou¹⁷⁰, A. Miucci¹⁸, P.S. Miyagawa¹⁴¹,
 A. Mizukami⁶⁹, J.U. Mjörnmark⁸⁴, T. Mkrtchyan¹⁸⁰, M. Mlynarikova¹³¹, T. Moa^{148a,148b},
 K. Mochizuki⁹⁷, P. Mogg⁵¹, S. Mohapatra³⁸, S. Molander^{148a,148b}, R. Moles-Valls²³, M.C. Mondragon⁹³,
 K. Mönig⁴⁵, J. Monk³⁹, E. Monnier⁸⁸, A. Montalbano¹⁵⁰, J. Montejo Berlingen³², F. Monticelli⁷⁴,
 S. Monzani^{94a,94b}, R.W. Moore³, N. Morange¹¹⁹, D. Moreno²¹, M. Moreno Llácer³², P. Morettini^{53a},
 S. Morgenstern³², D. Mori¹⁴⁴, T. Mori¹⁵⁷, M. Morii⁵⁹, M. Morinaga¹⁷⁴, V. Morisbak¹²¹, A.K. Morley³²,
 G. Mornacchi³², J.D. Morris⁷⁹, L. Morvaj¹⁵⁰, P. Moschovakos¹⁰, M. Mosidze^{54b}, H.J. Moss¹⁴¹,
 J. Moss^{145.ai}, K. Motohashi¹⁵⁹, R. Mount¹⁴⁵, E. Mountricha²⁷, E.J.W. Moyse⁸⁹, S. Muanza⁸⁸,
 F. Mueller¹⁰³, J. Mueller¹²⁷, R.S.P. Mueller¹⁰², D. Muenstermann⁷⁵, P. Mullen⁵⁶, G.A. Mullier¹⁸,
 F.J. Munoz Sanchez⁸⁷, W.J. Murray^{173,133}, H. Musheghyan³², M. Muškinja⁷⁸, A.G. Myagkov^{132.aj},
 M. Myska¹³⁰, B.P. Nachman¹⁶, O. Nackenhorst⁵², K. Nagai¹²², R. Nagai^{69,ae}, K. Nagano⁶⁹,
 Y. Nagasaka⁶¹, K. Nagata¹⁶⁴, M. Nagel⁵¹, E. Nagy⁸⁸, A.M. Nairz³², Y. Nakahama¹⁰⁵, K. Nakamura⁶⁹,
 T. Nakamura¹⁵⁷, I. Nakano¹¹⁴, R.F. Naranjo Garcia⁴⁵, R. Narayan¹¹, D.I. Narrias Villar^{60a},
 I. Naryshkin¹²⁵, T. Naumann⁴⁵, G. Navarro²¹, R. Nayyar⁷, H.A. Neal⁹², P.Yu. Nechaeva⁹⁸, T.J. Neep¹³⁸,
 A. Negri^{123a,123b}, M. Negrini^{22a}, S. Nektarijevic¹⁰⁸, C. Nellist⁵⁷, A. Nelson¹⁶⁶, M.E. Nelson¹²²,
 S. Nemecek¹²⁹, P. Nemethy¹¹², M. Nessi^{32.ak}, M.S. Neubauer¹⁶⁹, M. Neumann¹⁷⁸, P.R. Newman¹⁹,
 T.Y. Ng^{62c}, Y.S. Ng¹⁷, T. Nguyen Manh⁹⁷, R.B. Nickerson¹²², R. Nicolaidou¹³⁸, J. Nielsen¹³⁹,
 N. Nikiforou¹¹, V. Nikolaenko^{132.aj}, I. Nikolic-Audit⁸³, K. Nikolopoulos¹⁹, P. Nilsson²⁷, Y. Ninomiya⁶⁹,
 A. Nisati^{134a}, N. Nishu^{36c}, R. Nisius¹⁰³, I. Nitsche⁴⁶, T. Nitta¹⁷⁴, T. Nobe¹⁵⁷, Y. Noguchi⁷¹,
 M. Nomachi¹²⁰, I. Nomidis³¹, M.A. Nomura²⁷, T. Nooney⁷⁹, M. Nordberg³², N. Norjoharuddeen¹²²,
 O. Novgorodova⁴⁷, M. Nozaki⁶⁹, L. Nozka¹¹⁷, K. Ntekas¹⁶⁶, E. Nurse⁸¹, F. Nuti⁹¹, K. O'connor²⁵,
 D.C. O'Neil¹⁴⁴, A.A. O'Rourke⁴⁵, V. O'Shea⁵⁶, F.G. Oakham^{31.d}, H. Oberlack¹⁰³, T. Obermann²³,
 J. Ocariz⁸³, A. Ochi⁷⁰, I. Ochoa³⁸, J.P. Ochoa-Ricoux^{34a}, S. Oda⁷³, S. Odaka⁶⁹, A. Oh⁸⁷, S.H. Oh⁴⁸,
 C.C. Ohm¹⁴⁹, H. Ohman¹⁶⁸, H. Oide^{53a,53b}, H. Okawa¹⁶⁴, Y. Okumura¹⁵⁷, T. Okuyama⁶⁹, A. Olariu^{28b},
 L.F. Oleiro Seabra^{128a}, S.A. Olivares Pino^{34a}, D. Oliveira Damazio²⁷, M.J.R. Olsson³³, A. Olszewski⁴²,
 J. Olszowska⁴², A. Onofre^{128a,128e}, K. Onogi¹⁰⁵, P.U.E. Onyisi^{11.aa}, H. Oppen¹²¹, M.J. Oreglia³³,
 Y. Oren¹⁵⁵, D. Orestano^{136a,136b}, N. Orlando^{62b}, R.S. Orr¹⁶¹, B. Osculati^{53a,53b,*}, R. Ospanov^{36a},
 G. Otero y Garzon²⁹, H. Otono⁷³, M. Ouchrif^{137d}, F. Ould-Saada¹²¹, A. Ouraou¹³⁸, K.P. Oussoren¹⁰⁹,
 Q. Ouyang^{35a}, M. Owen⁵⁶, R.E. Owen¹⁹, V.E. Ozcan^{20a}, N. Ozturk⁸, K. Pachal¹⁴⁴, A. Pacheco Pages¹³,
 L. Pacheco Rodriguez¹³⁸, C. Padilla Aranda¹³, S. Pagan Griso¹⁶, M. Paganini¹⁷⁹, F. Paige²⁷,

G. Palacino⁶⁴, S. Palazzo^{40a,40b}, S. Palestini³², M. Palka^{41b}, D. Pallin³⁷, E.St. Panagiotopoulou¹⁰, I. Panagoulas¹⁰, C.E. Pandini⁵², J.G. Panduro Vazquez⁸⁰, P. Pani³², S. Panitkin²⁷, D. Pantea^{28b}, L. Paolozzi⁵², Th.D. Papadopoulou¹⁰, K. Papageorgiou^{9,s}, A. Paramonov⁶, D. Paredes Hernandez¹⁷⁹, A.J. Parker⁷⁵, M.A. Parker³⁰, K.A. Parker⁴⁵, F. Parodi^{53a,53b}, J.A. Parsons³⁸, U. Parzefall⁵¹, V.R. Pascuzzi¹⁶¹, J.M. Pasner¹³⁹, E. Pasqualucci^{134a}, S. Passaggio^{53a}, Fr. Pastore⁸⁰, S. Patariaia⁸⁶, J.R. Pater⁸⁷, T. Pauly³², B. Pearson¹⁰³, S. Pedraza Lopez¹⁷⁰, R. Pedro^{128a,128b}, S.V. Peleganchuk^{111,c}, O. Penc¹²⁹, C. Peng^{35a,35d}, H. Peng^{36a}, J. Penwell⁶⁴, B.S. Peralva^{26b}, M.M. Perego¹³⁸, D.V. Perepelitsa²⁷, F. Peri¹⁷, L. Perini^{94a,94b}, H. Pernegger³², S. Perrella^{106a,106b}, R. Peschke⁴⁵, V.D. Peshekhonov^{68,*}, K. Peters⁴⁵, R.F.Y. Peters⁸⁷, B.A. Petersen³², T.C. Petersen³⁹, E. Petit⁵⁸, A. Petridis¹, C. Petridou¹⁵⁶, P. Petroff¹¹⁹, E. Petrolo^{134a}, M. Petrov¹²², F. Petrucci^{136a,136b}, N.E. Pettersson⁸⁹, A. Peyaud¹³⁸, R. Pezoa^{34b}, F.H. Phillips⁹³, P.W. Phillips¹³³, G. Piacquadio¹⁵⁰, E. Pianori¹⁷³, A. Picazio⁸⁹, M.A. Pickering¹²², R. Piegaia²⁹, J.E. Pilcher³³, A.D. Pilkington⁸⁷, M. Pinamonti^{135a,135b}, J.L. Pinfold³, H. Pirumov⁴⁵, M. Pitt¹⁷⁵, L. Plazak^{146a}, M.-A. Pleier²⁷, V. Pleskot⁸⁶, E. Plotnikova⁶⁸, D. Pluth⁶⁷, P. Podberezko¹¹¹, R. Poettgen⁸⁴, R. Poggi^{123a,123b}, L. Poggioli¹¹⁹, I. Pogrebnyak⁹³, D. Pohl²³, I. Pokharel⁵⁷, G. Polesello^{123a}, A. Poley⁴⁵, A. Policicchio^{40a,40b}, R. Polifka³², A. Polini^{22a}, C.S. Pollard⁵⁶, V. Polychronakos²⁷, K. Pommès³², D. Ponomarenko¹⁰⁰, L. Pontecorvo^{134a}, G.A. Popeneci^{28d}, D.M. Portillo Quintero⁸³, S. Pospisil¹³⁰, K. Potamianos⁴⁵, I.N. Potrap⁶⁸, C.J. Potter³⁰, H. Potti¹¹, T. Poulsen⁸⁴, J. Poveda³², M.E. Pozo Astigarraga³², P. Pralavorio⁸⁸, A. Pranko¹⁶, S. Prell⁶⁷, D. Price⁸⁷, M. Primavera^{76a}, S. Prince⁹⁰, N. Proklova¹⁰⁰, K. Prokofiev^{62c}, F. Prokoshin^{34b}, S. Protopopescu²⁷, J. Proudfoot⁶, M. Przybycien^{41a}, A. Puri¹⁶⁹, P. Puzo¹¹⁹, J. Qian⁹², G. Qin⁵⁶, Y. Qin⁸⁷, A. Quadt⁵⁷, M. Queitsch-Maitland⁴⁵, D. Quilty⁵⁶, S. Raddum¹²¹, V. Radeka²⁷, V. Radescu¹²², S.K. Radhakrishnan¹⁵⁰, P. Radloff¹¹⁸, P. Rados⁹¹, F. Ragusa^{94a,94b}, G. Rahal¹⁸¹, J.A. Raine⁸⁷, S. Rajagopalan²⁷, C. Rangel-Smith¹⁶⁸, T. Rashid¹¹⁹, S. Raspopov⁵, M.G. Ratti^{94a,94b}, D.M. Rauch⁴⁵, F. Rauscher¹⁰², S. Rave⁸⁶, I. Ravinovich¹⁷⁵, J.H. Rawling⁸⁷, M. Raymond³², A.L. Read¹²¹, N.P. Readioff⁵⁸, M. Reale^{76a,76b}, D.M. Rebuzzi^{123a,123b}, A. Redelbach¹⁷⁷, G. Redlinger²⁷, R. Reece¹³⁹, R.G. Reed^{147c}, K. Reeves⁴⁴, L. Rehnisch¹⁷, J. Reichert¹²⁴, A. Reiss⁸⁶, C. Rembser³², H. Ren^{35a,35d}, M. Rescigno^{134a}, S. Resconi^{94a}, E.D. Resseguie¹²⁴, S. Rettie¹⁷¹, E. Reynolds¹⁹, O.L. Rezanova^{111,c}, P. Reznicek¹³¹, R. Rezvani⁹⁷, R. Richter¹⁰³, S. Richter⁸¹, E. Richter-Was^{41b}, O. Ricken²³, M. Ridel⁸³, P. Rieck¹⁰³, C.J. Riegel¹⁷⁸, J. Rieger⁵⁷, O. Rifki¹¹⁵, M. Rijssenbeek¹⁵⁰, A. Rimoldi^{123a,123b}, M. Rimoldi¹⁸, L. Rinaldi^{22a}, G. Ripellino¹⁴⁹, B. Ristic³², E. Ritsch³², I. Riu¹³, F. Rizatdinova¹¹⁶, E. Rizvi⁷⁹, C. Rizzi¹³, R.T. Roberts⁸⁷, S.H. Robertson^{90,o}, A. Robichaud-Veronneau⁹⁰, D. Robinson³⁰, J.E.M. Robinson⁴⁵, A. Robson⁵⁶, E. Rocco⁸⁶, C. Roda^{126a,126b}, Y. Rodina^{88,al}, S. Rodriguez Bosca¹⁷⁰, A. Rodriguez Perez¹³, D. Rodriguez Rodriguez¹⁷⁰, S. Roe³², C.S. Rogan⁵⁹, O. Røhne¹²¹, J. Roloff⁵⁹, A. Romaniouk¹⁰⁰, M. Romano^{22a,22b}, S.M. Romano Saez³⁷, E. Romero Adam¹⁷⁰, N. Rompotis⁷⁷, M. Ronzani⁵¹, L. Roos⁸³, S. Rosati^{134a}, K. Rosbach⁵¹, P. Rose¹³⁹, N.-A. Rosien⁵⁷, E. Rossi^{106a,106b}, L.P. Rossi^{53a}, J.H.N. Rosten³⁰, R. Rosten¹⁴⁰, M. Rotaru^{28b}, J. Rothberg¹⁴⁰, D. Rousseau¹¹⁹, A. Rozanov⁸⁸, Y. Rozen¹⁵⁴, X. Ruan^{147c}, F. Rubbo¹⁴⁵, E.M. Ruettinger⁴⁵, F. Rühr⁵¹, A. Ruiz-Martinez³¹, Z. Rurikova⁵¹, N.A. Rusakovich⁶⁸, H.L. Russell⁹⁰, J.P. Rutherford⁷, N. Ruthmann³², Y.F. Ryabov¹²⁵, M. Rybar¹⁶⁹, G. Rybkin¹¹⁹, S. Ryu⁶, A. Ryzhov¹³², G.F. Rzehorz⁵⁷, A.F. Saavedra¹⁵², G. Sabato¹⁰⁹, S. Sacerdoti²⁹, H.F.-W. Sadrozinski¹³⁹, R. Sadykov⁶⁸, F. Safai Tehrani^{134a}, P. Saha¹¹⁰, M. Sahinsoy^{60a}, M. Saimpert⁴⁵, M. Saito¹⁵⁷, T. Saito¹⁵⁷, H. Sakamoto¹⁵⁷, Y. Sakurai¹⁷⁴, G. Salamanna^{136a,136b}, J.E. Salazar Loyola^{34b}, D. Salek¹⁰⁹, P.H. Sales De Bruin¹⁶⁸, D. Salihagic¹⁰³, A. Salnikov¹⁴⁵, J. Salt¹⁷⁰, D. Salvatore^{40a,40b}, F. Salvatore¹⁵¹, A. Salvucci^{62a,62b,62c}, A. Salzburger³², D. Sammel⁵¹, D. Sampsonidis¹⁵⁶, D. Sampsonidou¹⁵⁶, J. Sánchez¹⁷⁰, V. Sanchez Martinez¹⁷⁰, A. Sanchez Pineda^{167a,167c}, H. Sandaker¹²¹, R.L. Sandbach⁷⁹, C.O. Sander⁴⁵, M. Sandhoff¹⁷⁸, C. Sandoval²¹, D.P.C. Sankey¹³³, M. Sannino^{53a,53b}, Y. Sano¹⁰⁵, A. Sansoni⁵⁰, C. Santoni³⁷, H. Santos^{128a}, I. Santoyo Castillo¹⁵¹, A. Saprnov⁶⁸, J.G. Saraiva^{128a,128d},

B. Sarrazin²³, O. Sasaki⁶⁹, K. Sato¹⁶⁴, E. Sauvan⁵, G. Savage⁸⁰, P. Savard^{161,d}, N. Savic¹⁰³,
 C. Sawyer¹³³, L. Sawyer^{82,u}, J. Saxon³³, C. Sbarra^{22a}, A. Sbrizzi^{22a,22b}, T. Scanlon⁸¹,
 D.A. Scannicchio¹⁶⁶, J. Schaarschmidt¹⁴⁰, P. Schacht¹⁰³, B.M. Schachtner¹⁰², D. Schaefer³³,
 L. Schaefer¹²⁴, R. Schaefer⁴⁵, J. Schaeffer⁸⁶, S. Schaepe³², S. Schaetzel^{60b}, U. Schäfer⁸⁶,
 A.C. Schaffer¹¹⁹, D. Schaile¹⁰², R.D. Schamberger¹⁵⁰, V.A. Schegelsky¹²⁵, D. Scheirich¹³¹,
 M. Schernau¹⁶⁶, C. Schiavi^{53a,53b}, S. Schier¹³⁹, L.K. Schildgen²³, C. Schillo⁵¹, M. Schioppa^{40a,40b},
 S. Schlenker³², K.R. Schmidt-Sommerfeld¹⁰³, K. Schmieden³², C. Schmitt⁸⁶, S. Schmitt⁴⁵, S. Schmitz⁸⁶,
 U. Schnoor⁵¹, L. Schoeffel¹³⁸, A. Schoening^{60b}, B.D. Schoenrock⁹³, E. Schopf²³, M. Schott⁸⁶,
 J.F.P. Schouwenberg¹⁰⁸, J. Schovancova³², S. Schramm⁵², N. Schuh⁸⁶, A. Schulte⁸⁶, M.J. Schultens²³,
 H.-C. Schultz-Coulon^{60a}, H. Schulz¹⁷, M. Schumacher⁵¹, B.A. Schumm¹³⁹, Ph. Schune¹³⁸,
 A. Schwartzman¹⁴⁵, T.A. Schwarz⁹², H. Schweiger⁸⁷, Ph. Schwemling¹³⁸, R. Schwienhorst⁹³,
 J. Schwindling¹³⁸, A. Sciandra²³, G. Sciolla²⁵, M. Scornajenghi^{40a,40b}, F. Scuri^{126a,126b}, F. Scutti⁹¹,
 J. Searcy⁹², P. Seema²³, S.C. Seidel¹⁰⁷, A. Seiden¹³⁹, J.M. Seixas^{26a}, G. Sekhniaidze^{106a}, K. Sekhon⁹²,
 S.J. Sekula⁴³, N. Semprini-Cesari^{22a,22b}, S. Senkin³⁷, C. Serfon¹²¹, L. Serin¹¹⁹, L. Serkin^{167a,167b},
 M. Sessa^{136a,136b}, R. Seuster¹⁷², H. Severini¹¹⁵, T. Sfiligoj⁷⁸, F. Sforza¹⁶⁵, A. Sfyrla⁵², E. Shabalina⁵⁷,
 N.W. Shaikh^{148a,148b}, L.Y. Shan^{35a}, R. Shang¹⁶⁹, J.T. Shank²⁴, M. Shapiro¹⁶, P.B. Shatalov⁹⁹,
 K. Shaw^{167a,167b}, S.M. Shaw⁸⁷, A. Shcherbakova^{148a,148b}, C.Y. Shehu¹⁵¹, Y. Shen¹¹⁵, N. Sherafati³¹,
 A.D. Sherman²⁴, P. Sherwood⁸¹, L. Shi^{153,am}, S. Shimizu⁷⁰, C.O. Shimmin¹⁷⁹, M. Shimojima¹⁰⁴,
 I.P.J. Shipsey¹²², S. Shirabe⁷³, M. Shiyakova^{68,an}, J. Shlomi¹⁷⁵, A. Shmeleva⁹⁸, D. Shoaleh Saadi⁹⁷,
 M.J. Shochet³³, S. Shojaii^{94a,94b}, D.R. Shope¹¹⁵, S. Shrestha¹¹³, E. Shulga¹⁰⁰, M.A. Shupe⁷, P. Sicho¹²⁹,
 A.M. Sickles¹⁶⁹, P.E. Sidebo¹⁴⁹, E. Sideras Haddad^{147c}, O. Sidiropoulou¹⁷⁷, A. Sidoti^{22a,22b}, F. Siegert⁴⁷,
 Dj. Sijacki¹⁴, J. Silva^{128a,128d}, S.B. Silverstein^{148a}, V. Simak¹³⁰, L. Simic⁶⁸, S. Simion¹¹⁹, E. Simioni⁸⁶,
 B. Simmons⁸¹, M. Simon⁸⁶, P. Sinervo¹⁶¹, N.B. Sinev¹¹⁸, M. Sioli^{22a,22b}, G. Siragusa¹⁷⁷, I. Siral⁹²,
 S.Yu. Sivoklovov¹⁰¹, J. Sjölin^{148a,148b}, M.B. Skinner⁷⁵, P. Skubic¹¹⁵, M. Slater¹⁹, T. Slavicek¹³⁰,
 M. Slawinska⁴², K. Sliwa¹⁶⁵, R. Slovak¹³¹, V. Smakhtin¹⁷⁵, B.H. Smart⁵, J. Smiesko^{146a}, N. Smirnov¹⁰⁰,
 S.Yu. Smirnov¹⁰⁰, Y. Smirnov¹⁰⁰, L.N. Smirnova^{101,ao}, O. Smirnova⁸⁴, J.W. Smith⁵⁷, M.N.K. Smith³⁸,
 R.W. Smith³⁸, M. Smizanska⁷⁵, K. Smolek¹³⁰, A.A. Snesarev⁹⁸, I.M. Snyder¹¹⁸, S. Snyder²⁷,
 R. Sobie^{172,o}, F. Socher⁴⁷, A. Soffer¹⁵⁵, A. Søggaard⁴⁹, D.A. Soh¹⁵³, G. Sokhrannyi⁷⁸,
 C.A. Solans Sanchez³², M. Solar¹³⁰, E.Yu. Soldatov¹⁰⁰, U. Soldevila¹⁷⁰, A.A. Solodkov¹³²,
 A. Soloshenko⁶⁸, O.V. Solovyanov¹³², V. Solovyev¹²⁵, P. Sommer¹⁴¹, H. Son¹⁶⁵, A. Sopczak¹³⁰,
 D. Sosa^{60b}, C.L. Sotiropoulou^{126a,126b}, S. Sottocornola^{123a,123b}, R. Soualah^{167a,167c}, A.M. Soukharev^{111,c},
 D. South⁴⁵, B.C. Sowden⁸⁰, S. Spagnolo^{76a,76b}, M. Spalla^{126a,126b}, M. Spangenberg¹⁷³, F. Spanò⁸⁰,
 D. Sperlich¹⁷, F. Spettel¹⁰³, T.M. Spieker^{60a}, R. Spighi^{22a}, G. Spigo³², L.A. Spiller⁹¹, M. Spousta¹³¹,
 R.D. St. Denis^{56,*}, A. Stabile^{94a}, R. Stamen^{60a}, S. Stamm¹⁷, E. Stanecka⁴², R.W. Stanek⁶,
 C. Stanescu^{136a}, M.M. Stanitzki⁴⁵, B.S. Stapf¹⁰⁹, S. Stapnes¹²¹, E.A. Starchenko¹³², G.H. Stark³³,
 J. Stark⁵⁸, S.H. Stark³⁹, P. Staroba¹²⁹, P. Starovoitov^{60a}, S. Stärz³², R. Staszewski⁴², M. Stegler⁴⁵,
 P. Steinberg²⁷, B. Stelzer¹⁴⁴, H.J. Stelzer³², O. Stelzer-Chilton^{163a}, H. Stenzel⁵⁵, T.J. Stevenson⁷⁹,
 G.A. Stewart⁵⁶, M.C. Stockton¹¹⁸, M. Stoebe⁹⁰, G. Stoica^{28b}, P. Stolte⁵⁷, S. Stonjek¹⁰³, A.R. Stradling⁸,
 A. Straessner⁴⁷, M.E. Stramaglia¹⁸, J. Strandberg¹⁴⁹, S. Strandberg^{148a,148b}, M. Strauss¹¹⁵,
 P. Strizenc^{146b}, R. Ströhmer¹⁷⁷, D.M. Strom¹¹⁸, R. Stroynowski⁴³, A. Strubig⁴⁹, S.A. Stucci²⁷,
 B. Stugu¹⁵, N.A. Styles⁴⁵, D. Su¹⁴⁵, J. Su¹²⁷, S. Suchek^{60a}, Y. Sugaya¹²⁰, M. Suk¹³⁰, V.V. Sulin⁹⁸,
 DMS Sultan^{162a,162b}, S. Sultansoy^{4c}, T. Sumida⁷¹, S. Sun⁵⁹, X. Sun³, K. Suruliz¹⁵¹, C.J.E. Suster¹⁵²,
 M.R. Sutton¹⁵¹, S. Suzuki⁶⁹, M. Svatos¹²⁹, M. Swiatlowski³³, S.P. Swift², I. Sykora^{146a}, T. Sykora¹³¹,
 D. Ta⁵¹, K. Tackmann⁴⁵, J. Taenzer¹⁵⁵, A. Taffard¹⁶⁶, R. Tafirout^{163a}, E. Tahirovic⁷⁹, N. Taiblum¹⁵⁵,
 H. Takai²⁷, R. Takashima⁷², E.H. Takasugi¹⁰³, K. Takeda⁷⁰, T. Takeshita¹⁴², Y. Takubo⁶⁹, M. Talby⁸⁸,
 A.A. Talyshev^{111,c}, J. Tanaka¹⁵⁷, M. Tanaka¹⁵⁹, R. Tanaka¹¹⁹, S. Tanaka⁶⁹, R. Tanioka⁷⁰,
 B.B. Tannenwald¹¹³, S. Tapia Araya^{34b}, S. Tapprogge⁸⁶, S. Tarem¹⁵⁴, G.F. Tartarelli^{94a}, P. Tas¹³¹,

M. Tasevsky¹²⁹, T. Tashiro⁷¹, E. Tassi^{40a,40b}, A. Tavares Delgado^{128a,128b}, Y. Tayalati^{137e}, A.C. Taylor¹⁰⁷,
A.J. Taylor⁴⁹, G.N. Taylor⁹¹, P.T.E. Taylor⁹¹, W. Taylor^{163b}, P. Teixeira-Dias⁸⁰, D. Temple¹⁴⁴,
H. Ten Kate³², P.K. Teng¹⁵³, J.J. Teoh¹²⁰, F. Tepel¹⁷⁸, S. Terada⁶⁹, K. Terashi¹⁵⁷, J. Terron⁸⁵, S. Terzo¹³,
M. Testa⁵⁰, R.J. Teuscher^{161,o}, S.J. Thais¹⁷⁹, T. Thevenaux-Pelzer⁸⁸, F. Thiele³⁹, J.P. Thomas¹⁹,
J. Thomas-Wilsker⁸⁰, P.D. Thompson¹⁹, A.S. Thompson⁵⁶, L.A. Thomsen¹⁷⁹, E. Thomson¹²⁴, Y. Tian³⁸,
M.J. Tibbetts¹⁶, R.E. Ticse Torres⁵⁷, V.O. Tikhomirov^{98,ap}, Yu.A. Tikhonov^{111,c}, S. Timoshenko¹⁰⁰,
P. Tipton¹⁷⁹, S. Tisserant⁸⁸, K. Todome¹⁵⁹, S. Todorova-Nova⁵, S. Todt⁴⁷, J. Tojo⁷³, S. Tokár^{146a},
K. Tokushuku⁶⁹, E. Tolley¹¹³, L. Tomlinson⁸⁷, M. Tomoto¹⁰⁵, L. Tompkins^{145,aq}, K. Toms¹⁰⁷, B. Tong⁵⁹,
P. Tornambe⁵¹, E. Torrence¹¹⁸, H. Torres⁴⁷, E. Torró Pastor¹⁴⁰, J. Toth^{88,ar}, F. Touchard⁸⁸,
D.R. Tovey¹⁴¹, C.J. Treado¹¹², T. Trefzger¹⁷⁷, F. Tresoldi¹⁵¹, A. Tricoli²⁷, I.M. Trigger^{163a},
S. Trincaz-Duvoid⁸³, M.F. Tripiana¹³, W. Trischuk¹⁶¹, B. Trocmé⁵⁸, A. Trofymov⁴⁵, C. Troncon^{94a},
M. Trottier-McDonald¹⁶, M. Trovatelli¹⁷², L. Truong^{147b}, M. Trzebinski⁴², A. Trzupiek⁴²,
K.W. Tsang^{62a}, J.C.-L. Tseng¹²², P.V. Tsiarshka⁹⁵, G. Tsipolitis¹⁰, N. Tsirintanis⁹, S. Tsiskaridze¹³,
V. Tsiskaridze⁵¹, E.G. Tskhadadze^{54a}, I.I. Tsukerman⁹⁹, V. Tsulaia¹⁶, S. Tsuno⁶⁹, D. Tsybychev¹⁵⁰,
Y. Tu^{62b}, A. Tudorache^{28b}, V. Tudorache^{28b}, T.T. Tulbure^{28a}, A.N. Tuna⁵⁹, S. Turchikhin⁶⁸,
D. Turgeman¹⁷⁵, I. Turk Cakir^{4b,as}, R. Turra^{94a}, P.M. Tuts³⁸, G. Uccielli^{22a,22b}, I. Ueda⁶⁹,
M. Ughetto^{148a,148b}, F. Ukegawa¹⁶⁴, G. Unal³², A. Undrus²⁷, G. Unel¹⁶⁶, F.C. Ungaro⁹¹, Y. Unno⁶⁹,
K. Uno¹⁵⁷, C. Unverdorben¹⁰², J. Urban^{146b}, P. Urquijo⁹¹, P. Urrejola⁸⁶, G. Usai⁸, J. Usui⁶⁹,
L. Vacavant⁸⁸, V. Vacek¹³⁰, B. Vachon⁹⁰, K.O.H. Vadla¹²¹, A. Vaidya⁸¹, C. Valderanis¹⁰²,
E. Valdes Santurio^{148a,148b}, M. Valente⁵², S. Valentineti^{22a,22b}, A. Valero¹⁷⁰, L. Valéry¹³, S. Valkar¹³¹,
A. Vallier⁵, J.A. Valls Ferrer¹⁷⁰, W. Van Den Wollenberg¹⁰⁹, H. van der Graaf¹⁰⁹, P. van Gemmeren⁶,
J. Van Nieuwkoop¹⁴⁴, I. van Vulpen¹⁰⁹, M.C. van Woerden¹⁰⁹, M. Vanadia^{135a,135b}, W. Vandelli³²,
A. Vaniachine¹⁶⁰, P. Vankov¹⁰⁹, G. Vardanyan¹⁸⁰, R. Vari^{134a}, E.W. Varnes⁷, C. Varni^{53a,53b}, T. Varol⁴³,
D. Varouchas¹¹⁹, A. Vartapetian⁸, K.E. Varvell¹⁵², J.G. Vasquez¹⁷⁹, G.A. Vasquez^{34b}, F. Vazeille³⁷,
D. Vazquez Furelos¹³, T. Vazquez Schroeder⁹⁰, J. Veatch⁵⁷, V. Veeraraghavan⁷, L.M. Veloce¹⁶¹,
F. Veloso^{128a,128c}, S. Veneziano^{134a}, A. Ventura^{76a,76b}, M. Venturi¹⁷², N. Venturi³², A. Venturini²⁵,
V. Vercesi^{123a}, M. Verducci^{136a,136b}, W. Verkerke¹⁰⁹, A.T. Vermeulen¹⁰⁹, J.C. Vermeulen¹⁰⁹,
M.C. Vetterli^{144,d}, N. Viaux Maira^{34b}, O. Viazlo⁸⁴, I. Vichou^{169,*}, T. Vickey¹⁴¹, O.E. Vickey Boeriu¹⁴¹,
G.H.A. Viehhauser¹²², S. Viel¹⁶, L. Vigani¹²², M. Villa^{22a,22b}, M. Villaplana Perez^{94a,94b}, E. Vilucchi⁵⁰,
M.G. Vincter³¹, V.B. Vinogradov⁶⁸, A. Vishwakarma⁴⁵, C. Vittori^{22a,22b}, I. Vivarelli¹⁵¹, S. Vlachos¹⁰,
M. Vogel¹⁷⁸, P. Vokac¹³⁰, G. Volpi¹³, H. von der Schmitt¹⁰³, E. von Toerne²³, V. Vorobel¹³¹,
K. Vorobev¹⁰⁰, M. Vos¹⁷⁰, R. Voss³², J.H. Vosseveld⁷⁷, N. Vranjes¹⁴, M. Vranjes Milosavljevic¹⁴,
V. Vrba¹³⁰, M. Vreeswijk¹⁰⁹, R. Vuillermet³², I. Vukotic³³, P. Wagner²³, W. Wagner¹⁷⁸,
J. Wagner-Kuhr¹⁰², H. Wahlberg⁷⁴, S. Wahrenmund⁴⁷, K. Wakamiya⁷⁰, J. Walder⁷⁵, R. Walker¹⁰²,
W. Walkowiak¹⁴³, V. Wallangen^{148a,148b}, C. Wang^{35b}, C. Wang^{36b,at}, F. Wang¹⁷⁶, H. Wang¹⁶, H. Wang³,
J. Wang⁴⁵, J. Wang¹⁵², Q. Wang¹¹⁵, R.-J. Wang⁸³, R. Wang⁶, S.M. Wang¹⁵³, T. Wang³⁸, W. Wang^{153,au},
W. Wang^{36a,av}, Z. Wang^{36c}, C. Wanotayaroj⁴⁵, A. Warburton⁹⁰, C.P. Ward³⁰, D.R. Wardrope⁸¹,
A. Washbrook⁴⁹, P.M. Watkins¹⁹, A.T. Watson¹⁹, M.F. Watson¹⁹, G. Watts¹⁴⁰, S. Watts⁸⁷,
B.M. Waugh⁸¹, A.F. Webb¹¹, S. Webb⁸⁶, M.S. Weber¹⁸, S.M. Weber^{60a}, S.W. Weber¹⁷⁷, S.A. Weber³¹,
J.S. Webster⁶, A.R. Weidberg¹²², B. Weinert⁶⁴, J. Weingarten⁵⁷, M. Weirich⁸⁶, C. Weiser⁵¹, H. Weits¹⁰⁹,
P.S. Wells³², T. Wenaus²⁷, T. Wengler³², S. Wenig³², N. Wermes²³, M.D. Werner⁶⁷, P. Werner³²,
M. Wessels^{60a}, T.D. Weston¹⁸, K. Whalen¹¹⁸, N.L. Whallon¹⁴⁰, A.M. Wharton⁷⁵, A.S. White⁹²,
A. White⁸, M.J. White¹, R. White^{34b}, D. Whiteson¹⁶⁶, B.W. Whitmore⁷⁵, F.J. Wickens¹³³,
W. Wiedenmann¹⁷⁶, M. Wielers¹³³, C. Wiglesworth³⁹, L.A.M. Wiik-Fuchs⁵¹, A. Wildauer¹⁰³, F. Wilk⁸⁷,
H.G. Wilkens³², H.H. Williams¹²⁴, S. Williams¹⁰⁹, C. Willis⁹³, S. Willocq⁸⁹, J.A. Wilson¹⁹,
I. Wingerter-Seez⁵, E. Winkels¹⁵¹, F. Winklmeier¹¹⁸, O.J. Winston¹⁵¹, B.T. Winter²³, M. Wittgen¹⁴⁵,
M. Wobisch^{82,u}, A. Wolf⁸⁶, T.M.H. Wolf¹⁰⁹, R. Wolff⁸⁸, M.W. Wolter⁴², H. Wolters^{128a,128c},

V.W.S. Wong¹⁷¹, N.L. Woods¹³⁹, S.D. Worm¹⁹, B.K. Wosiek⁴², J. Wotschack³², K.W. Wozniak⁴², M. Wu³³, S.L. Wu¹⁷⁶, X. Wu⁵², Y. Wu⁹², T.R. Wyatt⁸⁷, B.M. Wynne⁴⁹, S. Xella³⁹, Z. Xi⁹², L. Xia^{35c}, D. Xu^{35a}, L. Xu²⁷, T. Xu¹³⁸, W. Xu⁹², B. Yabsley¹⁵², S. Yacoob^{147a}, D. Yamaguchi¹⁵⁹, Y. Yamaguchi¹⁵⁹, A. Yamamoto⁶⁹, S. Yamamoto¹⁵⁷, T. Yamanaka¹⁵⁷, F. Yamane⁷⁰, M. Yamatani¹⁵⁷, T. Yamazaki¹⁵⁷, Y. Yamazaki⁷⁰, Z. Yan²⁴, H. Yang^{36c}, H. Yang¹⁶, Y. Yang¹⁵³, Z. Yang¹⁵, W-M. Yao¹⁶, Y.C. Yap⁴⁵, Y. Yasu⁶⁹, E. Yatsenko⁵, K.H. Yau Wong²³, J. Ye⁴³, S. Ye²⁷, I. Yeletsikh⁶⁸, E. Yigitbasi²⁴, E. Yildirim⁸⁶, K. Yorita¹⁷⁴, K. Yoshihara¹²⁴, C. Young¹⁴⁵, C.J.S. Young³², J. Yu⁸, J. Yu⁶⁷, S.P.Y. Yuen²³, I. Yusuff^{30,aw}, B. Zabinski⁴², G. Zacharis¹⁰, R. Zaidan¹³, A.M. Zaitsev^{132,aj}, N. Zakharchuk⁴⁵, J. Zalieckas¹⁵, A. Zaman¹⁵⁰, S. Zambito⁵⁹, D. Zanzi⁹¹, C. Zeitnitz¹⁷⁸, G. Zemaityte¹²², A. Zemla^{41a}, J.C. Zeng¹⁶⁹, Q. Zeng¹⁴⁵, O. Zenin¹³², T. Ženiš^{146a}, D. Zerwas¹¹⁹, D. Zhang^{36b}, D. Zhang⁹², F. Zhang¹⁷⁶, G. Zhang^{36a,aw}, H. Zhang¹¹⁹, J. Zhang⁶, L. Zhang⁵¹, L. Zhang^{36a}, M. Zhang¹⁶⁹, P. Zhang^{35b}, R. Zhang²³, R. Zhang^{36a,at}, X. Zhang^{36b}, Y. Zhang^{35a,35d}, Z. Zhang¹¹⁹, X. Zhao⁴³, Y. Zhao^{36b,ax}, Z. Zhao^{36a}, A. Zhemchugov⁶⁸, B. Zhou⁹², C. Zhou¹⁷⁶, L. Zhou⁴³, M. Zhou^{35a,35d}, M. Zhou¹⁵⁰, N. Zhou^{36c}, Y. Zhou⁷, C.G. Zhu^{36b}, H. Zhu^{35a}, J. Zhu⁹², Y. Zhu^{36a}, X. Zhuang^{35a}, K. Zhukov⁹⁸, A. Zibell¹⁷⁷, D. Zieminska⁶⁴, N.I. Zimine⁶⁸, C. Zimmermann⁸⁶, S. Zimmermann⁵¹, Z. Zinonos¹⁰³, M. Zinser⁸⁶, M. Ziolkowski¹⁴³, L. Živković¹⁴, G. Zobernig¹⁷⁶, A. Zoccoli^{22a,22b}, R. Zou³³, M. zur Nedden¹⁷, L. Zwalinski³².

¹ Department of Physics, University of Adelaide, Adelaide, Australia

² Physics Department, SUNY Albany, Albany NY, United States of America

³ Department of Physics, University of Alberta, Edmonton AB, Canada

⁴ (a) Department of Physics, Ankara University, Ankara; (b) Istanbul Aydin University, Istanbul; (c)

Division of Physics, TOBB University of Economics and Technology, Ankara, Turkey

⁵ LAPP, CNRS/IN2P3 and Université Savoie Mont Blanc, Annecy-le-Vieux, France

⁶ High Energy Physics Division, Argonne National Laboratory, Argonne IL, United States of America

⁷ Department of Physics, University of Arizona, Tucson AZ, United States of America

⁸ Department of Physics, The University of Texas at Arlington, Arlington TX, United States of America

⁹ Physics Department, National and Kapodistrian University of Athens, Athens, Greece

¹⁰ Physics Department, National Technical University of Athens, Zografou, Greece

¹¹ Department of Physics, The University of Texas at Austin, Austin TX, United States of America

¹² Institute of Physics, Azerbaijan Academy of Sciences, Baku, Azerbaijan

¹³ Institut de Física d'Altes Energies (IFAE), The Barcelona Institute of Science and Technology, Barcelona, Spain

¹⁴ Institute of Physics, University of Belgrade, Belgrade, Serbia

¹⁵ Department for Physics and Technology, University of Bergen, Bergen, Norway

¹⁶ Physics Division, Lawrence Berkeley National Laboratory and University of California, Berkeley CA, United States of America

¹⁷ Department of Physics, Humboldt University, Berlin, Germany

¹⁸ Albert Einstein Center for Fundamental Physics and Laboratory for High Energy Physics, University of Bern, Bern, Switzerland

¹⁹ School of Physics and Astronomy, University of Birmingham, Birmingham, United Kingdom

²⁰ (a) Department of Physics, Bogazici University, Istanbul; (b) Department of Physics Engineering, Gaziantep University, Gaziantep; (d) Istanbul Bilgi University, Faculty of Engineering and Natural Sciences, Istanbul; (e) Bahcesehir University, Faculty of Engineering and Natural Sciences, Istanbul, Turkey

²¹ Centro de Investigaciones, Universidad Antonio Narino, Bogota, Colombia

²² (a) INFN Sezione di Bologna; (b) Dipartimento di Fisica e Astronomia, Università di Bologna, Bologna, Italy

- 23 Physikalisches Institut, University of Bonn, Bonn, Germany
- 24 Department of Physics, Boston University, Boston MA, United States of America
- 25 Department of Physics, Brandeis University, Waltham MA, United States of America
- 26 ^(a) Universidade Federal do Rio De Janeiro COPPE/EE/IF, Rio de Janeiro; ^(b) Electrical Circuits Department, Federal University of Juiz de Fora (UFJF), Juiz de Fora; ^(c) Federal University of Sao Joao del Rei (UFSJ), Sao Joao del Rei; ^(d) Instituto de Fisica, Universidade de Sao Paulo, Sao Paulo, Brazil
- 27 Physics Department, Brookhaven National Laboratory, Upton NY, United States of America
- 28 ^(a) Transilvania University of Brasov, Brasov; ^(b) Horia Hulubei National Institute of Physics and Nuclear Engineering, Bucharest; ^(c) Department of Physics, Alexandru Ioan Cuza University of Iasi, Iasi; ^(d) National Institute for Research and Development of Isotopic and Molecular Technologies, Physics Department, Cluj Napoca; ^(e) University Politehnica Bucharest, Bucharest; ^(f) West University in Timisoara, Timisoara, Romania
- 29 Departamento de Física, Universidad de Buenos Aires, Buenos Aires, Argentina
- 30 Cavendish Laboratory, University of Cambridge, Cambridge, United Kingdom
- 31 Department of Physics, Carleton University, Ottawa ON, Canada
- 32 CERN, Geneva, Switzerland
- 33 Enrico Fermi Institute, University of Chicago, Chicago IL, United States of America
- 34 ^(a) Departamento de Física, Pontificia Universidad Católica de Chile, Santiago; ^(b) Departamento de Física, Universidad Técnica Federico Santa María, Valparaíso, Chile
- 35 ^(a) Institute of High Energy Physics, Chinese Academy of Sciences, Beijing; ^(b) Department of Physics, Nanjing University, Jiangsu; ^(c) Physics Department, Tsinghua University, Beijing 100084; ^(d) University of Chinese Academy of Science (UCAS), Beijing, China
- 36 ^(a) Department of Modern Physics and State Key Laboratory of Particle Detection and Electronics, University of Science and Technology of China, Anhui; ^(b) School of Physics, Shandong University, Shandong; ^(c) Department of Physics and Astronomy, Key Laboratory for Particle Physics, Astrophysics and Cosmology, Ministry of Education; Shanghai Key Laboratory for Particle Physics and Cosmology, Shanghai Jiao Tong University, Shanghai(also at PKU-CHEP), China
- 37 Université Clermont Auvergne, CNRS/IN2P3, LPC, Clermont-Ferrand, France
- 38 Nevis Laboratory, Columbia University, Irvington NY, United States of America
- 39 Niels Bohr Institute, University of Copenhagen, Kobenhavn, Denmark
- 40 ^(a) INFN Gruppo Collegato di Cosenza, Laboratori Nazionali di Frascati; ^(b) Dipartimento di Fisica, Università della Calabria, Rende, Italy
- 41 ^(a) AGH University of Science and Technology, Faculty of Physics and Applied Computer Science, Krakow; ^(b) Marian Smoluchowski Institute of Physics, Jagiellonian University, Krakow, Poland
- 42 Institute of Nuclear Physics Polish Academy of Sciences, Krakow, Poland
- 43 Physics Department, Southern Methodist University, Dallas TX, United States of America
- 44 Physics Department, University of Texas at Dallas, Richardson TX, United States of America
- 45 DESY, Hamburg and Zeuthen, Germany
- 46 Lehrstuhl für Experimentelle Physik IV, Technische Universität Dortmund, Dortmund, Germany
- 47 Institut für Kern- und Teilchenphysik, Technische Universität Dresden, Dresden, Germany
- 48 Department of Physics, Duke University, Durham NC, United States of America
- 49 SUPA - School of Physics and Astronomy, University of Edinburgh, Edinburgh, United Kingdom
- 50 INFN e Laboratori Nazionali di Frascati, Frascati, Italy
- 51 Fakultät für Mathematik und Physik, Albert-Ludwigs-Universität, Freiburg, Germany
- 52 Departement de Physique Nucleaire et Corpusculaire, Université de Genève, Geneva, Switzerland
- 53 ^(a) INFN Sezione di Genova; ^(b) Dipartimento di Fisica, Università di Genova, Genova, Italy
- 54 ^(a) E. Andronikashvili Institute of Physics, Iv. Javakhishvili Tbilisi State University, Tbilisi; ^(b) High

Energy Physics Institute, Tbilisi State University, Tbilisi, Georgia

⁵⁵ II Physikalisches Institut, Justus-Liebig-Universität Giessen, Giessen, Germany

⁵⁶ SUPA - School of Physics and Astronomy, University of Glasgow, Glasgow, United Kingdom

⁵⁷ II Physikalisches Institut, Georg-August-Universität, Göttingen, Germany

⁵⁸ Laboratoire de Physique Subatomique et de Cosmologie, Université Grenoble-Alpes, CNRS/IN2P3, Grenoble, France

⁵⁹ Laboratory for Particle Physics and Cosmology, Harvard University, Cambridge MA, United States of America

⁶⁰ ^(a) Kirchhoff-Institut für Physik, Ruprecht-Karls-Universität Heidelberg, Heidelberg; ^(b) Physikalisches Institut, Ruprecht-Karls-Universität Heidelberg, Heidelberg, Germany

⁶¹ Faculty of Applied Information Science, Hiroshima Institute of Technology, Hiroshima, Japan

⁶² ^(a) Department of Physics, The Chinese University of Hong Kong, Shatin, N.T., Hong Kong; ^(b) Department of Physics, The University of Hong Kong, Hong Kong; ^(c) Department of Physics and Institute for Advanced Study, The Hong Kong University of Science and Technology, Clear Water Bay, Kowloon, Hong Kong, China

⁶³ Department of Physics, National Tsing Hua University, Taiwan, Taiwan

⁶⁴ Department of Physics, Indiana University, Bloomington IN, United States of America

⁶⁵ Institut für Astro- und Teilchenphysik, Leopold-Franzens-Universität, Innsbruck, Austria

⁶⁶ University of Iowa, Iowa City IA, United States of America

⁶⁷ Department of Physics and Astronomy, Iowa State University, Ames IA, United States of America

⁶⁸ Joint Institute for Nuclear Research, JINR Dubna, Dubna, Russia

⁶⁹ KEK, High Energy Accelerator Research Organization, Tsukuba, Japan

⁷⁰ Graduate School of Science, Kobe University, Kobe, Japan

⁷¹ Faculty of Science, Kyoto University, Kyoto, Japan

⁷² Kyoto University of Education, Kyoto, Japan

⁷³ Research Center for Advanced Particle Physics and Department of Physics, Kyushu University, Fukuoka, Japan

⁷⁴ Instituto de Física La Plata, Universidad Nacional de La Plata and CONICET, La Plata, Argentina

⁷⁵ Physics Department, Lancaster University, Lancaster, United Kingdom

⁷⁶ ^(a) INFN Sezione di Lecce; ^(b) Dipartimento di Matematica e Fisica, Università del Salento, Lecce, Italy

⁷⁷ Oliver Lodge Laboratory, University of Liverpool, Liverpool, United Kingdom

⁷⁸ Department of Experimental Particle Physics, Jožef Stefan Institute and Department of Physics, University of Ljubljana, Ljubljana, Slovenia

⁷⁹ School of Physics and Astronomy, Queen Mary University of London, London, United Kingdom

⁸⁰ Department of Physics, Royal Holloway University of London, Surrey, United Kingdom

⁸¹ Department of Physics and Astronomy, University College London, London, United Kingdom

⁸² Louisiana Tech University, Ruston LA, United States of America

⁸³ Laboratoire de Physique Nucléaire et de Hautes Energies, UPMC and Université Paris-Diderot and CNRS/IN2P3, Paris, France

⁸⁴ Fysiska institutionen, Lunds universitet, Lund, Sweden

⁸⁵ Departamento de Física Teórica C-15, Universidad Autónoma de Madrid, Madrid, Spain

⁸⁶ Institut für Physik, Universität Mainz, Mainz, Germany

⁸⁷ School of Physics and Astronomy, University of Manchester, Manchester, United Kingdom

⁸⁸ CPPM, Aix-Marseille Université and CNRS/IN2P3, Marseille, France

⁸⁹ Department of Physics, University of Massachusetts, Amherst MA, United States of America

⁹⁰ Department of Physics, McGill University, Montreal QC, Canada

- ⁹¹ School of Physics, University of Melbourne, Victoria, Australia
- ⁹² Department of Physics, The University of Michigan, Ann Arbor MI, United States of America
- ⁹³ Department of Physics and Astronomy, Michigan State University, East Lansing MI, United States of America
- ⁹⁴ ^(a) INFN Sezione di Milano; ^(b) Dipartimento di Fisica, Università di Milano, Milano, Italy
- ⁹⁵ B.I. Stepanov Institute of Physics, National Academy of Sciences of Belarus, Minsk, Republic of Belarus
- ⁹⁶ Research Institute for Nuclear Problems of Byelorussian State University, Minsk, Republic of Belarus
- ⁹⁷ Group of Particle Physics, University of Montreal, Montreal QC, Canada
- ⁹⁸ P.N. Lebedev Physical Institute of the Russian Academy of Sciences, Moscow, Russia
- ⁹⁹ Institute for Theoretical and Experimental Physics (ITEP), Moscow, Russia
- ¹⁰⁰ National Research Nuclear University MEPhI, Moscow, Russia
- ¹⁰¹ D.V. Skobeltsyn Institute of Nuclear Physics, M.V. Lomonosov Moscow State University, Moscow, Russia
- ¹⁰² Fakultät für Physik, Ludwig-Maximilians-Universität München, München, Germany
- ¹⁰³ Max-Planck-Institut für Physik (Werner-Heisenberg-Institut), München, Germany
- ¹⁰⁴ Nagasaki Institute of Applied Science, Nagasaki, Japan
- ¹⁰⁵ Graduate School of Science and Kobayashi-Maskawa Institute, Nagoya University, Nagoya, Japan
- ¹⁰⁶ ^(a) INFN Sezione di Napoli; ^(b) Dipartimento di Fisica, Università di Napoli, Napoli, Italy
- ¹⁰⁷ Department of Physics and Astronomy, University of New Mexico, Albuquerque NM, United States of America
- ¹⁰⁸ Institute for Mathematics, Astrophysics and Particle Physics, Radboud University Nijmegen/Nikhef, Nijmegen, Netherlands
- ¹⁰⁹ Nikhef National Institute for Subatomic Physics and University of Amsterdam, Amsterdam, Netherlands
- ¹¹⁰ Department of Physics, Northern Illinois University, DeKalb IL, United States of America
- ¹¹¹ Budker Institute of Nuclear Physics, SB RAS, Novosibirsk, Russia
- ¹¹² Department of Physics, New York University, New York NY, United States of America
- ¹¹³ Ohio State University, Columbus OH, United States of America
- ¹¹⁴ Faculty of Science, Okayama University, Okayama, Japan
- ¹¹⁵ Homer L. Dodge Department of Physics and Astronomy, University of Oklahoma, Norman OK, United States of America
- ¹¹⁶ Department of Physics, Oklahoma State University, Stillwater OK, United States of America
- ¹¹⁷ Palacký University, RCPTM, Olomouc, Czech Republic
- ¹¹⁸ Center for High Energy Physics, University of Oregon, Eugene OR, United States of America
- ¹¹⁹ LAL, Univ. Paris-Sud, CNRS/IN2P3, Université Paris-Saclay, Orsay, France
- ¹²⁰ Graduate School of Science, Osaka University, Osaka, Japan
- ¹²¹ Department of Physics, University of Oslo, Oslo, Norway
- ¹²² Department of Physics, Oxford University, Oxford, United Kingdom
- ¹²³ ^(a) INFN Sezione di Pavia; ^(b) Dipartimento di Fisica, Università di Pavia, Pavia, Italy
- ¹²⁴ Department of Physics, University of Pennsylvania, Philadelphia PA, United States of America
- ¹²⁵ National Research Centre "Kurchatov Institute" B.P.Konstantinov Petersburg Nuclear Physics Institute, St. Petersburg, Russia
- ¹²⁶ ^(a) INFN Sezione di Pisa; ^(b) Dipartimento di Fisica E. Fermi, Università di Pisa, Pisa, Italy
- ¹²⁷ Department of Physics and Astronomy, University of Pittsburgh, Pittsburgh PA, United States of America
- ¹²⁸ ^(a) Laboratório de Instrumentação e Física Experimental de Partículas - LIP, Lisboa; ^(b) Faculdade

de Ciências, Universidade de Lisboa, Lisboa; ^(c) Department of Physics, University of Coimbra, Coimbra; ^(d) Centro de Física Nuclear da Universidade de Lisboa, Lisboa; ^(e) Departamento de Física, Universidade do Minho, Braga; ^(f) Departamento de Física Teórica y del Cosmos, Universidad de Granada, Granada; ^(g) Dep Física and CEFITEC of Faculdade de Ciências e Tecnologia, Universidade Nova de Lisboa, Caparica, Portugal

¹²⁹ Institute of Physics, Academy of Sciences of the Czech Republic, Praha, Czech Republic

¹³⁰ Czech Technical University in Prague, Praha, Czech Republic

¹³¹ Charles University, Faculty of Mathematics and Physics, Prague, Czech Republic

¹³² State Research Center Institute for High Energy Physics (Protvino), NRC KI, Russia

¹³³ Particle Physics Department, Rutherford Appleton Laboratory, Didcot, United Kingdom

¹³⁴ ^(a) INFN Sezione di Roma; ^(b) Dipartimento di Fisica, Sapienza Università di Roma, Roma, Italy

¹³⁵ ^(a) INFN Sezione di Roma Tor Vergata; ^(b) Dipartimento di Fisica, Università di Roma Tor Vergata, Roma, Italy

¹³⁶ ^(a) INFN Sezione di Roma Tre; ^(b) Dipartimento di Matematica e Fisica, Università Roma Tre, Roma, Italy

¹³⁷ ^(a) Faculté des Sciences Ain Chock, Réseau Universitaire de Physique des Hautes Energies - Université Hassan II, Casablanca; ^(b) Centre National de l'Energie des Sciences Techniques Nucleaires, Rabat; ^(c) Faculté des Sciences Semlalia, Université Cadi Ayyad, LPHEA-Marrakech; ^(d) Faculté des Sciences, Université Mohamed Premier and LPTPM, Oujda; ^(e) Faculté des sciences, Université Mohammed V, Rabat, Morocco

¹³⁸ DSM/IRFU (Institut de Recherches sur les Lois Fondamentales de l'Univers), CEA Saclay (Commissariat à l'Energie Atomique et aux Energies Alternatives), Gif-sur-Yvette, France

¹³⁹ Santa Cruz Institute for Particle Physics, University of California Santa Cruz, Santa Cruz CA, United States of America

¹⁴⁰ Department of Physics, University of Washington, Seattle WA, United States of America

¹⁴¹ Department of Physics and Astronomy, University of Sheffield, Sheffield, United Kingdom

¹⁴² Department of Physics, Shinshu University, Nagano, Japan

¹⁴³ Department Physik, Universität Siegen, Siegen, Germany

¹⁴⁴ Department of Physics, Simon Fraser University, Burnaby BC, Canada

¹⁴⁵ SLAC National Accelerator Laboratory, Stanford CA, United States of America

¹⁴⁶ ^(a) Faculty of Mathematics, Physics & Informatics, Comenius University, Bratislava; ^(b) Department of Subnuclear Physics, Institute of Experimental Physics of the Slovak Academy of Sciences, Kosice, Slovak Republic

¹⁴⁷ ^(a) Department of Physics, University of Cape Town, Cape Town; ^(b) Department of Physics, University of Johannesburg, Johannesburg; ^(c) School of Physics, University of the Witwatersrand, Johannesburg, South Africa

¹⁴⁸ ^(a) Department of Physics, Stockholm University; ^(b) The Oskar Klein Centre, Stockholm, Sweden

¹⁴⁹ Physics Department, Royal Institute of Technology, Stockholm, Sweden

¹⁵⁰ Departments of Physics & Astronomy and Chemistry, Stony Brook University, Stony Brook NY, United States of America

¹⁵¹ Department of Physics and Astronomy, University of Sussex, Brighton, United Kingdom

¹⁵² School of Physics, University of Sydney, Sydney, Australia

¹⁵³ Institute of Physics, Academia Sinica, Taipei, Taiwan

¹⁵⁴ Department of Physics, Technion: Israel Institute of Technology, Haifa, Israel

¹⁵⁵ Raymond and Beverly Sackler School of Physics and Astronomy, Tel Aviv University, Tel Aviv, Israel

¹⁵⁶ Department of Physics, Aristotle University of Thessaloniki, Thessaloniki, Greece

- ¹⁵⁷ International Center for Elementary Particle Physics and Department of Physics, The University of Tokyo, Tokyo, Japan
- ¹⁵⁸ Graduate School of Science and Technology, Tokyo Metropolitan University, Tokyo, Japan
- ¹⁵⁹ Department of Physics, Tokyo Institute of Technology, Tokyo, Japan
- ¹⁶⁰ Tomsk State University, Tomsk, Russia
- ¹⁶¹ Department of Physics, University of Toronto, Toronto ON, Canada
- ¹⁶² ^(a) INFN-TIFPA; ^(b) University of Trento, Trento, Italy
- ¹⁶³ ^(a) TRIUMF, Vancouver BC; ^(b) Department of Physics and Astronomy, York University, Toronto ON, Canada
- ¹⁶⁴ Faculty of Pure and Applied Sciences, and Center for Integrated Research in Fundamental Science and Engineering, University of Tsukuba, Tsukuba, Japan
- ¹⁶⁵ Department of Physics and Astronomy, Tufts University, Medford MA, United States of America
- ¹⁶⁶ Department of Physics and Astronomy, University of California Irvine, Irvine CA, United States of America
- ¹⁶⁷ ^(a) INFN Gruppo Collegato di Udine, Sezione di Trieste, Udine; ^(b) ICTP, Trieste; ^(c) Dipartimento di Chimica, Fisica e Ambiente, Università di Udine, Udine, Italy
- ¹⁶⁸ Department of Physics and Astronomy, University of Uppsala, Uppsala, Sweden
- ¹⁶⁹ Department of Physics, University of Illinois, Urbana IL, United States of America
- ¹⁷⁰ Instituto de Fisica Corpuscular (IFIC), Centro Mixto Universidad de Valencia - CSIC, Spain
- ¹⁷¹ Department of Physics, University of British Columbia, Vancouver BC, Canada
- ¹⁷² Department of Physics and Astronomy, University of Victoria, Victoria BC, Canada
- ¹⁷³ Department of Physics, University of Warwick, Coventry, United Kingdom
- ¹⁷⁴ Waseda University, Tokyo, Japan
- ¹⁷⁵ Department of Particle Physics, The Weizmann Institute of Science, Rehovot, Israel
- ¹⁷⁶ Department of Physics, University of Wisconsin, Madison WI, United States of America
- ¹⁷⁷ Fakultät für Physik und Astronomie, Julius-Maximilians-Universität, Würzburg, Germany
- ¹⁷⁸ Fakultät für Mathematik und Naturwissenschaften, Fachgruppe Physik, Bergische Universität Wuppertal, Wuppertal, Germany
- ¹⁷⁹ Department of Physics, Yale University, New Haven CT, United States of America
- ¹⁸⁰ Yerevan Physics Institute, Yerevan, Armenia
- ¹⁸¹ Centre de Calcul de l'Institut National de Physique Nucléaire et de Physique des Particules (IN2P3), Villeurbanne, France
- ¹⁸² Academia Sinica Grid Computing, Institute of Physics, Academia Sinica, Taipei, Taiwan
- ^a Also at Department of Physics, King's College London, London, United Kingdom
- ^b Also at Institute of Physics, Azerbaijan Academy of Sciences, Baku, Azerbaijan
- ^c Also at Novosibirsk State University, Novosibirsk, Russia
- ^d Also at TRIUMF, Vancouver BC, Canada
- ^e Also at Department of Physics & Astronomy, University of Louisville, Louisville, KY, United States of America
- ^f Also at Physics Department, An-Najah National University, Nablus, Palestine
- ^g Also at Department of Physics, California State University, Fresno CA, United States of America
- ^h Also at Department of Physics, University of Fribourg, Fribourg, Switzerland
- ⁱ Also at II Physikalisches Institut, Georg-August-Universität, Göttingen, Germany
- ^j Also at Departament de Física de la Universitat Autònoma de Barcelona, Barcelona, Spain
- ^k Also at Departamento de Física e Astronomia, Faculdade de Ciências, Universidade do Porto, Portugal
- ^l Also at Tomsk State University, Tomsk, and Moscow Institute of Physics and Technology State University, Dolgoprudny, Russia

- ^m Also at The Collaborative Innovation Center of Quantum Matter (CICQM), Beijing, China
- ⁿ Also at Università di Napoli Parthenope, Napoli, Italy
- ^o Also at Institute of Particle Physics (IPP), Canada
- ^p Also at Horia Hulubei National Institute of Physics and Nuclear Engineering, Bucharest, Romania
- ^q Also at Department of Physics, St. Petersburg State Polytechnical University, St. Petersburg, Russia
- ^r Also at Borough of Manhattan Community College, City University of New York, New York City, United States of America
- ^s Also at Department of Financial and Management Engineering, University of the Aegean, Chios, Greece
- ^t Also at Centre for High Performance Computing, CSIR Campus, Rosebank, Cape Town, South Africa
- ^u Also at Louisiana Tech University, Ruston LA, United States of America
- ^v Also at Institucio Catalana de Recerca i Estudis Avancats, ICREA, Barcelona, Spain
- ^w Also at Department of Physics, The University of Michigan, Ann Arbor MI, United States of America
- ^x Also at Graduate School of Science, Osaka University, Osaka, Japan
- ^y Also at Fakultät für Mathematik und Physik, Albert-Ludwigs-Universität, Freiburg, Germany
- ^z Also at Institute for Mathematics, Astrophysics and Particle Physics, Radboud University Nijmegen/Nikhef, Nijmegen, Netherlands
- ^{aa} Also at Department of Physics, The University of Texas at Austin, Austin TX, United States of America
- ^{ab} Also at Institute of Theoretical Physics, Iliia State University, Tbilisi, Georgia
- ^{ac} Also at CERN, Geneva, Switzerland
- ^{ad} Also at Georgian Technical University (GTU), Tbilisi, Georgia
- ^{ae} Also at Ochadai Academic Production, Ochanomizu University, Tokyo, Japan
- ^{af} Also at Manhattan College, New York NY, United States of America
- ^{ag} Also at The City College of New York, New York NY, United States of America
- ^{ah} Also at Departamento de Física Teórica y del Cosmos, Universidad de Granada, Granada, Portugal
- ^{ai} Also at Department of Physics, California State University, Sacramento CA, United States of America
- ^{aj} Also at Moscow Institute of Physics and Technology State University, Dolgoprudny, Russia
- ^{ak} Also at Departement de Physique Nucleaire et Corpusculaire, Université de Genève, Geneva, Switzerland
- ^{al} Also at Institut de Física d'Altes Energies (IFAE), The Barcelona Institute of Science and Technology, Barcelona, Spain
- ^{am} Also at School of Physics, Sun Yat-sen University, Guangzhou, China
- ^{an} Also at Institute for Nuclear Research and Nuclear Energy (INRNE) of the Bulgarian Academy of Sciences, Sofia, Bulgaria
- ^{ao} Also at Faculty of Physics, M.V.Lomonosov Moscow State University, Moscow, Russia
- ^{ap} Also at National Research Nuclear University MEPhI, Moscow, Russia
- ^{aq} Also at Department of Physics, Stanford University, Stanford CA, United States of America
- ^{ar} Also at Institute for Particle and Nuclear Physics, Wigner Research Centre for Physics, Budapest, Hungary
- ^{as} Also at Giresun University, Faculty of Engineering, Turkey
- ^{at} Also at CPPM, Aix-Marseille Université and CNRS/IN2P3, Marseille, France
- ^{au} Also at Department of Physics, Nanjing University, Jiangsu, China
- ^{av} Also at Institute of Physics, Academia Sinica, Taipei, Taiwan
- ^{aw} Also at University of Malaya, Department of Physics, Kuala Lumpur, Malaysia
- ^{ax} Also at LAL, Univ. Paris-Sud, CNRS/IN2P3, Université Paris-Saclay, Orsay, France
- * Deceased